HCN channel regulation by the cAMP-binding fold is facilitated by interdomain interactions

by

Dana A. Page

B.Sc., Simon Fraser University, 2013

Thesis Submitted in Partial Fulfillment of the
Requirements for the Degree of
Doctor of Philosophy

in the
Department of Molecular Biology and Biochemistry
Faculty of Science

SIMON FRASER UNIVERSITY
Fall 2019

Approval

Name:	**Dana A. Page**
Degree:	**Doctor of Philosophy**
Title:	**HCN channel regulation by the cAMP-binding fold is facilitated by interdomain interactions**
Examining Committee:	**Chair:** Harald Hutter Professor Department of Biological Sciences
	Edgar Young Senior Supervisor Associate Professor
	Jenifer Thewalt Supervisor Professor
	Thomas Claydon Supervisor Professor Department of Biomedical Physiology and Kinesiology
	Peter Ruben Internal Examiner Professor Department of Biomedical Physiology and Kinesiology
	Sharona Gordon External Examiner Professor Department of Physiology and Biophysics University of Washington
Date Defended/Approved:	November 7, 2019

Ethics Statement

The author, whose name appears on the title page of this work, has obtained, for the research described in this work, either:

a. human research ethics approval from the Simon Fraser University Office of Research Ethics

or

b. advance approval of the animal care protocol from the University Animal Care Committee of Simon Fraser University

or has conducted the research

c. as a co-investigator, collaborator, or research assistant in a research project approved in advance.

A copy of the approval letter has been filed with the Theses Office of the University Library at the time of submission of this thesis or project.

The original application for approval and letter of approval are filed with the relevant offices. Inquiries may be directed to those authorities.

Simon Fraser University Library
Burnaby, British Columbia, Canada

Update Spring 2016

Abstract

Hyperpolarization and Cyclic Nucleotide-gated (HCN) channels regulate electrical activity in rhythmically firing cells of the brain and heart. Their voltage-gating is mediated by a transmembrane (TM) region and also by direct binding of cAMP to a cyclic nucleotide-binding (CNB) fold in the cytoplasmic C-terminal region. In its unliganded form, the CNB fold mediates autoinhibition, a mechanism that thermodynamically and kinetically stabilizes the closed channel state; cAMP binding relieves this inhibition. The CNB fold mediates two additional regulatory mechanisms called Open-State Trapping (OST) and Quick-Activation (QA), which can govern the kinetic stability of the open and closed states, respectively. Structural studies have shown direct interactions of the TM region with the cytoplasmic C-linker which connects the TM region to the CNB fold, but the functional role of these interdomain interactions is poorly understood. In this work I found functional evidence for interdomain interactions facilitating autoinhibition, OST and QA, using domain replacements and site directed mutagenesis combined with voltage-clamp assays of channel gating. First, I replaced the TM region of HCN2 with that of HCN4, which augmented the magnitude of autoinhibition by the unliganded CNB fold. This implies that HCN2 channels have an interdomain interaction that limits the magnitude of autoinhibition. The augmentation of autoinhibition was also associated with disruption of the OST and QA mechanisms which are characteristic of HCN2. This resulted in autoinhibition becoming the dominant mechanism contributed by the C-terminal region determining kinetics for both activation and deactivation. Second, I used site-directed mutagenesis to identify a C-linker residue (E457) which stabilizes the open state but exerts different effects on thermodynamics and kinetics, most likely through an electrostatic interaction with the HCN4 TM region. A charge reversal mutation (E457R) limited the thermodynamic effect of autoinhibition while augmenting the kinetic effect of autoinhibition. Notably, in full-length autoinhibited channels E457 undergoes a conformational change such that it no longer stabilizes the open state. Overall, my work suggests that the molecular mechanisms of autoinhibition, OST, and QA must include participation of TM region structures and provides functional evidence for interdomain interactions that facilitate HCN channel regulation by CNB fold-mediated mechanisms.

Keywords: HCN channels; cyclic AMP binding fold; transmembrane region; interdomain interactions; autoinhibition; regulation

To Anita, who taught me to be positive and to persevere through the worst life can throw at you,

To Heather, for teaching me about passion and dedication,

To Lindsae, for teaching me about kindness and giving,

To Janis, for teaching me to be curious and to love unconditionally,

And to Al, for making me laugh.

Acknowledgements

My time in grad school, like many other students, had both highs and lows, but through it all I benefited immensely from the help and support of many people.

I first must thank my supervisor, Dr. Edgar Young who stuck with me as a shy young undergrad and whose mentorship allowed me to blossom into a confident scientist. He took me from someone who was too afraid to answer questions when called upon to someone who is not only ready to answer but is willing to fight for their opinion. Dr. Young supported me through illness; as I hit the biggest low of my grad school experience he stayed by my side and helped me up, and for that I will be eternally grateful. I also used that semi-colon just for him.

Thank you to my committee members, Dr. Thomas Claydon and Dr. Jenifer Thewalt, for challenging me and contributing to my projects since my undergraduate honors degree. Every committee meeting was both informative and enjoyable and for that I am appreciative. I also must thank Dr. Peter Ruben and Dr. Sharona Gordon for agreeing to take the time to be my examiners.

My time in graduate school was greatly enhanced by the other members of the Young Lab. Thank you all for the advice and camaraderie you provided. A special thank you to the wonderful undergraduate research assistants who helped with my project Jessica Li, Matt Jung, and Allaa Ela-Alim. I would also be remiss if I did not thank Dr. Kaylee Magee, who became a close friend and confidante throughout our time working together. Your support and friendship has meant the world to me. I am so glad you took me under your wing seven years ago and that even now you continue to listen to me and keep me laughing.

Lastly, I must thank my friends and family, who let me vent any frustrations and talk to them excitedly about ion channels, something they definitely cared very little about. Without their support I assuredly would not be here today.

Table of Contents

List of Tables

List of Figures

List of Acronyms

cAMP	Cyclic Adenosine 3’,5’- monophosphate
CNB fold	Cyclic Nucleotide Binding fold
CNG	Cyclic Nucleotide Gated Channel
cryoEM	Cryo-electron microscopy
HCN	Hyperpolarization and Cyclic-Nucleotide Gated Channel
hERG	human ether-à-go-go
I_F	Funny Current
I_H	Hyperpolarization-activated current
IOPC	Inside Out Patch Clamp
K_V	Voltage gated potassium channel
OST	Open-State Trapping
PIP_2	Phosphatidylinositol 4,5-bisphosphate
QA	Quick-Activation
RMP	Resting Membrane Potential
SA	Sino-Atrial
SD	Standard deviation
SEM	Standard error of the mean
spHCN	Sea urchin HCN
TEVC	Two Electrode Voltage Clamp
TM	Transmembrane
VSD	Voltage Sensing Domain
XC	Extreme C-terminus
αC	C-helix

Chapter 1.

Introduction

1.1. General overview of HCN channels

1.1.1. HCN channel discovery and characterization

Hyperpolarization and Cyclic Nucleotide gated (HCN) channels are the voltage gated ion channel responsible for the funny current (I_F) which was first described in the sino-atrial (SA) node of the heart in 1979 (Brown et al., 1979; DiFrancesco, 1981, 1986; DiFrancesco et al., 1986). This current is an inward mixed cation current (composed of sodium and potassium ions) that occurs at hyperpolarizing membrane potentials following the action potential and helps depolarize the cell membrane, leading to action potential initiation (DiFrancesco, 1981, 1984, 1986; DiFrancesco et al., 1986). I_F was also found to help mediate the increased heart rate in response to adrenaline, largely as a response to increases in levels of the second messenger cyclic AMP (cAMP) (DiFrancesco and Tortora, 1991; DiFrancesco et al., 1986). An analogous current (I_h) was found in neurons and is mainly involved in neuronal integration and regulation of action potential initiation and duration (Santoro and Tibbs, 1999).

When the gene products responsible for the I_F current (the HCN channel) were cloned (Ludwig et al., 1998, 1999; Santoro et al., 1997, 1998), they were found to be homologous to human ether-à-go-go (hERG) channels and Cyclic Nucleotide Gated (CNG) channels, which are distantly related to classical voltage-gated potassium channels. Like voltage-gated potassium channels, HCN channels are tetramers where each subunit contains a transmembrane (TM) region flanked by cytoplasmic N-terminal and C-terminal regions. Notably, like CNG channels, HCN channels have a Cyclic Nucleotide-Binding (CNB) fold in their C-terminal region, which allows for regulation of channel conductance by cyclic nucleotides like cAMP (Zagotta and Siegelbaum, 1996; Zagotta et al., 2003). The four subtypes of mammalian HCN channels (HCN1-4) that were cloned each have distinct expression patterns. The main subtype found in the SA node is HCN4; HCN1 or HCN2 are also expressed in the SA node to lesser degrees depending on the organism (Brioschi et al., 2009; Santoro et al., 2000). In contrast,

HCN1 and HCN2 are highly expressed across various specific neuronal tissues with limited HCN4 expression, while HCN3 is mainly expressed in the kidney (Santoro and Tibbs, 1999).

1.1.2. Physiological roles of HCN channels

Role of HCN Channels in the heart

As previously stated, HCN channels are involved in maintaining rhythmicity in the heart as well as increasing heart rate in response to beta-adrenergic stimulation. For this reason, mutations in HCN channels (mainly HCN4 channels) underlie a variety of heart disease states, including bradycardia, atrial fibrillation, sick sinus syndrome and Brugada syndrome (Duhme et al., 2013; Macri et al., 2014; Netter et al., 2012; Schulze-Bahr et al., 2003; Schweizer et al., 2010; Ueda et al., 2004, 2009; Zhou et al., 2014). HCN channels may also be important during heart development, as a knockout of HCN4 channels in mice led to embryonic death (Stieber et al., 2003a). Demonstrating the importance of proper cardiac HCN channel function, one mutation in an interdomain linker has been found to cause severe bradycardia, QT prolongation and Torsade de pointes (Netter et al., 2012; Ueda et al., 2004). Another mutation in the same interdomain linker caused tachycardia/bradycardia syndrome and atrial fibrillation, possibly due to an increased response to cAMP (Duhme et al., 2013).

Role of HCN Channels in neurons

HCN channels are involved in various neuronal activities including maintaining resting membrane potential, dendritic integration in pyramidal neurons, control of synaptic plasticity and the production of long-term potentiation (LTP), working and spatial memory, synaptic transmission, resonance and oscillations, and motor learning (reviewed in Biel & Wahl-Schott, 2009). Most of these roles are related to the fact that in neurons HCN channels are open at the negative potentials typical of a resting neuron, but produce a current that depolarizes the potential. Deviations from rest caused by excitatory stimuli, called excitatory post synaptic potentials, result in fast HCN channel closure and therefore membrane repolarization (Doan and Kunze, 1999; Lupica et al., 2001; Meuth et al., 2019; Nolan et al., 2003, 2004, 2007). This stabilization of the resting membrane potential of the cell is a key role of neuronal HCN channels.

The role of HCN channels in neuronal diseases is less studied than in heart disease, in part due to the increased complexity of HCN channel function in various neuronal cell types (see review of HCN channel disease states in Baruscotti et al., 2010). However, there is some evidence for dysregulation or changes in expression patterns of HCN1 or HCN2 channels resulting in epilepsy (DiFrancesco and DiFrancesco, 2015; DiFrancesco et al., 2011; Nava et al., 2014). Increased neuronal activity and action potential production due to a loss of HCN channels could cause hyperexcitability and consequently, epilepsy. In support of this, epileptic mouse models with HCN2 knock-outs have been created (Ludwig et al., 2003).

1.1.3. Basic HCN channel functions

It is important to understand the structural mechanisms that underlie different functions of HCN channels so that we can understand how mutations like the ones described in 1.1.2 can result in the described disease states. The HCN transmembrane (TM) region contains voltage sensing structures as well as a pore mediating ion conductance (Lee and MacKinnon, 2017). HCN channels activate (i.e. pore opens) at hyperpolarizing voltages and deactivate (i.e. pore closes) at depolarizing voltages (DiFrancesco, 1984; DiFrancesco et al., 1986). Opening of the pore results in conduction of an inward mixed cation current (DiFrancesco, 1984; DiFrancesco et al., 1986). These basic functions of HCN channels (i.e. ion conductance in response to voltage) can be modulated by ligands; of particular interest in this thesis is cAMP mentioned above, as well as the lipid messenger phosphatidylinositol 4,5-bisphosphate (PIP_2).

The binding of cAMP to the channel's CNB fold results in potentiation (increase), of channel activity, causing a positive shift in the voltage dependence of HCN channels so they are easier to open, as well as speeding activation and slowing deactivation (DiFrancesco and Tortora, 1991; Wainger et al., 2001). As stated earlier, this function is important for mediating increased heart rate in response to beta-adrenergic stimulation (DiFrancesco and Tortora, 1991; DiFrancesco et al., 1986). It is thought that cAMP binding to the CNB fold is coupled to conformational changes in the voltage-sensing and/or pore domains in the TM region, stabilizing the open state of the channel; detailed structural models for cAMP potentiation will be discussed in detail later in this Chapter and this thesis. Binding of the lipid PIP_2 also potentiates HCN channels, which can be

demonstrated by removing PIP_2 by enzymatic degradation or by chemical inhibition of PIP_2 synthesis enzymes (Pian et al., 2006, 2007; Zolles et al., 2006). A PIP_2 binding site has been located in the C-terminal region of the HCN channel homolog found in sea urchin (spHCN) (Flynn and Zagotta, 2011); the amino acid residues in this site are conserved in mammalian HCN channels. There is also a PIP_2 binding site in the TM region, although the specific amino acids involved have not been identified (Flynn and Zagotta, 2011).

1.2. Detailed structure of HCN channels

The recent cryoEM structure of the human HCN1 channel (Lee and MacKinnon, 2017) confirmed many structural aspects of HCN channels that had been suggested previously (see Wahl-Schott and Biel, 2009 for review of the suggested HCN channel structure). The TM region of HCN channels (i.e. the voltage sensing domain and the pore) is formed by six transmembrane helices (S1 to S6; Figure 1-1) (Lee and MacKinnon, 2017). The pore domain consists of the S5 and S6 helices plus the intervening sequence. The pore domains in the four subunits in the tetramer interact to form the pore of the channel (Figure 1-2). Between the S5 and S6 helices is the selectivity filter which selects for Na^+ or K^+ ions passing through the pore. The C-terminal region of S6 forms the activation gate of the channel, which is opened in response to hyperpolarization. The S1-S4 helices make up the voltage sensing domain so that the tetramer has four voltage-sensing domains on the periphery of the pore (Figure 1-1, Figure 1-2). The S4 helix is known as the voltage sensor as it contains nine positively charged residues (Lee and MacKinnon, 2017). This positively charged helix moves through the membrane in response to voltage changes, resulting in the activation gate opening (Bell et al., 2004; Vemana et al., 2004).

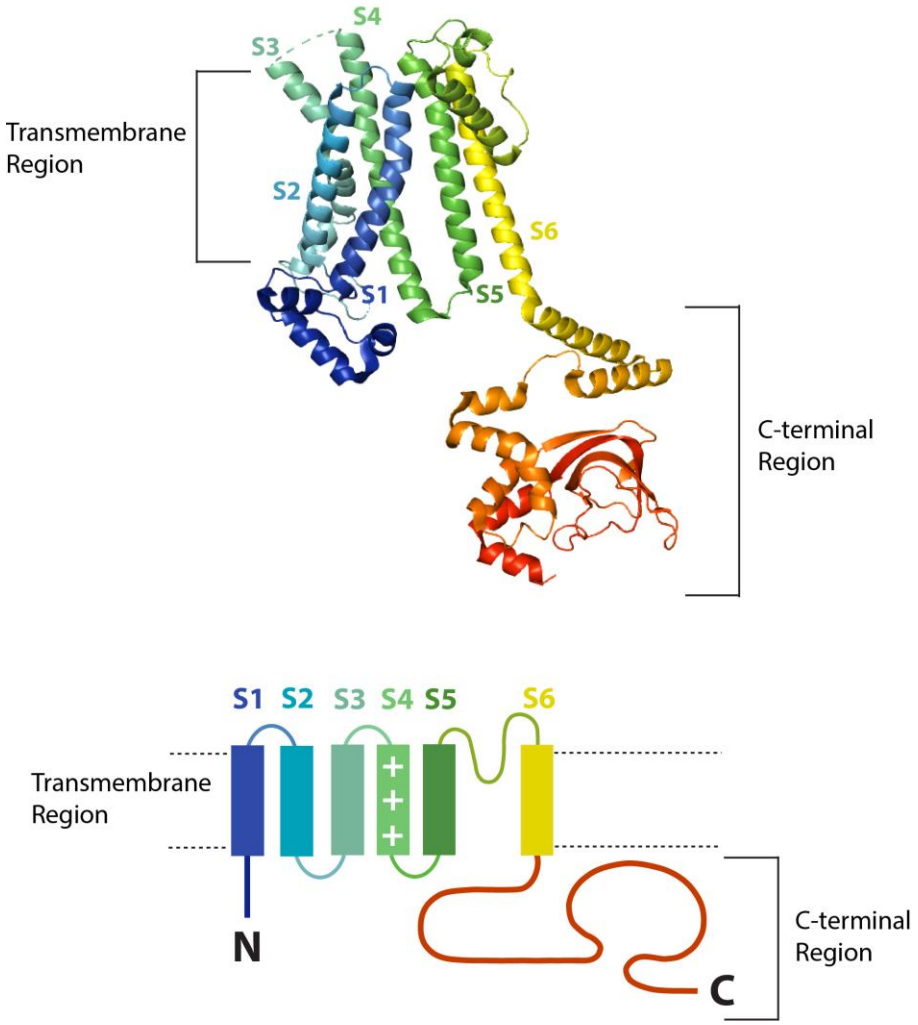

Figure 1-1: Structure of the human HCN1 (hHCN1) subunit

Upper, Single human HCN subunit (unliganded) (Lee and MacKinnon, 2017) with the Transmembrane and C-terminal regions indicated and six membrane spanning helices labelled S1 to S6 **Lower,** Schematic of a single HCN subunit colored as in *upper panel*. The S4 voltage sensor has three positive symbols to indicate the nine positively charged residues on S4. The S5 and S6 helices are connected by a pore loop. The C-terminal region is colored orange with the CNB fold represented by the round loop structure, connected to the TM region by the C-linker. This schematic will be used throughout this thesis to indicate sequence composition of HCN channel derivatives studied

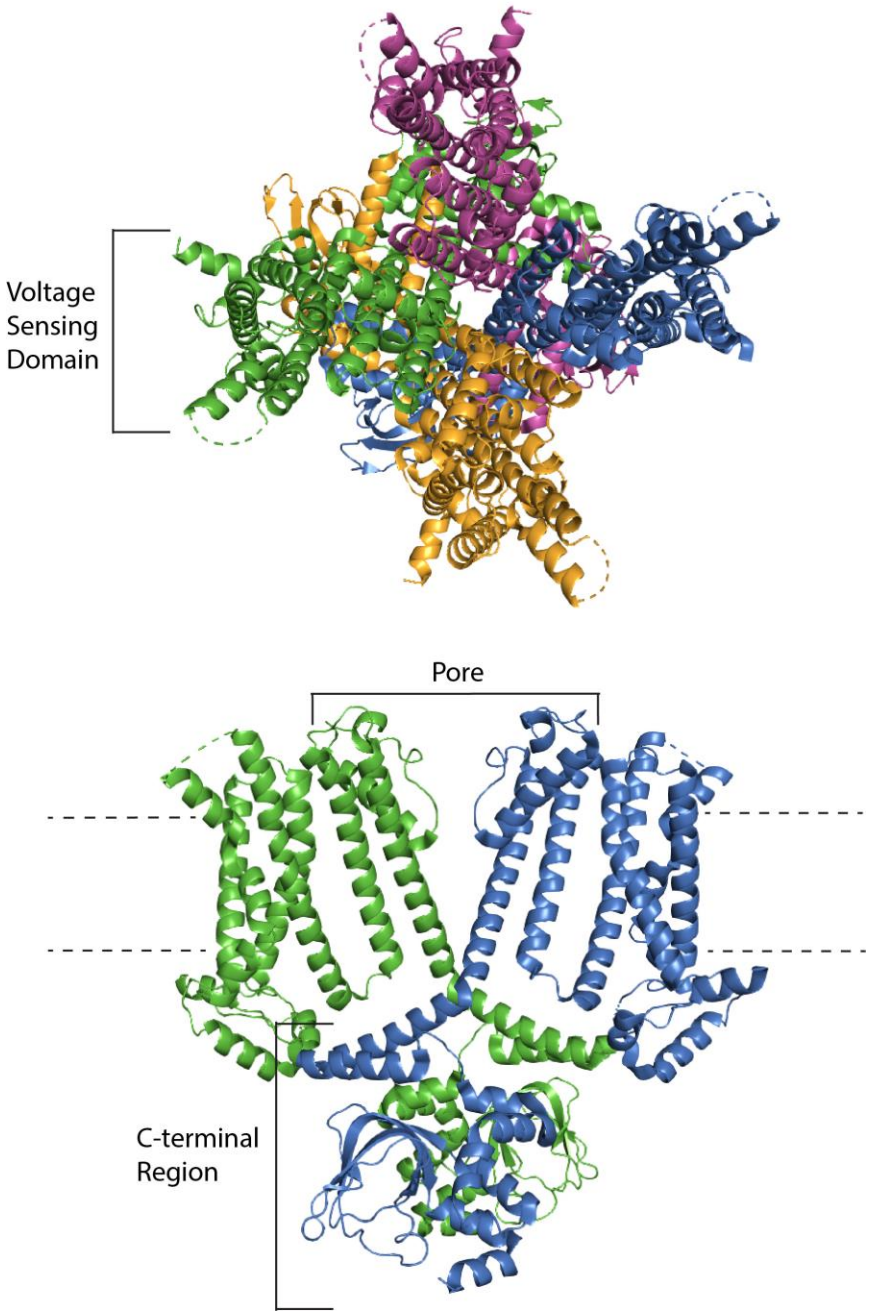

Figure 1-2: General structure of the hHCN1 channel

Upper, Top-down view of the unliganded hHCN1 tetramer (Lee and MacKinnon, 2017) where the four subunits are colored blue, orange, green and pink. The voltage sensing domains (S1-S4) are on the periphery of the channel. The central pore contains the S5 and S6 helices of each subunit. **Lower,** Side-view of the green and blue subunits of the tetramer from the *upper panel*. The pink and orange subunits are removed for clarity. The central pore contains the selectivity filter between the S5 and S6 helices, extending into the middle of the pore. The proposed location of the phospholipid membrane is indicated with dashed lines. The C-terminal region is indicated below. Note the proximity of the blue subunit's C-linker to the green subunit's TM region, suggesting the possibility of interactions between the two.

The C-terminal end of the S6 helix is directly connected to the C-terminal region of the channel (Figure 1-1, Figure 1-2) (Lee and MacKinnon, 2017). The C-terminal region contains, in order: the C-linker; the CNB fold; and, the extreme C-terminal region (Figure 1-3) (Lee and MacKinnon, 2017; Zagotta et al., 2003). The C-linker contains six alpha helices (Figure 1-3, Figure 1-4) (Lee and MacKinnon, 2017; Zagotta et al., 2003). The proximal position of the C-linker to the transmembrane regions could allow for C-terminal structures to modify TM region functions (Figure 1-2) (Lee and MacKinnon, 2017). The CNB fold has a beta-roll and three alpha-helices (A, B and C) (Figure 1-3, Figure 1-4) (Lee and MacKinnon, 2017; Zagotta et al., 2003). The C-helix, which is C-terminal of the beta-roll, has been implicated in cAMP binding, by acting as a gate, trapping cAMP in the active site (Figure 1-3, Figure1-4) (Puljung and Zagotta, 2013; Taraska et al., 2009). Binding of cAMP to the CNB fold leads to a rearrangement of the C-linker with formation of a ring assembly ("tetramerization") (Akimoto et al., 2014; Craven and Zagotta, 2004; Lee and MacKinnon, 2017; Zagotta et al., 2003). This assembly is thought to stabilize the open state of the channel, which could explain how cAMP potentiation occurs.

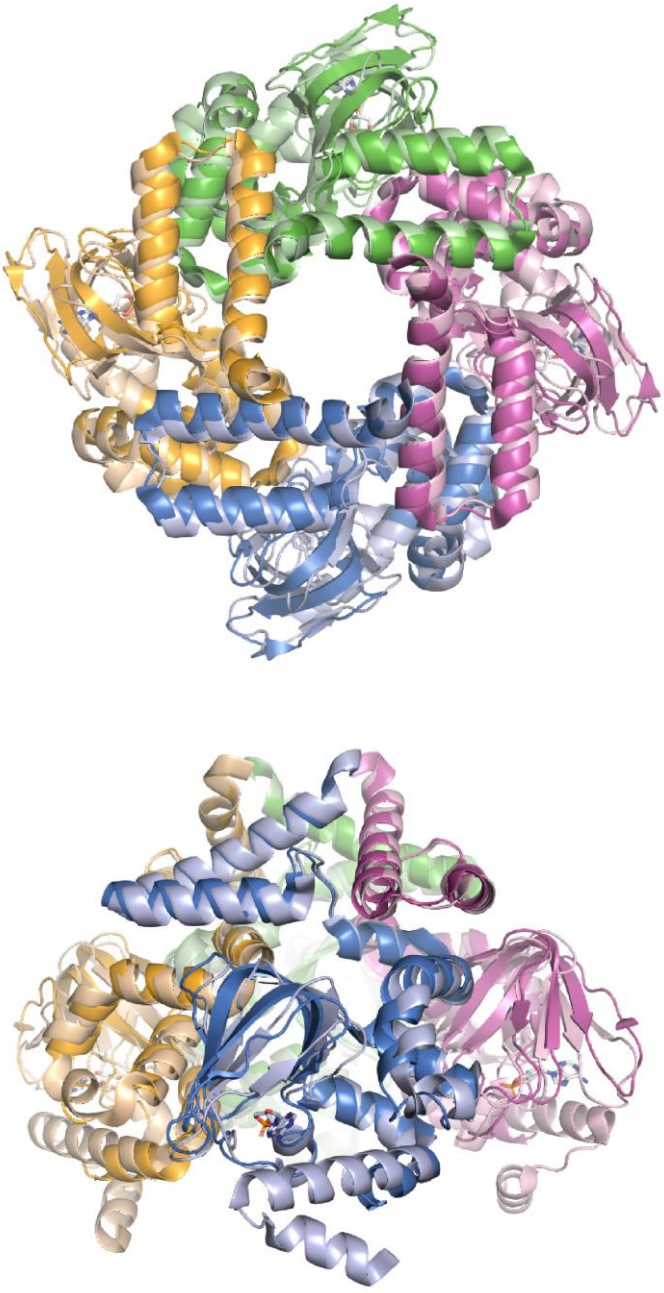

Figure 1-3: CNB fold and C-linker of the hHCN1 channel

Upper, Top-down view of a superimposition of the liganded and unliganded C-terminal regions of the hHCN1 tetramer from Figure 1-2 (Lee and MacKinnon, 2017). Unliganded channel structure is colored in dark colors, as in Figure 1-2, while the liganded channel structure is colored in light colors (light blue, light orange, light green and light pink). Note the conformational changes that occur upon cAMP binding, specifically the A' helices (helices that form a square, closest to the center of the channel) rotating outwards away from the center of the channel. **Lower,** Side-view of the superimposition of the liganded and unliganded C-terminal regions from the *upper panel.* Coloring as in *upper panel.* The A' helices are at the top connecting to the C-terminal region of the S6 helix. Note the conformational change upon cAMP binding, where the C-helix lengthens to interact with cAMP

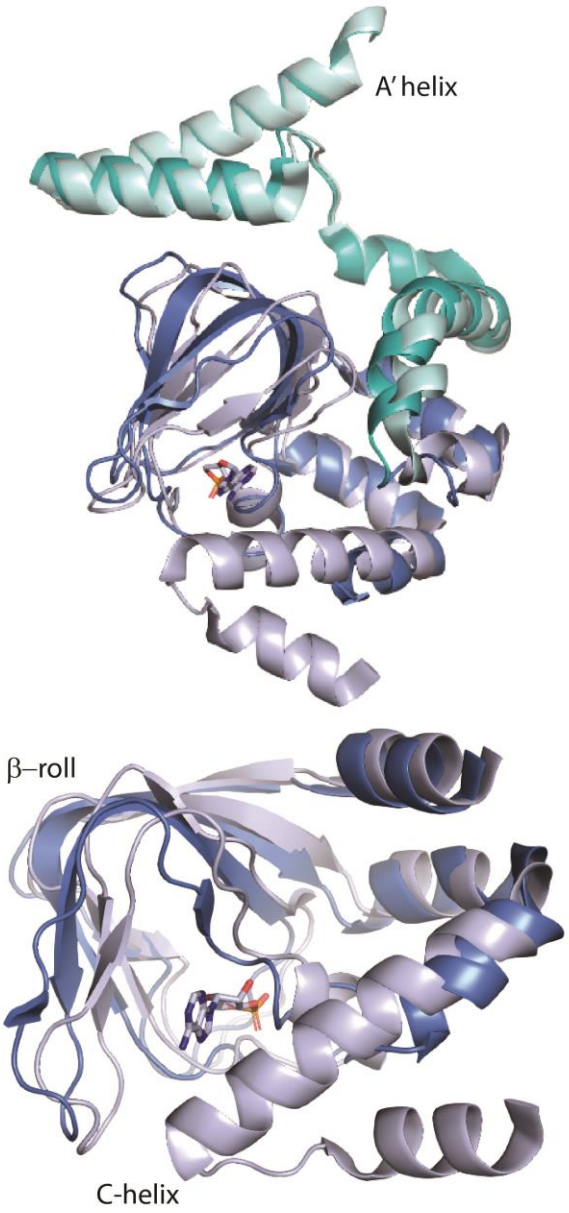

Figure 1-4: Single subunit superimposition of unliganded and liganded C-terminal regions

Upper, Single subunit from the superimposition of the liganded and unliganded C-terminal regions shown in Figure 1-3. The C-linker is shown in teal (unliganded) and light teal (liganded), while the unliganded CNB fold is in blue and the liganded CNB fold is in light blue. **Lower,** CNB fold from *upper panel.* Note the conformational change upon cAMP binding, where the C-helix lengthens to interact with cAMP

1.3. Coupling Voltage Sensing to Pore Opening

In contrast to classical voltage-gated potassium (K_V) channels which activate in response to depolarized membrane potentials, HCN channels activate in response to hyperpolarizing membrane potentials and deactivate in response to depolarizing membrane potentials (Ludwig et al., 1998, 1999; Santoro et al., 1998). HCN channel activation starts with the S4 voltage sensor moving inwards in response to a hyperpolarizing membrane potential, which is followed by pore opening (Bell et al., 2004; Männikkö et al., 2005; Vemana et al., 2004). In crystal structures of classical Kv channels an alpha-helical segment was observed between the S4 and S5 helices, which therefore connected the voltage sensor to the pore; this was labelled the S4-S5 linker (Jiang et al., 2003; Long et al., 2005a, 2007). A well-established model used to explain voltage-gating in Kv channels is that the movement of the S4 voltage sensor is allosterically coupled to opening of the S6 activation gate in the pore through the S4-S5 linker (Long et al., 2005a).

Based on homology models with classical Kv channels a putative HCN S4-S5 linker sequence was proposed and subsequently probed to identify residues involved in coupling voltage-dependent movement of S4 to pore opening, similar to classical Kv channels (Chen et al., 2001a). The researchers performed an alanine scan of the putative HCN channel S4-S5 linker and identified three residues where mutation to alanine inhibited channel closure (Chen et al., 2001a). This was explained by proposing that the alanine mutations disrupted important interactions between the mutated S4-S5 linker residues and the S6 activation gate (Chen et al., 2001a). Based on these results researchers concluded that the putative S4-S5 linker can couple S4 movement to the S6 activation gate in HCN channels (Chen et al., 2001a). Since HCN channels also have a regulatory C-terminal domain that can modulate voltage dependence, could this regulation be occurring through interactions with the S4-S5 linker?

1.4. Interactions between the TM and C-terminal regions in HCN channels

In addition to showing that the S4-S5 linker was helical, classical K_V channel crystal structures showed that the S4-S5 linker was accessible to the cytoplasm (Jiang et al., 2003; Long et al., 2005b, 2005a, 2007). Based on this it was thought that the

putative S4-S5 linker of HCN channels was also accessible to the cytoplasm, and thus accessible to the C-terminal region of the channel (Chen et al., 2001a; Jiang et al., 2003; Kwan et al., 2012; Long et al., 2005b, 2005a, 2007; Prole and Yellen, 2006). This led to the hypothesis that the C-terminal region could interact with the S4-S5 linker in order to modulate channel activity (Decher et al., 2004; Kwan et al., 2012; Prole and Yellen, 2006; Zagotta et al., 2003). Crystal structures of the isolated C-linker and CNB fold of HCN channels suggested that the first alpha-helix of the C-linker (A') could be close and parallel to the membrane, where it could interact with the S4-S5 linker (Taraska et al., 2009; Xu et al., 2010; Zagotta et al., 2003). In fact, Kwan et al. found that by replacing A' and S4-S5 linker residues with cysteines and then applying Cd^{2+}, they were able to form crosslinks between the cysteines that were within 4 Å of eachother; this showed that various residues in the A' helix and S4-S5 linker are in very close proximity in either the closed state, the open state or both (Kwan et al., 2012). In another study (Decher et al., 2004), alanine scans of both the A' helix and S4-S5 linker not only found residues of both regions that are important for normal channel gating, but also identified a pair of residues, one in the A' helix and one in the S4-S5 linker, that could form an electrostatic interaction. This interaction was demonstrated using charge reversal mutations of the individual residues, which affected normal channel gating, as well as double charge-reversal mutants which regenerated normal channel functions (Decher et al., 2004).

Notably, unlike crystal structures of classical K_V channels, the recent cryoEM structure of human HCN1 (hHCN1) in the closed state did not show a helical S4-S5 linker connecting S4 to the pore (Figure 1-1, Figure 1-2) (Jiang et al., 2003; Lee and MacKinnon, 2017; Long et al., 2005b, 2007). Instead, the S4 and S5 helices extended into the cytoplasm with a small three-residue linker connecting them (Lee and MacKinnon, 2017). The portions of these helices that extended into the cytoplasm formed extensive interactions with the cytoplasmic portions of the HCN channel, including the N-terminal HCN domain and the C-linker. Markedly, the TM region of one subunit interacts with the A' helix of the adjacent subunit's C-linker due to a phenomenon called "domain swapping" (Figure 1-1, Figure 1-2, Figure 1-5) (Lee and MacKinnon, 2017). In fact, a recent study (Flynn and Zagotta, 2018) has suggested that it is not the physical connection of the VSD and the pore through the S4-S5 linker that couples voltage sensing to pore opening, but instead S4 residues interact with the pore directly to couple voltage sensing to pore opening. While these findings change our idea

of the general structure of the S4-S5 linker in HCN channels, it does not change the findings that there are TM region residues (in what we now know are the S4 and S5 helices) that are involved in coupling voltage sensor movement to pore opening, and that could interact with the residues of the A' helix (Figure 1-5).

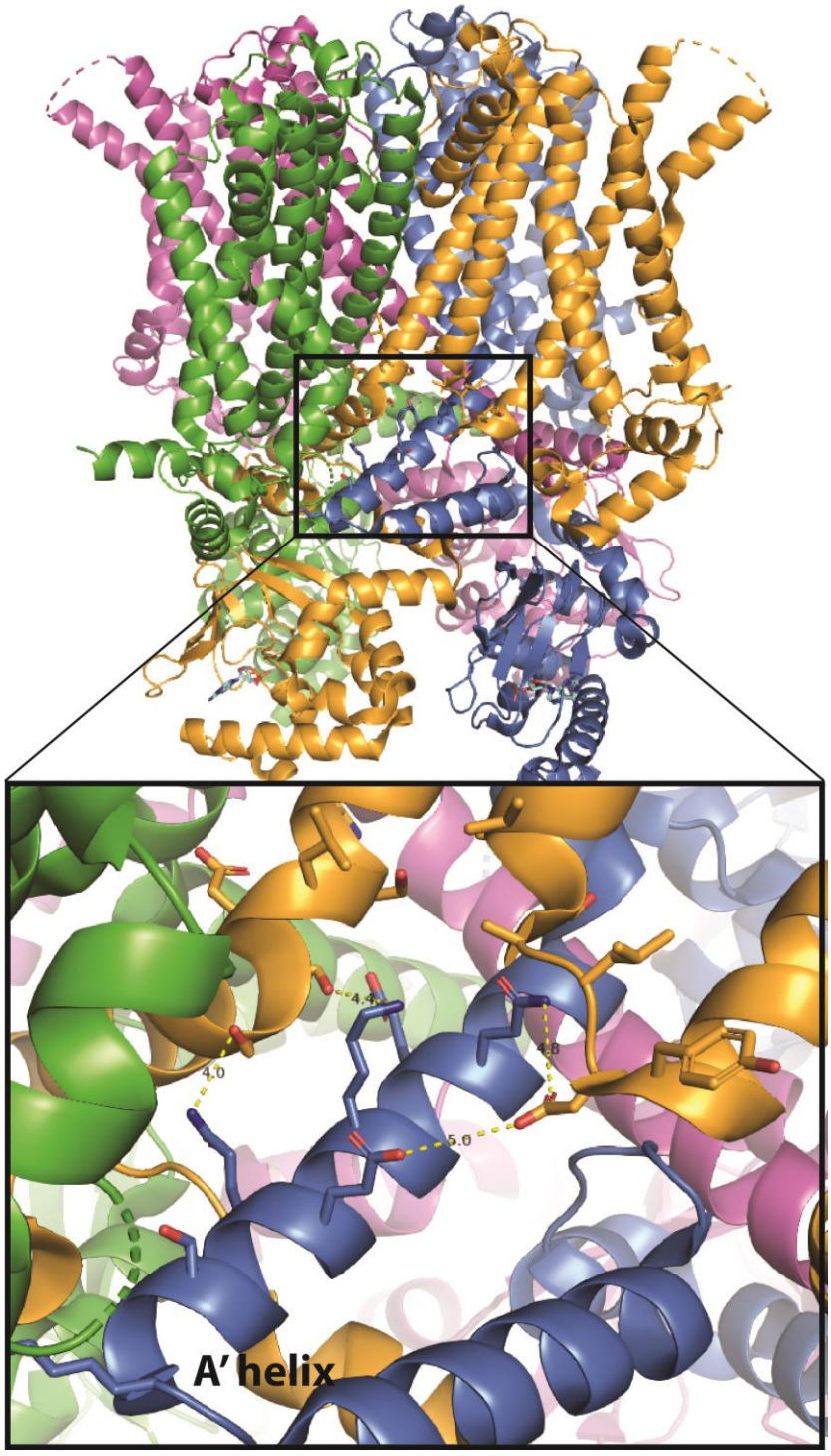

Figure 1-5: Possible A' helix interactions in the hHCN1 structure

Upper, Side-view of the closed, liganded hHCN1 tetramer (Lee and MacKinnon, 2017). Each subunit is colored separately, blue, orange, green and pink. The side-chains of the blue A' helix and potential interacting residues from the TM region are shown as sticks. **Lower,** Magnification of the A' helix from the *upper panel*. The distance between charged A' helix residues and potential partner residues in TM region. Distances shown are 5.0 Å or less.

In conclusion, structural interdomain interactions are known to occur between the TM and C-terminal regions, specifically the S4 and S5 helices and the A' helix (Figure 1-5) (Lee and MacKinnon, 2017). These interactions are hypothesized to modify channel activity in a variety of ways, including changing the relative thermodynamic stability of either the open or closed states, or changing gating kinetics (Chen et al., 2001a; Decher et al., 2004; Kwan et al., 2012; Lee and MacKinnon, 2017; Prole and Yellen, 2006). In general, however, there is little direct evidence of what detailed mechanisms in channel function these interdomain interactions are involved in. I have attempted to identify channel functions that can be modulated by interdomain interactions. I will now discuss these channel functions in detail.

1.5. Voltage Dependence of HCN channels

The voltage dependence of HCN channels is regulated by the relative thermodynamic stability of the HCN channel open and closed states. The more stable the closed state is, the stronger (i.e. more hyperpolarized) the membrane voltage required to open the channel. Therefore, one measure of channel voltage dependence and therefore, thermodynamic stability, is the voltage where half of the channels have opened ($V_{1/2}$) (Hille, 1992). While HCN channel subtypes have been reported to differ in $V_{1/2}$ (Wahl-Schott and Biel, 2009), there can be a large range of reported $V_{1/2}$ values for each subtype as $V_{1/2}$ is sensitive to factors that can vary with cell type, including ligand concentrations and the presence of different accessory proteins (Baruscotti et al., 2005).

1.5.1. Modification of voltage dependence by the C-terminal region

The cAMP potentiation of HCN channels is apparent by a positive shift in the $V_{1/2}$ (DiFrancesco and Tortora, 1991; Wainger et al., 2001; Wang et al., 2001). Different HCN subtypes differ in their responses to cAMP (Ludwig et al., 1998, 1999; Santoro et al., 1998). HCN2 and HCN4 both have a strong response to cAMP, with a reported positive shift in $V_{1/2}$ between 10 and 25 mV (Ludwig et al., 1998, 1999; Santoro et al., 1998). In contrast, HCN1 and HCN3 have a weak response to cAMP; the positive shift in $V_{1/2}$ reported for HCN1 is only around 5 mV (Ludwig et al., 1998; Santoro et al., 1998; Stieber et al., 2005). In conclusion, cAMP binding changes the relative stability of the

open and closed states of HCN channels, causing changes in the channel voltage dependence, which can be observed through shifts in the $V_{1/2}$.

The difference in voltage-dependence between cAMP-liganded and unliganded HCN channels has been proposed to arise through a model of autoinhibition and cAMP-dependent relief of autoinhibition. According to this "autoinhibition model", the unliganded CNB fold inhibits the channel by stabilizing the closed state relative to the open state of the channel (Figure 1-6) (Magee et al., 2015; Wainger et al., 2001). This inhibition can be demonstrated by deletion of the CNB fold because autoinhibited (unliganded) channels display more hyperpolarized $V_{1/2}$ values than the corresponding CNB-fold deletion channels (Magee et al., 2015; Wainger et al., 2001). The autoinhibition model explains cAMP potentiation by proposing that cAMP binding can partially relieve autoinhibition, so that liganded channels display more depolarized $V_{1/2}$ values than unliganded channels (Figure 1-6) (Magee et al., 2015; Wainger et al., 2001). However, because cAMP binding may not completely relieve autoinhibition, the difference in $V_{1/2}$ between cAMP-liganded and unliganded channels may not reflect the full magnitude of autoinhibition. Rather, the magnitude of autoinhibition can be calculated by comparing the $V_{1/2}$ of unliganded channels to the $V_{1/2}$ of channels with a CNB fold deletion (Wainger et al., 2001).

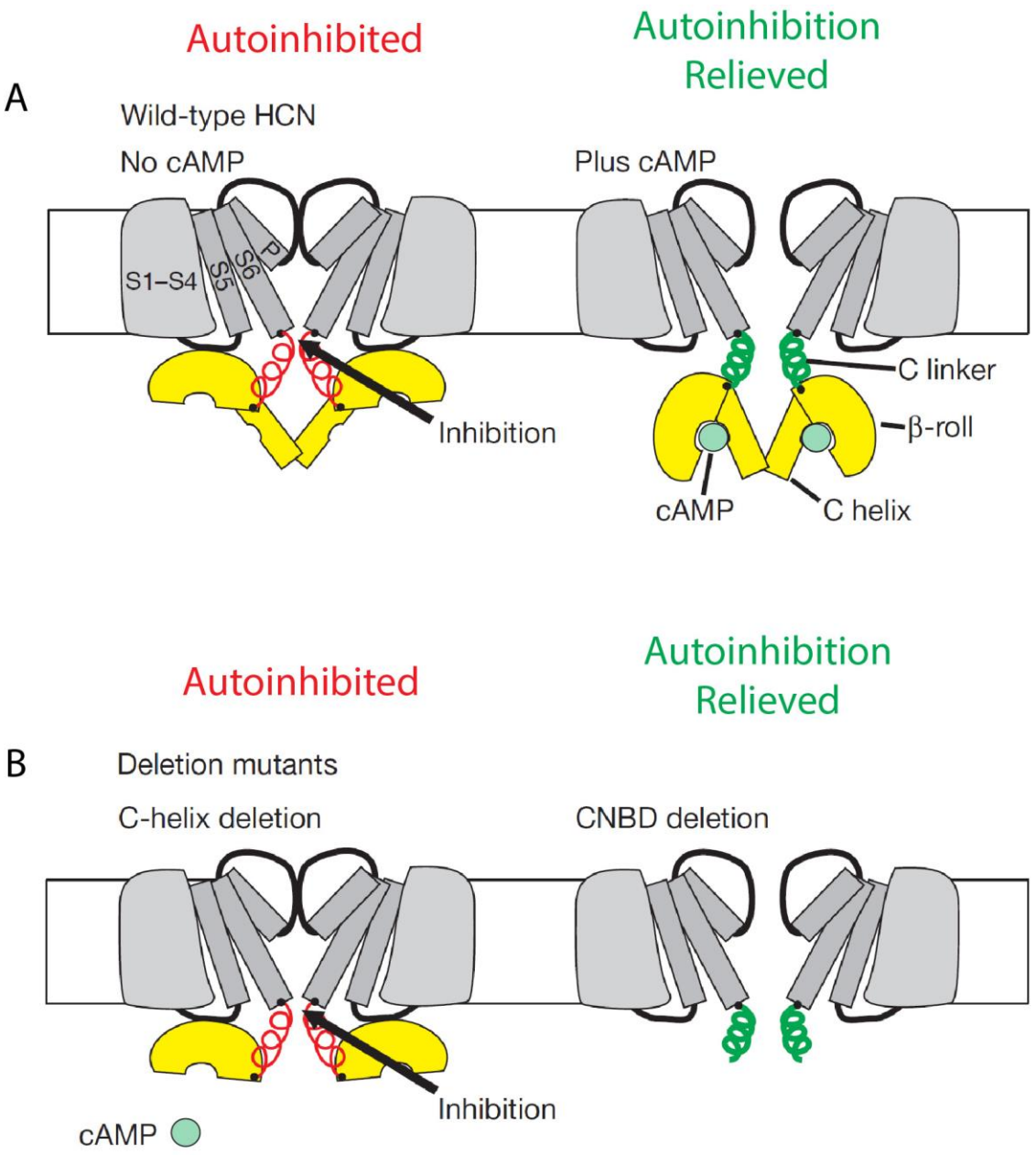

Figure 1-6: The unliganded CNB fold inhibits HCN channels

A, The autoinhibition mechanism in full length channels. *Left,* the unliganded CNB fold inhibits the open state of the channel. *Right,* the autoinhibition can be relieved by cAMP binding. **B,** The autoinhibition mechanism in deletion channels. *Left,* the C-helix deletion prevents cAMP binding, resulting in autoinhibition of the open state by the remaining CNB fold. *Right,* channels with the full CNB fold deleted are autoinhibition free. Adapted from (Wainger et al., 2001) with permission.

The autoinhibition model follows a simple conception of gating that we could call "parallel stabilization", where preferential thermodynamic stabilization of the closed state is accompanied by kinetic stabilization of the closed state (slower activation) and kinetic destabilization of the open state (faster deactivation) (Wainger et al., 2001). In other words, the autoinhibition model allows for prediction of channel kinetics based on the relative stability of the closed and open state in any given channel. The effects of cAMP potentiation on HCN channels also follow "parallel stabilization", with a positive shift in $V_{1/2}$, speeding of activation and slowing of deactivation. As expected, however, parallel stabilization of thermodynamics and kinetics does not always occur. Different mechanisms have been discovered that control HCN kinetics yet do not affect channel $V_{1/2}$, like the Quick-Activation mechanism for activation and the Open-State Trapping mechanism for deactivation (Magee et al., 2015; Wicks et al., 2009, 2011); these mechanisms will be discussed in detail later in this introduction. The implication is that when examining the functional effect of interdomain interactions on channel activity it is important to examine activation kinetics and deactivation kinetics in addition to thermodynamic stability and $V_{1/2}$ values.

1.6. Activation kinetics of HCN channels

HCN channels activate in response to hyperpolarized membrane potentials, and similar to thermodynamics, activation kinetics vary depending on the HCN subtype (Ludwig et al., 1998, 1999; Santoro et al., 1998; Stieber et al., 2003b; Xu et al., 2010). In parallel with differences in $V_{1/2}$ reflecting differences in thermodynamics, HCN4 activates slower than HCN2 channels (Stieber et al., 2003b). Quantifying HCN channel kinetics is typically done by determining time constants of channel activation. These activation time constants are calculated by fitting the activation transients to an exponential decay curve (Magee et al., 2015). There is also a portion of the activation transient known as the lag that cannot be fit to an exponential decay, (Magee et al., 2015).

In experiments using intact *Xenopus laevis* oocytes such as those in this thesis, a double exponential equation is often the best fit for activation transients (Magee et al., 2015; Wang et al., 2002). This observation has been explained as due to HCN channels slowly binding cAMP that is present at low endogenous levels in the intact oocyte, with the assumption of a cyclic allostery model for cAMP binding (Chen et al., 2007; Wang et

al., 2002). According to the cyclic allostery model, if cAMP binding stabilizes the open state then a consequence is that the closed state of HCN channels has a low affinity for cAMP while the open state has a high affinity for cAMP. This means that at low endogenous concentations of cAMP, the activation reaction pathway is the following portion of the cyclic allostery model without significant population of liganded closed channels:

$$C_{unliganded} \leftrightarrow O_{unliganded} \leftrightarrow O_{liganded}.$$

Initially, the closed HCN channels are predominantly unliganded ($C_{unliganded}$). Upon hyperpolarization, the pore opens ($O_{unliganded}$). This opening is allosterically coupled to conformational changes in the CNB fold, increasing the cAMP affinity. Consequently, cAMP binding becomes energetically more favourable and the open channels can slowly become liganded ($O_{liganded}$). This shifts the $C_{unliganded}$ –$O_{unliganded}$ equilibrium to the right, resulting in a slow increase in the number of open channels. Overall, this model predicts that in intact oocytes the first component of activation transients corresponds to unliganded channels opening, and then a slow second component appears, corresponding to the shift in equilibrium due to cAMP binding. This slow second component has been observed in HCN2 channels in intact oocytes (Magee et al., 2015; Wang et al., 2002) and would be expected for any HCN channel that has a large response to cAMP, like HCN4.

1.6.1. Mechanisms of regulating activation: Autoinhibition

Applying the concept of parallel stabilization to the autoinhibition model, it would be expected that the autoinhibition mechanism would not only negatively shift $V_{1/2}$ but would also affect activation kinetics to disfavor opening. In other words, channels with a CNB fold deletion would have strong kinetic destabilization of the closed state and would open faster than autoinhibited channels. Channels with a liganded CNB fold might have moderate kinetic destabilization of the closed state, since autoinhibition might be only partially relieved by cAMP binding. Experiments using inside-out patch clamp of HCN1 and HCN2 channels supported the autoinhibition mechanism affecting activation kinetics in parallel with thermodynamics: unliganded channels opened slower than CNB-fold deletion channels and liganded channels opened at intermediate speeds (i.e. faster than unliganded channels but slower than CNB-fold deletion channels) (Wainger et al., 2001).

1.6.2. Mechanisms of regulating activation: Quick-Activation

Quick-Activation is a mechanism that is dependent on the C-terminal region but distinct from autoinhibition. The Quick-Activation mechanism was discovered as a mechanism that controls the activation kinetics of HCN2 channels (Magee et al., 2015). Specifically, HCN2 with a CNB fold deletion exhibited slow activation compared to full length HCN2 (Figure 1-7). This is the opposite of what is expected from the autoinhibition model assuming parallel stabilization and indicated the presence of a distinct Quick-Activation that was missing in CNB fold deletion channels. At the same time, the $V_{1/2}$ of HCN2 with CNB fold deletion was more depolarized than full length, unliganded channels and not significantly different than full length, liganded channels; this is expected from the autoinhibition model (Figure 1-7). In addition, CNB fold deletion channels deactivated slower than full length, unliganded channels, also expected from the autoinhibition model. Thus, the Quick-Activation mechanism exemplifies how CNB fold-mediated gating mechanisms of HCN channels do not always follow the rule of parallel stabilization.

The speeding of activation in full length HCN2 due to Quick-Activation is dependent on the correct structure of the C-terminal region, evidenced by the fact that even when the HCN2 channel could not bind cAMP, the Quick-Activation mechanism was present as long as the channel had an intact CNB fold. (Magee et al., 2015) A channel with partial deletion of the CNB fold (deletion of the C-helix) did not support Quick-Activation and exhibited an intermediate activation speed that was slower than a channel with an intact CNB fold but faster than a channel with a complete CNB fold deletion (Figure 1-7) (Magee et al., 2015).

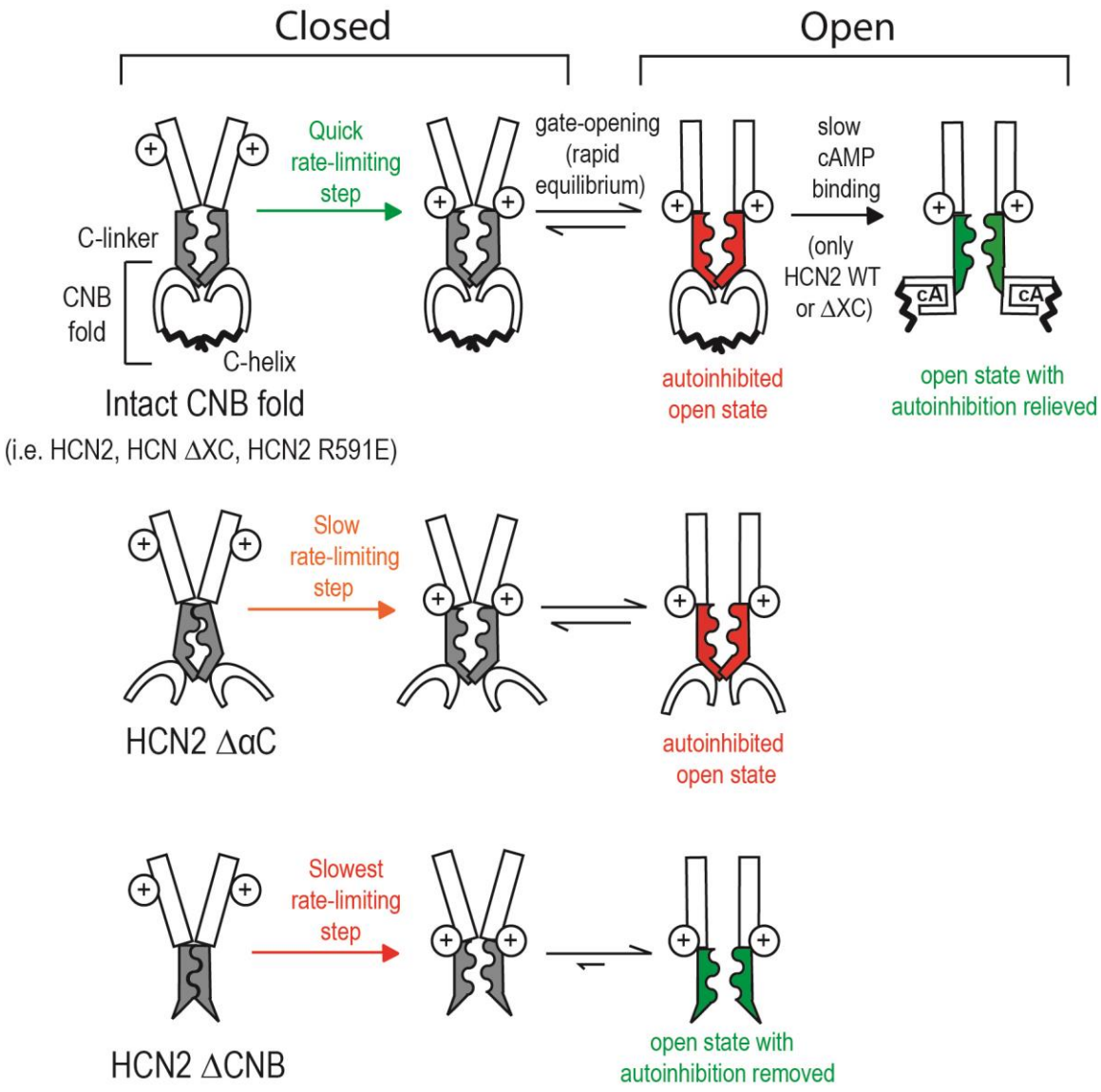

Figure 1-7: The Quick-Activation mechanism regulates HCN2 activation kinetics

Schematic explaining the effects of the Quick-Activation mechanism and the autoinhibition mechanism in HCN2 channels. The Quick-Activation conformation is supported by channels with an intact CNB fold (quick rate-limiting step, green arrow), consequently these channels will open quickly. However, if these channels are unliganded (e.g. HCN2 R591E) the open sate is destabilized by the autoinhibition mechanism (red C-linker), leading to a negative $V_{1/2,}$ a shift that is not parallel to the activation kinetics. If these channels can bind cAMP (HCN2 and HCN2 ΔXC), the autoinhibition can be relieved (green C-linker) leading to a positive shift in $V_{1/2}$ compared to the autoinhibited channel. Partial truncation of the CNB fold (HCN2 ΔαC) disrupts the Quick-Activation conformation (slow rate-limiting step, orange arrow) and prevents cAMP binding, leading to autoinhibition (red C-linker). Full truncation of the CNB fold (HCN2 ΔCNB) completely disrupts the Quick-Activation conformation (slowest rate-limiting step, red arrow) and completely relieves autoinhibition (green C-linker). Adapted from (Magee et al., 2015) with permission.

The Quick-Activation mechanism is not supported in an excised patch-clamp experimental configuration (Wainger et al., 2001) but is supported in intact oocytes (Magee et al., 2015). The excision of the membrane patch and subsequent perfusion of bath solution will wash out cellular factors which are present in intact oocytes. This suggested that a cellular factor was necessary for the Quick-Activation mechanism to act. PIP_2 is one known cellular factor that is gradually hydrolyzed in excised patch-clamp experiments, in a process commonly known as "rundown". However, when PIP_2 was depleted in intact oocytes using the drug wortmannin, the Quick-Activation mechanism was still supported (Magee et al., 2015). This suggests that there are multiple cellular factors that can affect HCN channel gating mechanisms dependent on the C-terminal region, which can be investigated using intact oocytes.

1.6.3. Comparison of Autoinhibition and Quick-Activation models

The autoinhibition and Quick-Activation models differ in expectations for channels with the CNB fold deleted and the C-helix deleted (Magee et al., 2015; Wainger et al., 2001). According to the autoinhibition model, CNB fold deletion will speed channel activation, while according to the Quick-Activation model, CNB fold deletion will slow channel activation. Additionally, according to the autoinhibition model, since a C-helix deletion results in autoinhibition, such channels will activate at the same speed as full length unliganded (i.e. autoinhibited) channels. In contrast, according to the Quick-Activation model, a C-helix deletion channel, while thermodynamically autoinhibited, will have the Quick-Activation mechanism disrupted and will therefore open slower than full length unliganded (i.e. autoinhibited) channels. Notably, the $V_{1/2}$ is not predicted to change after the Quick-Activation mechanism has been disrupted due to C-terminal deletion; however $V_{1/2}$ will change positively if an autoinhibition mechanism is disrupted by C-terminal deletion. Finally, the example of HCN2 shows that one channel can possess both the autoinhibition mechanism which regulates $V_{1/2}$ and the Quick-Activation mechanism which regulates activation kinetics.

These two models for the regulation of activation kinetics by the C-terminal region also differ in their dependence on cellular factors (Magee et al., 2015; Wainger et al., 2001). Autoinhibition was been found in excised patch configurations after rundown of PIP2 occured, and therefore does not require cellular factors to slow channel activation. In contrast, the Quick-Activation mechanism has only been identified in intact

oocyte configurations, implying that, as stated previously, cellular factors are required to facilitate speeding of activation. Therefore, when examining how interdomain interactions may affect these two mechanisms for C-terminal regulation of activation kinetics, it will be important to use intact oocytes, considering the importance of cellular factors for the Quick-Activation mechanism.

1.7. Deactivation kinetics of HCN channels

HCN channels deactivate in response to depolarized membrane potentials and while activation kinetics of HCN channels is a well-studied phenomenon, deactivation kinetics tend to be less examined. Similar to activation, it could be assumed in a simple conception that the four different subtypes of HCN channels might have distinctive deactivation kinetics that follow parallel stabilization in relation to $V_{1/2}$. Consistent with this, HCN2 channels deactivate faster than HCN4 channels (Xu et al., 2010).

The process of deactivation is known to be separate from activation as multiple studies have been able to affect one process without affecting the other. For example, deactivation kinetics for HCN4 are also slowed by the C-terminal region, in a process that is independent of the transmembrane region (Xu et al., 2010). Another well described example of this is the phenomenon of hysteresis between activation and deactivation voltage dependence, where HCN channels voltage dependence for activation is different from the voltage dependence for deactivation. More specifically, HCN channels require a stronger driving force for deactivation than for activation. This phenomenon was explained by the Mode Shift model (Elinder et al., 2006; Männikkö et al., 2005). According to Mode Shift, HCN channels have two open states with different thermodynamic stabilities: Mode I and Mode II. The closed channel initially opens in Mode I but given sufficient time (i.e. generally longer than 1 second) the channels transition from the Mode I state into the Mode II state, which is the more stable open state (Elinder et al., 2006; Männikkö et al., 2005). Consequently, a stronger driving force is required to transition to the closed state from the Mode II open state than the Mode I open state. The simple 4-state reaction diagram for mode shift proposed by the Larsson lab is shown in Figure 1-8 (Elinder et al., 2006; Männikkö et al., 2005). In general, the concept of Mode Shift suggests that the mechanisms that control deactivation are separate from activation, and therefore, might involve a separate set of structural features like interdomain interactions.

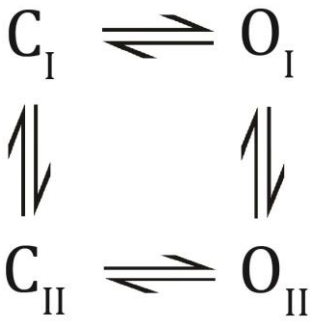

Figure 1-8: Reaction mechanism for mode shift

A simple four state reaction mechanism to explain HCN channel mode shift, where the C to O transitions represent the pore opening or closing. The mode shift model states that O_{II} is more stable than O_I, whereas C_{II} is less stable than C_I. The activation pathway proceeds from C_I to O_I and then to O_{II}, whereas the deactivation pathway proceeds from O_{II} to C_{II} and then to C_I.

1.7.1. Mechanisms of regulating deactivation: Autoinhibition

As stated above, full length unliganded HCN2 channels deactivate faster than HCN2 with a CNB fold deletion, as expected from an autoinhibition model with parallel stabilization; this is observed both in excised patch-clamp and intact oocyte experiments. (Magee et al., 2015; Wainger et al., 2001). According to an autoinhibition model, channels with a cAMP-liganded CNB fold might have intermediate kinetic stabilization of the open state, since autoinhibition might be only partially relieved by cAMP binding, and thus liganded channels should not deactivate slower than a CNB fold deletion channel. In agreement with this model, studies of HCN channel response to cAMP in the SA node found that deactivation slowed after cAMP was bound to the CNB fold, and cAMP had a greater effect on deactivation kinetics than on activation kinetics. (DiFrancesco and Tortora, 1991). This suggests that autoinhibition has a strong influence on deactivation kinetics.

1.7.2. Mechanisms of regulating deactivation: Open-State Trapping

Open-State Trapping (OST) is a mechanism dependent on the C-terminal region but distinct from autoinhibition, like Quick-Activation, but OST specifically regulates deactivation kinetics. (Wicks et al., 2009, 2011). OST kinetically stabilizes the open state in a channel with an intact CNB fold, resulting in slower deactivation than in a channel with CNB fold deletion (Figure 1-9). This is the opposite of what is expected from the autoinhibition model assuming parallel stabilization. The kinetic stabilization of

the open state in the OST mechanism is weaker in channels with an unliganded CNB fold compared to a channel with CNB fold deletion (Figure 1-9). The OST mechanism was first found in a chimeric channel consisting of the N- and C-terminal regions of HCN2 with the TM region of HCN4 containing a K381E mutation of a residue in S4 (Wicks et al., 2009, 2011). Deletion of the CNB fold speeded deactivation kinetics, and moreover substitution of the C-terminal region from HCN1 speeded deactivation kinetics but decreased the magnitude of autoinhibition (measured by $V_{1/2}$). In another study, OST was shown to operate in HCN2: liganded HCN2 channels were found to close slower than HCN2 channels with a CNB fold deletion (Magee et al., 2015). The OST mechanisms applies to deactivation kinetics with significant voltage-dependence at intermediate voltages (e.g. -40 mV) where S4 movement is predicted to be the rate limiting step of deactivation. This implies the involvement of the S4 voltage sensor in the OST mechanism and suggests an interaction between the TM region and C-terminal region.

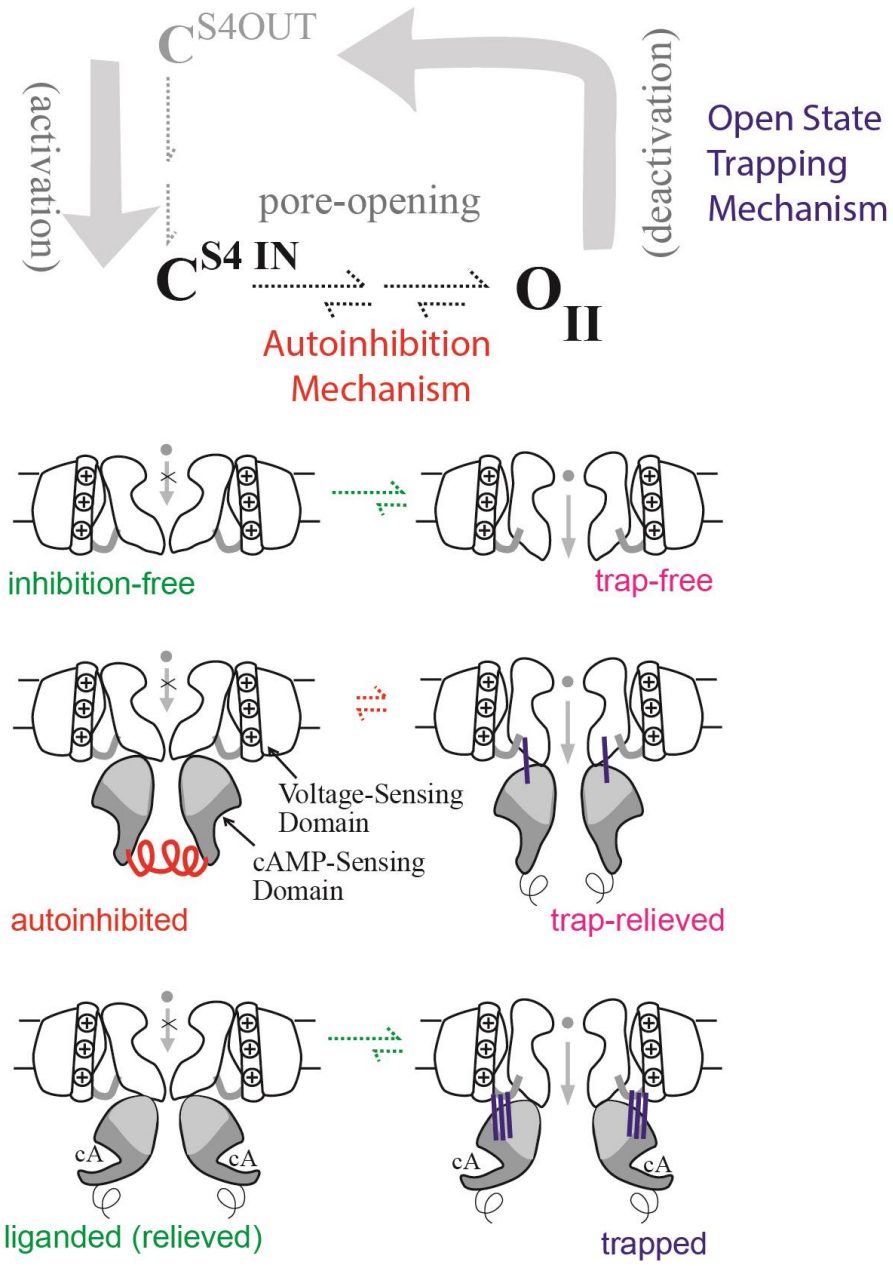

Figure 1-9: Open-State Trapping mechanism regulates deactivation kinetics while the Autoinhibition mechanism regulates the relative stability of the open and closed states

Schematic explaining the effects of the Autoinhibition mechanism and the Open-State Trapping mechanism. The autoinhibition mechanism controls the relative stability of the open and closed states ($C^{S4\text{-}IN}$ to O_{II} transition), while the OST mechanism controls the rate of deactivation. Inhibition free and liganded channels have a more stable open state (green) than the autoinhibited channel (red). Once the channel has opened the OST mechanism may be present. The CNB fold deletion completely relieves autoinhibition and prevents the channel from being trapped in the open state (pink). The unliganded channel was autoinhibited, but once open has been partially relieved of "trap." The liganded channel, while relieved of autoinhibition has the full-strength Open-State Trapping mechanism present (blue), consequently slowing deactivation. Adapted from (Wicks et al., 2011) with permission.

1.7.3. Comparison of Autoinhibition and Open-State Trapping models

Consistent with the known slowing of HCN channel deactivation during cAMP potentiation, according to both the autoinhibition and OST models a liganded channel will deactivate slower than the unliganded channel (Magee et al., 2015; Wainger et al., 2001; Wicks et al., 2009, 2011). However, these two models differ with regards to a CNB fold deletion (ΔCNB). According to the autoinhibition model, the autoinhibition-free ΔCNB channel will deactivate faster (or at least no slower) than the channel with an intact CNB (liganded or unliganded). In contrast, according to the OST model the OST-free ΔCNB channel will deactivate slower than (or at least no faster than) the channel with an intact CNB (liganded or unliganded). According to the autoinhibition model, cAMP slows deactivation by relieving autoinhibition, whereas according to the OST model, cAMP slows deactivation by strengthening Open-State Trapping. Notably, the example of HCN2 (Magee et al., 2015) illustrates that autoinhibition and OST can be operating simultaneously in one channel: the unliganded channel deactivates faster than the ΔCNB channel (autoinhibition) but the liganded channel deactivates slower than the ΔCNB channel (OST). Here, cAMP slows deactivation by both relieving autoinhibition and strengthening OST.

As another hypothetical example, it is possible that in a new HCN channel both OST and autoinhibition are operating, such that the unliganded channel deactivates at a similar speed to the ΔCNB channel. This could be explained by a model for unliganded channels where (relative to a ΔCNB channel) an autoinhibition mechanism is acting to speed deactivation, but an OST mechanism is simultaneously acting to slow deactivation; this would result in an intermediate deactivation speed that is similar in magnitude to that of ΔCNB channels.

If OST affected thermodynamics in parallel to the kinetic stabilization of the open state, it would be expected that cAMP-liganded channels with OST would have a positively shifted $V_{1/2}$ compared to OST-free ΔCNB channels. However, in the channels examined having OST (HCN2 and the HCN2-HCN4 chimera), the changes in $V_{1/2}$ due to CNB fold deletion could be fully explained by the autoinhibition model. Thus, OST slows the rate limiting step of deactivation but does not affect channel thermodynamics in a parallel manner. Based on the existence of OST and Quick-Activation mechanisms in addition to autoinhibition, an interdomain interaction that modulates channel function

may not fit the notion of parallel stabilization, but may affect only one or two of the three different aspects of gating: kinetic stability of the open state, kinetic stability of the closed state, or overall thermodynamic stability of the open vs. closed state

1.8. Objectives and hypotheses of my work

I hypothesized that interdomain interactions between the C-terminal region and the TM region facilitated CNB fold-mediated regulatory mechanisms. Therefore, the main objective of this work has been to find functional evidence for interdomain interactions between general regions and specific residues in HCN channels. This will allow for better understanding of the role of interdomain interactions in regulating HCN channel activity. To accomplish this objective, I analyzed different channel backgrounds, using truncation or mutation to disrupt interdomain interactions. This involved electrophysiology measures of thermodynamics and kinetics with and without key modulators in intact cells. Figure 1-10 (using the hHCN1 structure published by Lee and MacKinnon, 2017 as an example) and table summarize the different types of C-terminal channel truncations and mutations used in both Chapters 2 and 3, and their general effect on cAMP potentiation and other mechanisms mediated by the C-terminal region. The mouse HCN2 channel (Magee et al., 2015) is used as an example, although other HCN channel derivatives are also explored in this thesis.

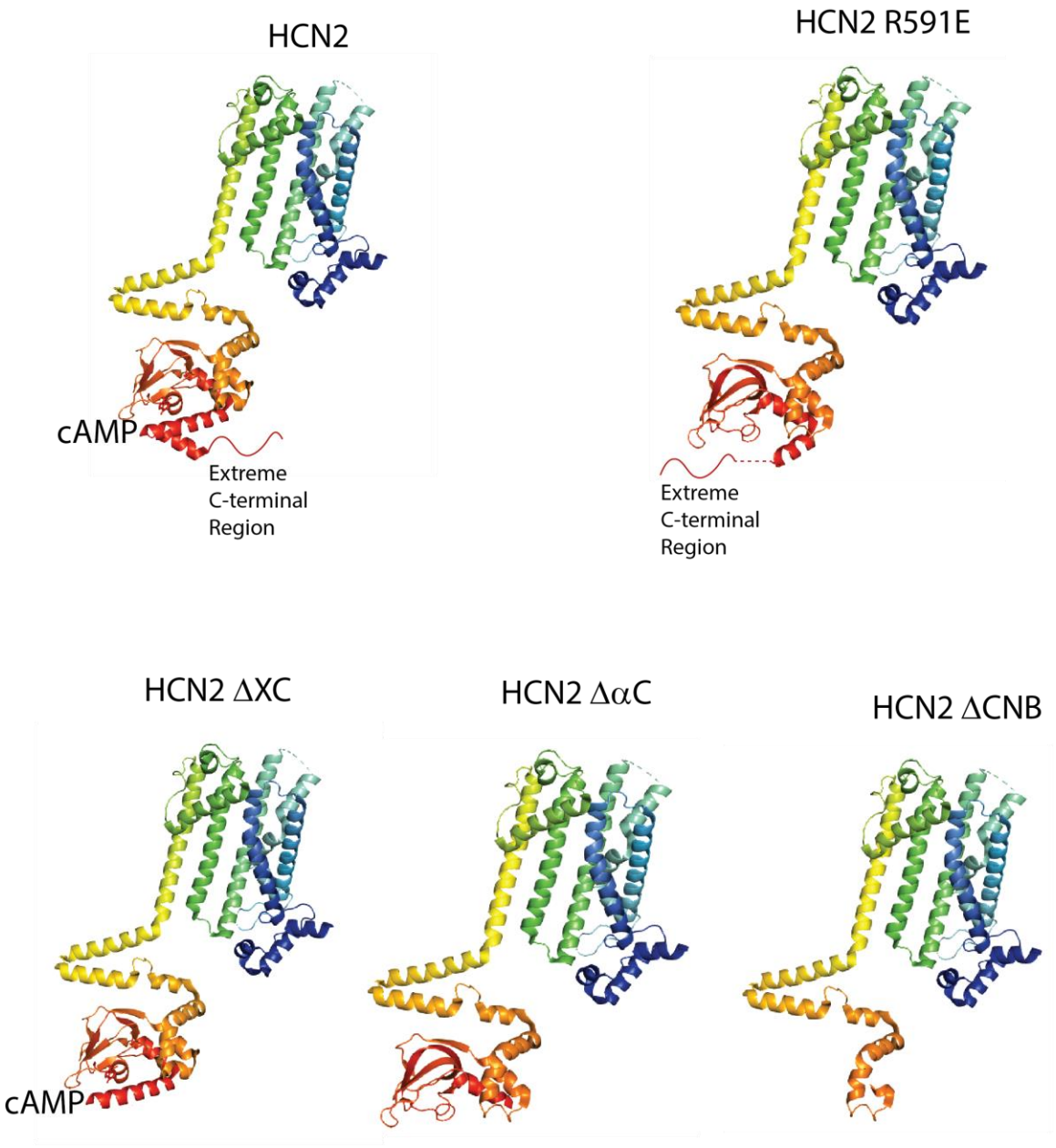

Figure1-10: Pictorial summary of C-terminal variants characterized prior to this work

Top panels, Full length constructs indicated by the addition of an Extreme C-terminal region (wavy line) to the cryoEM structure of hHCN1. Unliganded hHCN1 structure used in place of the unliganded R591E mutation. **Top left,** full length HCN2 with a CNB-fold that can bind cAMP (liganded). **Top right,** full length HCN2 R591E which cannot bind cAMP (unliganded). C-terminal portion of the C-helix is disordered (dashed line) along with the extreme C-terminal region (wavy line). **Bottom panels,** Various C-terminal truncations of the cryoEM structure. **Bottom left,** HCN2 channel with the extreme C-terminal region truncated. The CNB fold of this channel can still bind cAMP (liganded). **Bottom center,** HCN2 channel with truncation of the C-helix. The CNB fold of this channel cannot bind cAMP (unliganded). **Bottom right,** HCN2 channel with the entire CNB fold truncated. This channel cannot bind cAMP (unliganded).

Table 1-1: Summary of C-terminal variants characterized prior to this work

	Truncation of?	cAMP binding status	Auto-inhibition status	Quick-Activation status	Open-State Trapping status
HCN2	n/a	Can bind cAMP	Autoinhibition relieved	Quick-Activation	Open State Trapped
HCN2 R591E	n/a	Cannot bind cAMP	Autoinhibited	Quick-Activation	Not apparent
HCN2 ΔXC	Extreme C-terminal region	Binds cAMP at a lower affinity than HCN2	Partial autoinhibition relief	Quick-Activation	Open State Trapped
HCN2 ΔαC	C-helix	Cannot bind cAMP	Autoinhibited	Disrupted Quick-Activation	Disruption of Open-State Trapping
HCN2 ΔCNB	CNB fold	Cannot bind cAMP	Autoinhibition free	Quick-Activation free	Open-State Trapping free

Truncations include all structures C-terminal to the region indicated. For example, a channel with a C-helix truncation has the C-helix truncated as well as the Extreme C-terminal region.

In general, I aimed to answer these questions:

Do interdomain interactions exist that are subtype-specific?

Which C-terminal functions (OST, QA, autoinhibition, and cAMP-relief of autoinhibition) are supported by interdomain interactions?

Chapter 2: Subtype specific interdomain interactions control C-terminal functions: autoinhibition, Open-State Trapping, and Quick-Activation

In chapter 2 I determined that autoinhibition produced by the C-terminal region was limited by an interaction between the HCN2 TM region and the C-terminal region. By replacing the HCN2 TM region with the HCN4 TM region, the limitation was removed and autoinhibition became augmented. This augmentation was disrupted after truncation after the beta-roll of the CNB fold. Augmentation of autoinhibition led to hyperpolarizing shifts in the $V_{1/2}$ compared to HCN2. Moreover, the autoinhibition mechanism became the dominant kinetic mechanism for both activation and deactivation. In other words, the HCN4 TM-replacement also disrupted interdomain

interactions that supported other kinetic mechanisms present in HCN2 channels (Quick-Activation and Open-State Trapping).

Chapter 3: Characterization of an interdomain interaction in HCN channels: E457 interacts with the transmembrane region to stabilize the open state and regulate the autoinhibition mechanism

In Chapter 3, I used site-directed mutagenesis to identify functional evidence for an interdomain interaction between the E457 residue in the A' helix and a TM region residue. This interdomain interaction stabilizes the open state in autoinhibition-relieved channels. This was true of both channels that had autoinhibition relieved by cAMP binding or by deletion of the CNB fold. In one form of an autoinhibited channel (with C-helix deletion), E457 also stabilizes the open state. A charge reversal mutation here (E457R) limited the thermodynamic effect of autoinhibition while augmenting the kinetic effect of autoinhibition. However, in another form of an autoinhibited channel (full-length with the R591E mutation), I found some evidence for a new conformation of E457 that acts to destabilize the open state, such that an E457R mutation stabilizes the open state with attenuation of autoinhibition. The conformation of the E457 residue appears to be dependent on cellular factors, the activity of which is disrupted by either membrane patch excision or C-helix deletion. Finally, I made a mutation series in autoinhibition relieved channels that suggested that the E457 interdomain interaction is a salt-bridge. Combined, these results suggest a model where a salt bridge between E457 and an unidentified TM region residue which stabilizes the open state in full length, possibly facilitating the autoinhibition relief seen in full length liganded channels. However, under certain conditions in full-length autoinhibited channels, E457 rotates away from this partner residue so that the open state is no longer stabilized. This conformational change could result in E457 repelling a second residue, thus facilitating the additional destabilization of the open state that occurs in full-length, autoinhibited channels.

Chapter 2.

HCN channel autoinhibition is regulated by the transmembrane region

The research presented in Chapter 2 has been compiled into an unpublished manuscript, with the intent of submitting the work for publication in the near future. The HCN2 data acquisition was performed by Dr. Kaylee Magee (published in Magee et al., 2015). New construct construction (i.e. Ch4-2 channels) and data acquisition was completed by either myself or undergraduate students (Jessica Li and Matt Jung) whom I trained and supervised. I completed the majority of the data analysis, made the initial figures, and wrote the first draft of the manuscript and participated in extensive editing. Comments on the manuscript were provided by Dr. Kaylee Magee and Dr. Tom Claydon. I also presented a poster based on parts of this work at the Biophysical Society Meeting (2018).

Page, D.A., Magee, K.E., Li, J., Jung, M., Young, E.C. Role of Interactions between transmembrane and C-terminal regions in voltage-dependent activation of HCN4 channels. Poster presented at Biophysical Society's Annual Meeting, February 2018.

2.1. Introduction

Hyperpolarization-activated cation (HCN) channels produce the I_h or I_f "pacemaker" currents that regulate rhythmic firing in excitable tissues including the brain and heart (Wahl-Schott and Biel, 2009). HCN channels are activated by membrane hyperpolarization, leading to an inward mixed Na^+ / K^+ current which promotes action potential initiation (Wahl-Schott and Biel, 2009). Of the four mammalian HCN channel subtypes, the HCN2 and HCN4 subtypes exhibit the largest degree of potentiation by direct binding of cytosolic cAMP, with consequent shifting of the conductance – voltage relation to more positive voltages, speeding of activation kinetics, and slowing of deactivation kinetics (DiFrancesco and Tortora, 1991; Ludwig et al., 1998, 1999; Santoro et al., 1998). This cAMP-dependent activity is proposed to help regulate thalamocortical oscillations associated with sleep states and epileptic seizures (Bal and Mccormick, 1996) as well as heartbeat pacing in the sinoatrial node (DiFrancesco, 1986). The transmembrane (TM) region of HCN channels is homologous to the tetrameric Kv channel superfamily with six transmembrane helices (S1-S6), including a positively charged S4 voltage sensor and a pore domain containing the permeation pathway (S5 through S6) (Wahl-Schott and Biel, 2009). Cyclic AMP potentiation is mediated by a large cytoplasmic C-terminal region which includes a C-linker consisting of multiple helices, a cyclic nucleotide-binding (CNB) fold, and an extreme C-terminal region (Zagotta et al., 2003). But there remains incomplete understanding of the molecular events by which the C-terminal region would modify the energetics and kinetics of voltage-gating mediated by the TM region.

The functional features of HCN channel modification by the C-terminal region are complex, indicating involvement of more than one mechanism. While all of these regulatory mechanisms depend on the presence of the CNB fold and affect channel function, the specific structural mechanism for how they occur (e.g. inhibiting voltage sensor movement or inhibiting coupling of VSD and pore) are not understood. The best-known mechanism is autoinhibition, where the presence of the unliganded CNB fold inhibits channel activity (relative to a truncated channel lacking the CNB fold, called ΔCNB), and cAMP binding relieves this autoinhibition (Wainger et al., 2001). We determine whether a channel is autoinhibited by whether it has an autoinhibitory shift in $V_{1/2}$ compared to the ΔCNB channel. However, the kinetics of HCN channel activation

and deactivation can be additionally regulated by the C-terminal region in mechanisms distinct from autoinhibition. For instance, cAMP-liganded HCN2 channels exhibit an open-state trapping mechanism, with deactivation that is slower than in the autoinhibition-free ΔCNB channel (Magee et al., 2015; Wicks et al., 2009, 2011). And even when unliganded and hence autoinhibited, HCN2 channels exhibit a Quick-Activation mechanism, with activation that is faster than in the autoinhibition-free ΔCNB channel (Magee et al., 2015). Moreover, HCN channels exhibit hysteresis such that the deactivation pathway is not the reverse of the activation pathway (Kusch et al., 2010; Männikkö et al., 2005; Wicks et al., 2009). Therefore, a full understanding of HCN channel gating requires elucidation of multiple, co-existing mechanisms that all depend on the CNB fold, and yet have different structural determinants and target different reaction steps.

Conformational changes have been shown in the CNB fold and C-linker due to cAMP binding (Akimoto et al., 2014; Goldschen-Ohm et al., 2016; Taraska et al., 2009; VanSchouwen et al., 2015; Zagotta et al., 2003; Zhou et al., 2004), and these are presumably coupled to conformational changes in the TM region by an as yet unknown mechanism. Physical contacts between the C-linker and the TM region are apparent in a cryoEM structure of the hHCN1 channel in the closed state (Lee and MacKinnon, 2017). This observation validated previous mutagenesis and cross-linking studies that identified residues in the C-linker and the TM region as proximal to each other (Decher et al., 2004; Kwan et al., 2012; Prole and Yellen, 2006). Those previous studies established that these interdomain interactions influenced the relative stability of the open vs. closed state. However, these studies did not clarify how significant these interactions would be for the multiple regulatory mechanisms of the C-terminal region. This is especially true for the magnitude of autoinhibition which can only be measured by comparing an autoinhibited channel to the autoinhibition-free ΔCNB channel, and for the deactivation kinetics which have been less commonly studied in HCN channels.

In this study we report evidence for functional interaction between the TM region and the C-terminal region, by demonstrating that the multiple regulatory mechanisms mediated by the C-terminal region additionally depend on the subtype sequence of the TM region. We replaced the HCN2 TM region with that of HCN4 and found that the magnitude of autoinhibition imposed by the unliganded CNB fold was significantly augmented. Additionally, the open-state trapping and Quick-Activation mechanisms

characteristic of HCN2 were disrupted, such that the augmented autoinhibition became the dominant mechanism contributed by the C-terminal region to determine kinetics for both activation and deactivation. This establishes that interaction with the TM region supports the complex control of both thermodynamics and kinetics by the C-terminal region.

2.2. Methods

2.2.1. Construct composition

All chimera constructs (Ch4-2 series) include residues M1-G130 from mouse HCN2 fused to the transmembrane region M214-D521 of mouse HCN4 (Santoro and Tibbs, 1999). This invariant sequence was then fused to various portions of the C-terminal region derived from mouse HCN2 (Magee et al., 2015): for Ch4-2, S444-L863; for Ch4-2 ΔαC, S444-E617; for Ch4-2 ΔCNB, S444-F525. The Ch4-2 R591E C-terminal region is identical to the Ch4-2 channel with the exception of the R591E mutation. All constructs were subcloned into the pGEM-HE vector for high expression in *Xenopus laevis* oocytes as previously reported for the corresponding HCN2 channel derivatives (Magee et al., 2015).

2.2.2. Electrophysiology

As previously described (Magee et al., 2015), all channels were expressed as homomers from in vitro transcribed RNA injected into *X. laevis* oocytes, obtained using established procedures through ovariectomies following guidelines from the Canadian Council on Animal Care. Two-electrode voltage clamp (TEVC) recordings for each construct or condition were obtained from oocytes of at least three frogs. Each frog contributed no more than two data points per ovariectomy to overall average calculations for each Ch4-2 construct. As previously described (Magee et al., 2015), the bath solution (ND-96) consisted of (in mM): 96 NaCl, 3 KCl, 5 HEPES (pH 7.4), 1 $MgCl_2$, and 0.75 $CaCl_2$.

Oocytes were excluded if they exhibited inward leak (time-independent) current larger than 100 nA at the holding voltage of -40 mV; leak stability was verified with a “staircase” of steps to +40, 0 and -40 mV applied after each test sweep. The activation

protocol stepped from the holding voltage to voltages between +20 mV and -170 mV (Δ10 mV) for a 3-s activation epoch, followed by a tail epoch at -120 mV and a 4-s deactivation epoch at +20 mV. As described previously (Magee et al., 2015), late in the activation epoch at extreme hyperpolarizing voltages, some oocytes exhibited currents not typical of HCN channels; this atypical behaviour included a decrease in inward current or a second inflection point leading to concave-negative curvature. Individual sweeps at -150 mV or more negative were excluded from analysis if they had atypical behaviour. Oocytes were excluded from analysis entirely if atypical behaviour was exhibited at -140 mV or less negative.

The deactivation protocol stepped from the holding voltage to -130 mV for a 4-s activation epoch, followed by a step to voltages between 0 mV and +40 mV (Δ20 mV) for a 4-s deactivation epoch. The deactivation epoch was followed by a tail epoch at -120 mV and a second deactivation epoch at 0 mV for 5 s. This second deactivation epoch was performed to ensure all channels are in the closed state before returning to the holding voltage. Channel behaviour was typically stable over at least 10 minutes, as verified with a control protocol which was identical to the deactivation protocol except it had a single sweep with 0 mV in the deactivation epoch. Oocytes were excluded from analysis if absolute tail currents differed by more than 100 nA in control protocols before and after a deactivation protocol.

2.2.3. Data analysis

Isochronal $V_{1/2}$ measurements were completed using the 3-s activation protocol as described previously (Magee et al., 2015). The four-parameter Boltzmann equation was used:

$$I = y_0 + \frac{a}{(1 + e^{-(V - V_{1/2})/s})}.$$

Deactivation transients reached endpoint consistently in the 4-s deactivation epoch, and the midpoint time of deactivation ($t_{1/2}$) was determined as previously described (Magee et al., 2015).

Activation time constants were calculated from a single or double exponential fit equation using an iterative fit procedure as previously described (Magee et al., 2015; Wicks et al., 2009). The double exponential fit equation was:

$$I(t) = A_{early}e^{-t/\tau_{early}} + A_{late}e^{-t/\tau_{late}} + C.$$

The fractional contribution of the early component to the curve (f_{early}) was calculated using:

$$f_{early} = A_{early}/(A_{early} + A_{late}).$$

The weighted-average time constant (τ_w) was calculated using:

$$\tau_w = (\tau_{early} * f_{early}) + (\tau_{late} * (1 - f_{early})).$$

Mean values are reported ± SD where *n* is the number of oocytes recorded. Comparisons of mean values were assessed by two-sided t-tests with a significance threshold of $p = 0.05$. Magnitude of autoinhibition ($\Delta V_{1/2}$) values are calculated from mean $V_{1/2}$ values, ± errors propagated from the SEM.

2.3. Results

2.3.1. HCN4 TM-replacement inhibits activation of HCN2 channels

We sought to investigate whether interactions between the HCN2 TM region and the C-terminal region have a role in different CNB fold mediated functional mechanisms (i.e. Autoinhibition, cAMP relief of Autoinhibition, Open State Trapping, and Quick-Activation). To prepare for this investigation we constructed a chimeric channel called Ch4-2 by replacing the TM region of mouse HCN2 with the TM region of mouse HCN4 — a substitution which we term an "HCN4 TM-replacement" — and found that Ch4-2 had less efficient gating than HCN2. Channels were expressed in *X. laevis* oocytes for two-electrode voltage clamp experiments (Figure 2-1*A, B*) (Dascal, 1987; Magee et al., 2015). The $V_{1/2}$ of Ch4-2 (-93.2 ± 3.2 mV, *n* = 8) was significantly more negative ($p < 10^{-4}$) than the $V_{1/2}$ of HCN2 (-83.4 ± 5.0 mV, *n* = 49) (Figure 2-1*C*). This 10-mV shift resulting from HCN4 TM-replacement is a sizable effect, on the scale of $V_{1/2}$ shifts from regulators like cAMP or PIP_2 (Magee et al., 2015). Qualitatively, the HCN4 TM replacement also slowed channel gating (Figure 2-1*B*) which will be quantitatively

addressed in later sections. We concluded that the HCN4 TM-replacement decreased channel activity, which could be accomplished by one or more of the following: (1) by disrupting cAMP potentiation, (2) by augmenting the autoinhibitory $V_{1/2}$ shift, or (3) through an intrinsic property of the TM region alone without involvement of the C-terminal region.

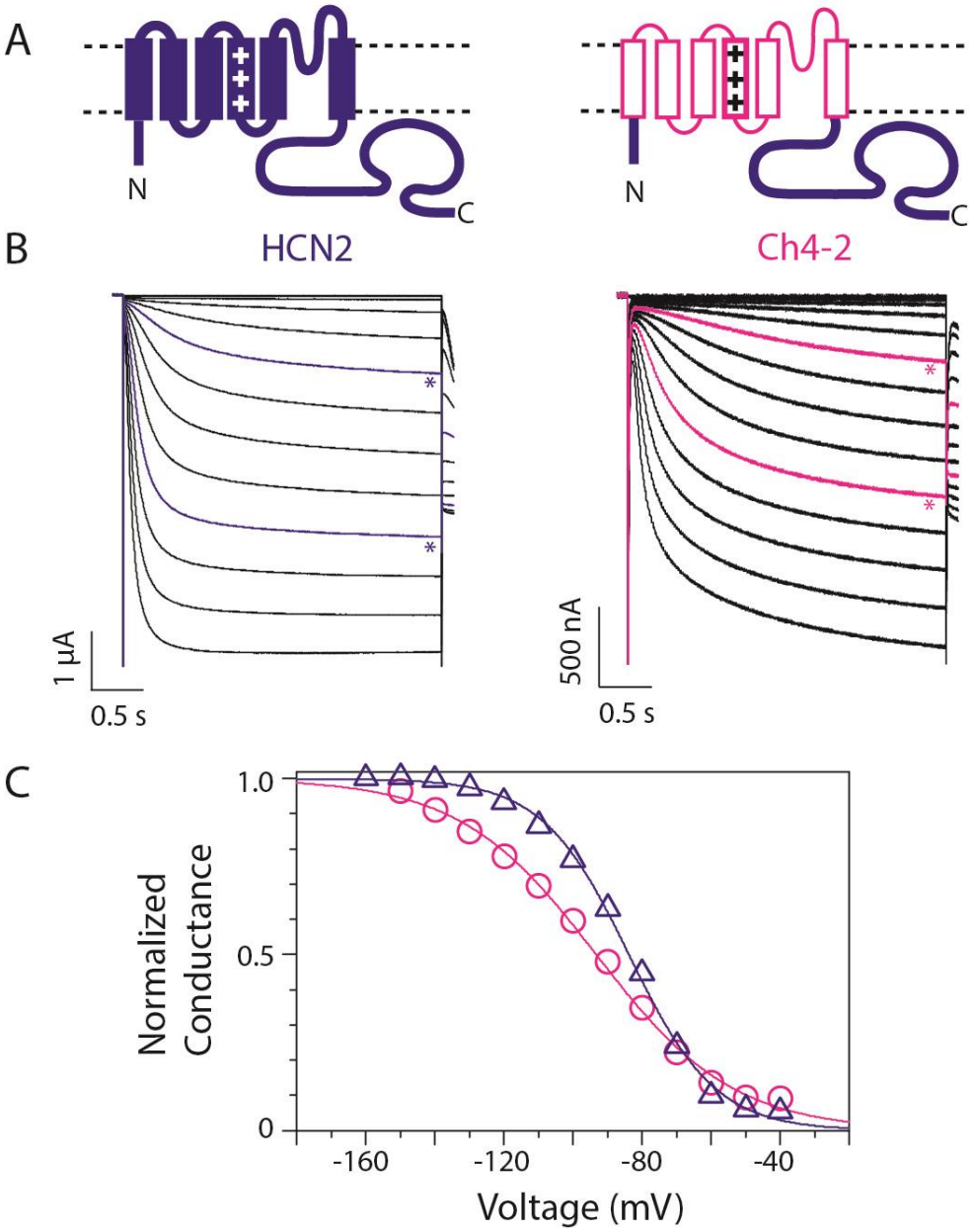

Figure 2-1: HCN4 TM-replacement inhibits activation of cAMP-liganded HCN2

A, Schematics of HCN2 channel and the Ch4-2 channel produced by HCN4 TM-replacement in HCN2. *Rectangles* represent transmembrane helices S1 through S6. HCN2 sequence is shown in *thick curves* and *solid rectangles*; HCN4 sequence is shown in *thin curves* and *open rectangles*. **B,** Representative inward currents of HCN2 and Ch4-2. Channel currents were elicited by step hyperpolarisations to various voltages followed by a tail epoch at -120 mV for $V_{1/2}$ determination. In each dataset, *stars* indicate traces for -90 mV and -130 mV. **C**, Conductance-voltage relationships for HCN2 (*triangles*) and Ch4-2 (*circles*) using tail current data from panel *B* after leak-subtraction and normalization to maximal amplitude determined from Boltzmann equation fit (*curves*, see "Methods"). These channels are bound to endogenous cAMP. Boltzmann fit parameters of the representative curves are as follows: HCN2 (blue), −83.8 mV, s = 12.5 mV; Ch4-2 (pink), −93.3 mV, s = 19.8 mV;

2.3.2. HCN4 TM-replacement does not disrupt cAMP potentiation

The recent hHCN1 cryo-EM structure shows the C-terminal region, which mediates cAMP potentiation, is in contact with S4 in the TM region (Lee and MacKinnon, 2017). Based on this structural interaction, we considered the hypothesis that a functional interaction between the HCN4 TM region and C-terminal region inhibits cAMP potentiation, resulting in decreased channel activity. To test this, we determined the magnitude of $V_{1/2}$ shift due to cAMP potentiation – comparing the $V_{1/2}$ of the unliganded vs. cAMP-liganded channel – in HCN2 and Ch4-2. The $V_{1/2}$ of the unliganded state cannot be assessed with these channels alone in intact oocytes, since the oocytes contain sufficient endogenous cAMP to bind channels during activation (Magee et al., 2015; Wang et al., 2001). To generate an unliganded CNB fold for use in intact oocytes, we used the previously characterized R591E mutation which is a charge reversal mutation of the critical arginine that contacts the cyclic phosphate group of cAMP (Chen et al., 2001b; Magee et al., 2015). The $V_{1/2}$ of HCN2 R591E was previously found to be -99.4 ± 3.1 mV (*n* = 10) in intact oocytes, so the magnitude of $V_{1/2}$ shift due to cAMP potentiation in HCN2 channels was a 15.9 ± 1.2 mV positive shift (Magee et al., 2015). We performed an HCN4 TM-replacement on the HCN2 R591E channel, equivalent to introducing R591E mutation into Ch4-2. The $V_{1/2}$ of Ch4-2 R591E was -107.9 ± 5.0 mV (n = 16), so cAMP potentiation resulted in a 14.7 ± 1.7 mV positive $V_{1/2}$ shift, matching that of the corresponding HCN2 channels within the uncertainty (Fig. 2-2*A, B*) (Magee et al., 2015). Therefore, we found no evidence from our examination of $V_{1/2}$ to suggest that the HCN4 TM-replacement disrupts cAMP potentiation.

The measurements above also showed that the HCN4 TM-replacement shifted $V_{1/2}$ in the unliganded HCN2 R591E channel by the same amount as in the cAMP-liganded HCN2 channel. That is, the HCN4 TM-replacement negatively shifted the $V_{1/2}$ by approximately 10 mV in both HCN2 and HCN2 R591E sequence backgrounds. HCN4 TM-replacement in HCN2 R591E (unliganded) also qualitatively slowed channel gating, similar to the results seen after HCN4 TM-replacement in HCN2 (liganded).

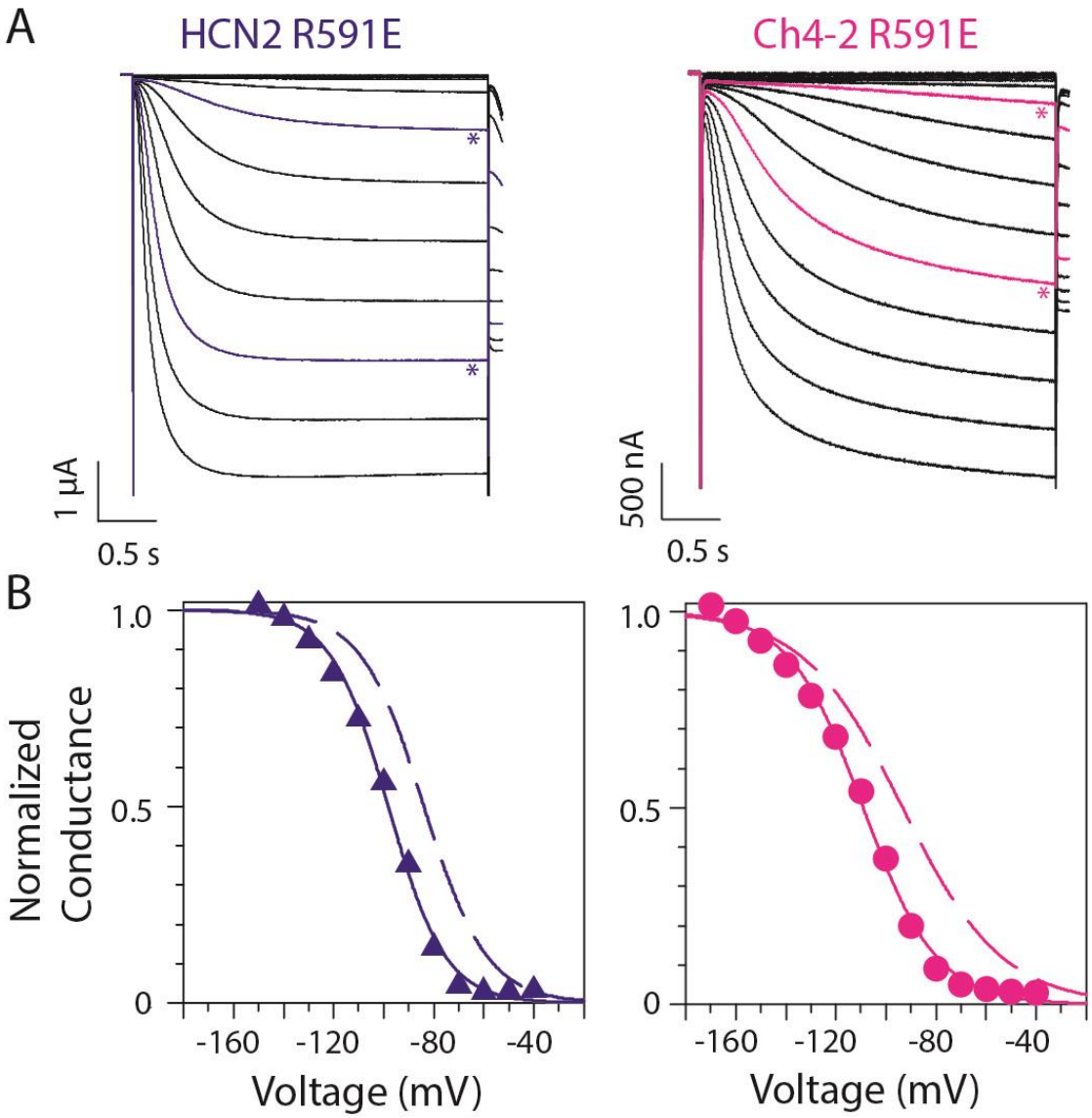

Figure 2-2: HCN4 TM-replacement inhibits activation of unliganded HCN2

A, Representative inward currents of HCN2 R591E and Ch4-2 R591E mutants lacking cAMP binding. Channel currents were elicited by step hyperpolarizations to various voltages followed by a tail epoch at -120 mV for $V_{1/2}$ determination. In each dataset, *stars* indicate traces for -90 mV and -130 mV. **B***,* Conductance-voltage relationships for unliganded channels HCN2 R591E (filled triangles) and Ch4-2 R591E (filled circles), using data from panel *D*. In each graph, the data for an unliganded R591E channel (*points and solid curve*) is compared with data for the corresponding cAMP-liganded channel (*dashed curve, repeated from Fig 2-1 C*.) Boltzmann fit parameters of the representative curves are as follows: HCN2 R591E, −98.2 mV, s = 11.4 mV; Ch4-2 R591E, −109.1 mV, s = 14.7 mV.

2.3.3. HCN4 TM-replacement augments autoinhibitory $V_{1/2}$ shift

Decreased channel activity after HCN4 TM-replacement is not caused by disruption of cAMP potentiation but could be caused by augmentation of the autoinhibition mediated by the unliganded C-terminal region. We hypothesized that an interaction between the HCN4 TM region and the C-terminal region augments autoinhibition, resulting in decreased channel activity. If this were true, it would be the first time that the TM region has been implicated in altering autoinhibition. To test this, we determined the magnitude of $V_{1/2}$ shift due to autoinhibition in our channels. The magnitude of autoinhibition in HCN2 channels was determined previously in intact oocytes by comparing the $V_{1/2}$ of HCN2 R591E to the $V_{1/2}$ of HCN2 ΔCNB, which is a channel truncated after the C-linker, so that both the CNB fold and extreme C-terminal region were deleted. HCN2 ΔCNB completely lacks autoinhibition, while HCN2 R591E is fully autoinhibited (Wainger et al., 2001); in this comparison, HCN2 channels displayed a 16.5 ± 3.2 mV negative shift due to autoinhibition (Magee et al., 2015). We performed an HCN4 TM-replacement on HCN2 ΔCNB, equivalent to truncating Ch4-2 R591E to remove autoinhibition and found that the $V_{1/2}$ of Ch4-2 ΔCNB was -82.9 ± 5.2 mV (*n* = 11) (Figure 2-3*A*-*C*). This means that Ch4-2 channels displayed 25.0 ± 2.0 mV negative shift due to autoinhibition, greater than that of HCN2 by 10 mV (Figure 2-3*C*). We concluded that HCN4 TM-replacement decreased channel activity by augmenting autoinhibition. Moreover, our finding that the $V_{1/2}$ of Ch4-2 ΔCNB is not significantly different from that of HCN2 ΔCNB ($p > 0.97$) suggests that the negative shift of $V_{1/2}$ after HCN4 TM-replacement in full length channels is not caused by an intrinsic property of the TM region alone. This is the first evidence that the strength of the autoinhibition mediated by the CNB fold can be augmented by the HCN4 TM region.

In summary, the $V_{1/2}$ for the cAMP-liganded Ch4-2 channel in intact oocytes can be explained by the following: The magnitude of autoinhibition for an unliganded Ch4-2 channel reflects contributions from conventional autoinhibition (like HCN2) and from augmented autoinhibition (absent from HCN2). The conventional autoinhibition contribution is sufficient to negatively shift $V_{1/2}$ by 15 mV relative to Ch4-2 ΔCNB, and the augmented autoinhibition contribution is sufficient to negatively shift the $V_{1/2}$ an additional 10 mV. The net result for unliganded Ch4-2 would be a negative $V_{1/2}$ shift of 25 mV relative to Ch4-2 ΔCNB (as exhibited by Ch4-2 R591E, Figure 2-3*D left panel*, "*Autoinhibition magnitude*"). We presume that full length Ch4-2 and HCN2 channels

have similar cAMP affinity and thus similar extent of cAMP potentiation in intact oocytes. Therefore, cAMP potentiation in Ch4-2 is sufficient to positively shift the $V_{1/2}$ by 15 mV, as with HCN2 (Figure 2-3*D right panel*, "*cAMP relief*"). This results in a $V_{1/2}$ for liganded Ch4-2 channels that is 10 mV more negative than that of liganded HCN2 (Figure 2-3*C*).

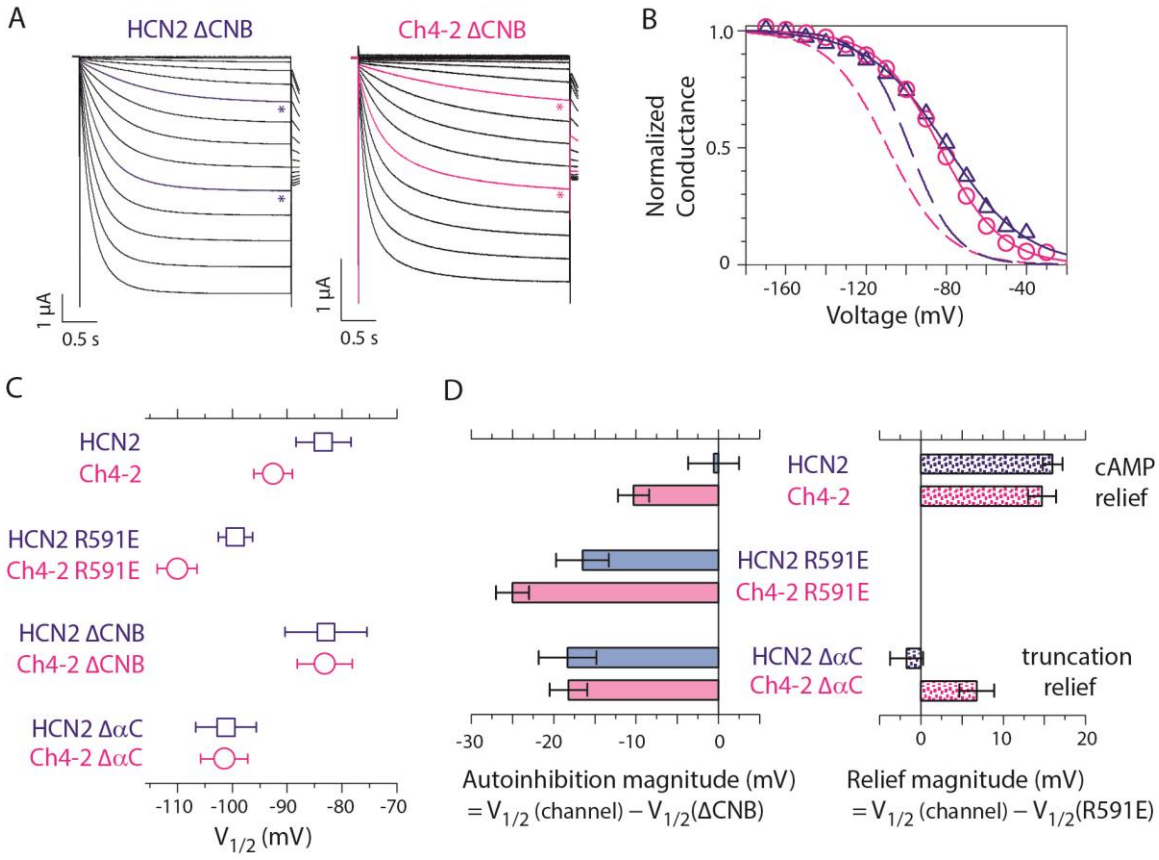

Figure 2-3: HCN4 TM-replacement in truncated HCN2 derivatives does not negatively shift $V_{1/2}$

A, Representative inward currents of HCN2 ΔCNB and Ch4-2 ΔCNB, formatted as in *Fig. 2-1B*. **B**, Conductance-voltage relationships for HCN2 ΔCNB (*triangles*) and Ch4-2 ΔCNB (*circles*) using data from panel *A* and constructed as in *Fig. 2-1C*. For comparison with fully autoinhibited channels, the relations for HCN2 R591E (*long-dash curve*) and Ch4-2 R591E (*short-dash curve*) are shown *repeated from Fig.2-2B*. Boltzmann fit parameters of the representative curves are as follows: HCN2 ΔCNB, −79.4 mV, s = 19.2 mV; Ch4-2 ΔCNB, −83.2 mV, s = 15.4 mV. **C**, Mean $V_{1/2}$ values for full-length and truncated channels with the HCN2 TM region (squares) or the HCN4 TM region (circles). *Error bars* show SD, with >6 recordings for each channel. **D**, The autoinhibition magnitude of each channel (*left panel*) was calculated from that channel's mean $V_{1/2}$ after subtracting the mean $V_{1/2}$ of the corresponding ΔCNB channel (i.e., having the same TM region sequence). The relief magnitude (*right panel*) was calculated from that channel's mean $V_{1/2}$ after subtracting the mean $V_{1/2}$ of the corresponding R591E channel. *Error bars* show uncertainties from error propagation using SEM as uncertainty of individual mean $V_{1/2}$ values.

2.3.4. Augmentation of autoinhibition can be disrupted by truncation after the beta-roll of the CNB fold

Previous studies identified the beta-roll of the CNB fold as a key structure for autoinhibition by characterizing a channel called HCN2 ΔαC which was truncated after the beta-roll (that is, lacking the helix ΔαC and the extreme C-terminal region) (Wainger et al., 2001). HCN2 ΔαC channels are unliganded and therefore are autoinhibited (Magee et al., 2015; Wainger et al., 2001), but they fail to support the Quick-Activation mechanism that controls activation kinetics in unliganded full-length HCN2 channels (Magee et al., 2015). So, we considered a hypothesis where, although the beta-roll may be sufficient to impart conventional autoinhibition, the presence of helix αC or the extreme C-terminal region is necessary for the interaction between the HCN4 TM region and C-terminal region that augments autoinhibition. To test this, we performed the HCN4 TM-replacement in HCN2 ΔαC to make Ch4-2 ΔαC and determined whether its autoinhibition magnitude would be less than that of an unliganded channel known to have augmented autoinhibition (i.e. Ch4-2 R591E). The $V_{1/2}$ value for Ch4-2 ΔαC was -101.2 ± 4.5 mV (n = 7) (Figure 2-3*C, D*). This means that Ch4-2 ΔαC channels display 18.2 ± 2.3 mV negative $V_{1/2}$ shift due to autoinhibition. This is significantly less than the autoinhibition magnitude for Ch4-2 R591E (25.0 ± 2.0 mV) and matches the conventional autoinhibition previously found for HCN2 ΔαC (18.3 ± 3.5 mV (Magee et al., 2015); see Figure 2-3*D* left panel, "Autoinhibition magnitude"). This suggests that augmented autoinhibition has been disrupted by the truncation after the beta-roll, producing approximately 10 mV of autoinhibition relief relative to Ch4-2 R591E (Figure 2-3*D* right panel, "truncation relief"). In other words, the beta-roll of the CNB fold in the absence of helix αC or the extreme C-terminal region is sufficient for conventional autoinhibition but is not sufficient for augmentation of autoinhibition by the HCN4 TM region.

2.3.5. Augmented autoinhibition leads to kinetic dominance of the autoinhibition mechanism during deactivation

We examined augmented autoinhibition further by looking at how HCN4 TM-replacement affected deactivation kinetics (activation kinetics are treated in the next section). There are two proposed models (Magee et al., 2015; Wicks et al., 2009, 2011) in which the CNB fold governs HCN channel deactivation kinetics: autoinhibition and

open-state trapping. In an autoinhibition model, channels with an intact CNB fold have a kinetically destabilized open state and hence faster deactivation compared to channels lacking the CNB fold (i.e. ΔCNB). The opposite is true in an open-state trapping model, so that channels with an intact CNB fold have slower deactivation compared to ΔCNB channels (Wicks et al., 2009, 2011). Autoinhibition and open-state trapping are exemplified by unliganded and cAMP-liganded HCN2 respectively (Magee et al., 2015), although open-state trapping has also been observed for an unliganded HCN4 derivative with a mutation in S4 (Wicks et al., 2009, 2011). Thus, for each channel in our study we compared its deactivation kinetics with those of the corresponding ΔCNB channel to distinguish autoinhibition from open-state trapping effects.

Deactivation kinetics were quantified by $t_{1/2}$ (time required for 50% deactivation completion) over a 40-mV range, exhibiting depolarization-dependence that was similar for all HCN2 and Ch4-2 derivatives (Fig. 2-4*A*, Table 2-1). Over the voltages tested, HCN4 TM-replacement in HCN2 ΔCNB significantly ($p < 10^{-4}$) increased $t_{1/2}$ by a factor of 4.1 or more. This suggests an influence on deactivation kinetics intrinsic to the HCN4 TM region without involvement of the CNB fold or extreme C-terminal region. HCN4 TM-replacement in the longer HCN2 sequence backgrounds also significantly slowed deactivation ($p < 10^{-4}$ for all cases) but the slowing effect was not as marked as for HCN2 ΔCNB, being limited to a factor from 1.5 to 2.2. We hypothesized that in the longer backgrounds, HCN4 TM-replacement augmented the conventional autoinhibitory effect of the C-terminal region to speed deactivation kinetics, partially mitigating the 4-fold slowing effect intrinsic to the HCN4 TM region.

This hypothesis was validated for unliganded full-length channels: HCN4 TM-replacement in HCN2 R591E not only preserved the known effect of autoinhibition on deactivation kinetics, it also augmented the magnitude of this autoinhibition effect. Specifically, over the voltages tested, Ch4-2 R591E deactivated faster than Ch4-2 ΔCNB by a factor of 2.6 or more, whereas HCN2 R591E deactivated faster than HCN2 ΔCNB by a factor of only 1.2-fold or less (Fig. 2-4*A, B*). We considered a simple hypothesis where the 25-mV negative shift of $V_{1/2}$ from augmented autoinhibition results in a parallel 25-mV negative shifting of the $t_{1/2}$ vs. V relation, thus speeding deactivation kinetics. But this hypothesis is insufficient to explain the quantitative speeding of deactivation observed; for instance, $t_{1/2}$ of Ch4-2 R591E at 0 mV was 2.0-fold smaller than $t_{1/2}$ of Ch4-2 ΔCNB at the much stronger depolarization of +40 mV. Figure 2-4B provides a succinct

visualization of autoinhibition magnitudes by plotting $t_{1/2}$ (for +20 mV deactivation) vs. $V_{1/2}$ for R591E and ΔCNB channels, with a correlation line drawn between to represent the magnitude of autoinhibition. Compared to HCN2 channels, the correlation line for Ch4-2 channels is longer in both the horizonal and vertical dimensions, and moreover has a steeper slope. This illustrates how HCN4 TM-replacement in HCN2 channels introduced an augmented contribution to autoinhibition which applies to both $V_{1/2}$ and $t_{1/2}$ compared to HCN2 channels, and also has a disproportionately large effect on $t_{1/2}$ compared to $V_{1/2}$.

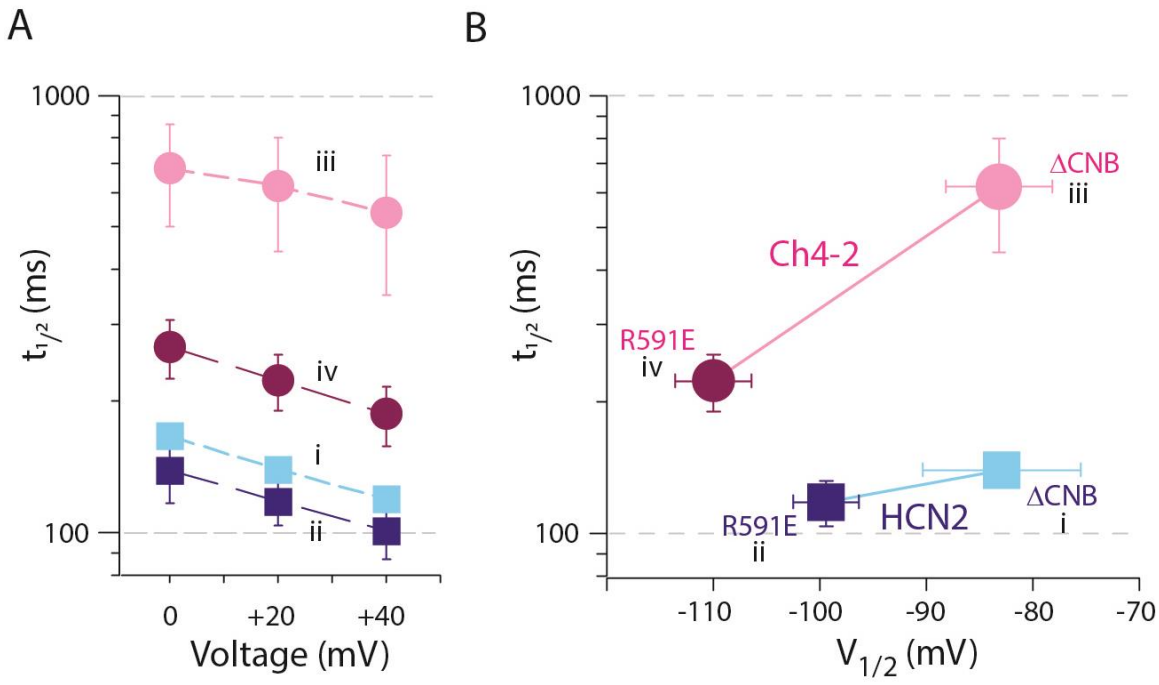

Figure 2-4: Effect of augmented autoinhibition on deactivation kinetics on unliganded channels

A, Mean $t_{1/2}$ values with error bars showing SD, with ≥ 6 recordings for each channel; for some channels the bars are drawn wider for clarity. Selected datasets are labelled with roman numerals for reference in panel *B*. Datasets are plotted for channels lacking cAMP potentiation: HCN2 ΔCNB, light solid squares, label *i*; HCN2 R591E, dark solid squares, label *ii*; HCN2 ΔαC, half-shaded squares; Ch4-2 ΔCNB, light solid circles, label *iii*; Ch4-2 R591E, dark solid circles, label *iv*; Ch4-2 ΔαC, half-shaded circles. **B,** Correlation plot of deactivation $t_{1/2}$ (+20 mV, from panel A) vs $V_{1/2}$ (from *Fig. 2-3C*). Point symbols and roman numeral labels are as in *panel A.* The datapoints for ΔCNB and R591E channels are connected by a straight line representing autoinhibition.

Sigmoidal shape with a delay phase is a characteristic feature of deactivation transients in HCN channels and is believed to reflect multiple sequential S4 movement steps in the voltage-sensing domain that precede the open-closed transition in the pore domain (Elinder et al., 2006; Kusch et al., 2010). Deactivation transients of HCN2 ΔCNB and Ch4-2 ΔCNB showed reduced sigmoidicity in comparison with those of R591E channels, so that at early times the fraction completion was greater for each ΔCNB channel than for the corresponding R591E channels (Figure 2-4*A*). This suggests that while truncation after the C-linker slowed overall progress through the deactivation pathway, it also loosened the requirement for multiple S4 movements before pore closure. This argues in support of the existence of functional interactions between the voltage-sensing region and the C-terminal region, where the C-terminal region structures that impose autoinhibition are also involved with imposing cooperativity between subunits of the tetramer.

The $t_{1/2}$ values of cAMP-liganded Ch4-2 and Ch4-2 ΔαC were both intermediate between Ch4-2 R591E and Ch4-2 ΔCNB, which is consistent with partial relief of autoinhibition through either cAMP binding or truncation within the CNB fold. Over the voltages tested, liganded Ch4-2 deactivated at least 1.2-fold faster than Ch4-2 ΔCNB which indicates autoinhibition but deactivated at least 1.7-fold slower than Ch4-2 R591E which demonstrates a slowing effect of cAMP potentiation on deactivation kinetics (Figure 2-5*B left)*. Similarly, Ch4-2 ΔαC deactivated at least 1.8-fold faster than Ch4-2 ΔCNB but at least 1.4-fold slower than Ch4-2 R591E (Figure 2-5*B right*). Fig. 4*C* shows that the Ch4-2 derivatives as a group conform to a regular progression well described by the correlation line from no autoinhibition (ΔCNB) to maximal autoinhibition (R591E) with varying degrees of autoinhibition relief from partial truncation (ΔαC) or cAMP binding (Ch4-2 lig.).

The straightforward progression of Ch4-2 derivatives in Fig. 2-5*C* contrasts with the group of HCN2 derivatives, where datapoints for liganded HCN2 and HCN2 ΔαC do not conform to the correlation line defined by comparing HCN2 R591E vs. HCN2 ΔCNB. Liganded HCN2 deactivates markedly slower than HCN2 ΔCNB due to open-state trapping (Magee et al., 2015) (Figure 2-5*C* "*HCN2 lig.*"). HCN2 ΔαC deactivates slightly slower than HCN2 ΔCNB despite exhibiting conventional autoinhibition as evaluated by $V_{1/2}$. This suggests that truncation after the beta-roll enables the open-state trapping mechanism and autoinhibition mechanism to operate simultaneously with opposing

influence on deactivation kinetics. All together these results suggest that HCN2 and Ch4-2 differ in their complexity of mechanistic contributions to deactivation kinetics. HCN2 possesses two distinct mechanisms of open-state trapping and autoinhibition which in some cases operate simultaneously, whereas the HCN4 TM-replacement disrupted the Open-State Trapping mechanism, leaving autoinhibition (with partial relief by cAMP binding) to be the dominant mechanism contributed by the C-terminal region to determine deactivation kinetics.

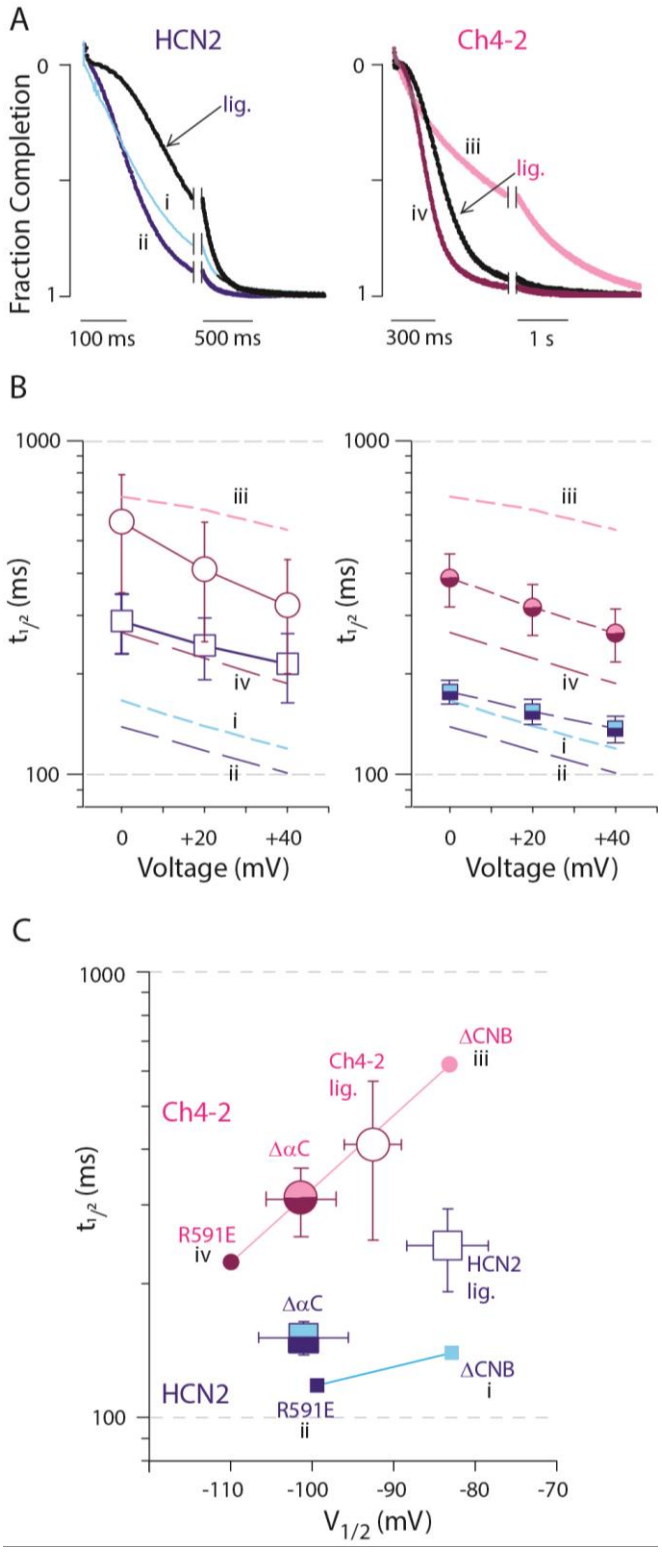

Figure 2-5: Effect of augmented autoinhibition on deactivation kinetics

A, Representative deactivation currents at +20 mV, each normalized to total decay amplitude. Selected datasets are marked from those channels whose datasets are shown in *Fig. 2-4A*.

Within each channel family, the maximally autoinhibited channel (full length R591E, *ii* and *iv*) exhibits the smallest $t_{1/2}$ values. For these example traces, the $t_{1/2}$ are as follows: HCN2 ΔCNB (label *i*), $t_{1/2}$ = 133 ms; HCN2 R591E (label *ii*), $t_{1/2}$ = 119 ms; HCN2 lig. $t_{1/2}$ = 255 ms; Ch4-2 ΔCNB (label *iii*), $t_{1/2}$ = 632 ms; Ch4-2 R591E (label *iv*), $t_{1/2}$ = 245 ms; Ch4-2 lig. $t_{1/2}$ = 340 ms. .**B,** Mean $t_{1/2}$ values with error bars showing SD, with ≥6 recordings for each channel; for some channels the bars are drawn wider for clarity. Datasets are plotted as points for the following channels: HCN2, open squares; Ch4-2 open circles; HCN2 ΔαC, half-shaded squares; Ch4-2 ΔαC, half-shaded circles. For reference, datasets are repeated from *upper panels* for corresponding ΔCNB and R591E channels (*dashed lines*, *labels i through iv*). **C**, Correlation plot of deactivation $t_{1/2}$ (+20 mV, from *Fig. 2-4A and this figure panel B*) vs. $V_{1/2}$ (from *Fig. 2-3C*). Point symbols and roman numeral labels are as in *panel B*. For each of the HCN2 and Ch4-2 groups of derivatives, the datapoints for ΔCNB and R591E channels are connected by a straight line.

2.3.6. Augmented autoinhibition leads to kinetic dominance of the autoinhibition mechanism during activation

As with deactivation, there are two proposed models in which the CNB fold governs HCN channel activation kinetics: these are the autoinhibition and Quick-Activation (Magee et al., 2015; Wainger et al., 2001). Compared to ΔCNB channels, channels with an intact CNB fold have activation that is either slower (autoinhibition model) or faster (Quick-Activation model). Autoinhibition and Quick-Activation are exemplified by unliganded and liganded HCN2 respectively, so we tested whether HCN4 TM-replacement leads to the kinetic dominance of the autoinhibition mechanism during activation as it did for deactivation. Notably, the activation kinetics of liganded HCN2 channels cannot be tested in intact oocytes. This is because the cAMP affinity of closed channels is too weak to enable binding of the low endogenous concentration of cAMP; rather, cAMP binding occurs over the course of the activation epoch as channels reach the open state with strong cAMP affinity (Magee et al., 2015; Wang et al., 2001). Therefore, we limited our quantitative analysis of activation to the constitutively unliganded channels (R591E, ΔαC, and ΔCNB).

The sigmoidal activation transients were fitted to a sum of two exponentials following a delay (Magee et al., 2015; Wang et al., 2001), and the overall activation kinetics was then quantified with a weighted-average time constant (τ_w, see Methods). Over the voltages tested (-110 to -150 mV), HCN4 TM-replacement in HCN2 ΔCNB significantly ($p < 10^{-3}$) increased τ_w by a factor from 1.6 to 2.0, indicating a slowing influence intrinsic to the HCN4 TM region (Figure 2-6*A,* Table 2-2). The slowing effect of HCN4 TM-replacement was even more pronounced for longer HCN2 sequence backgrounds, with τ_w increasing at least 2.6-fold. As with deactivation, the different degrees of slowing from HCN4 TM-replacement in different sequence backgrounds

indicates that the TM-replacement modified how the C-terminal region governed activation kinetics. Another observation that echoes the findings for deactivation is the reduction in sigmoidicity of the activation transients upon truncation after the C-linker (Figure 2-6*B*), suggesting a loss of S4 cooperativity. Over the voltages tested, Ch4-2 R591E exhibited autoinhibition of activation kinetics, activating at least 1.4-fold slower than Ch4-2 ΔCNB, whereas HCN2 R591E exhibited Quick-Activation, activating at least 1.8-fold faster than HCN2 ΔCNB (Figure 2-6*A, B*). This suggests that the Quick-Activation mechanism of unliganded HCN2 was disrupted by the HCN4 TM-replacement providing the first evidence that a key structural determinant of the Quick-Activation mechanism is in the HCN2 TM region.

The disruption of Quick-Activation can be visualized in the correlation plot of τ_w vs. $V_{1/2}$ (Figure 2-6*C*). The correlation lines drawn between ΔCNB and R591E datapoints have opposite slopes for Ch4-2 and HCN2, because Ch4-2 R591E exhibited autoinhibition of activation kinetics whereas HCN2 R591E exhibited Quick-Activation. In contrast, for deactivation kinetics, both Ch4-2 R591E and HCN2 R591E exhibited autoinhibition and hence both correlation lines had positive slopes.

For each of Ch4-2 ΔαC and HCN2 ΔαC, the activation kinetics were intermediate between the corresponding ΔCNB and R591E channels. Notably, HCN2 ΔαC exhibited a weaker degree of Quick-Activation compared to HCN2 R591E, despite these two channels having the same autoinhibition magnitude as evaluated by $V_{1/2}$ (Magee et al., 2015). Consequently, in the correlation plot Figure 2-6*C*, the HCN2 ΔαC datapoint falls well above the correlation line defined by ΔCNB and R591E channels. This complex combination of opposing gating characteristics in HCN2 — thermodynamic closed-state stabilization indicated by $V_{1/2}$, yet kinetic closed-state destabilization indicated by τ_w — contrasts with the Ch4-2 derivatives which form a straightforward progression in the correlation plot. Therefore, HCN4 TM-replacement had the effect of simplifying the complex gating of HCN2 so that autoinhibition was the dominant mechanism contributed by the C-terminal region to determine activation kinetics, just as for deactivation kinetics.

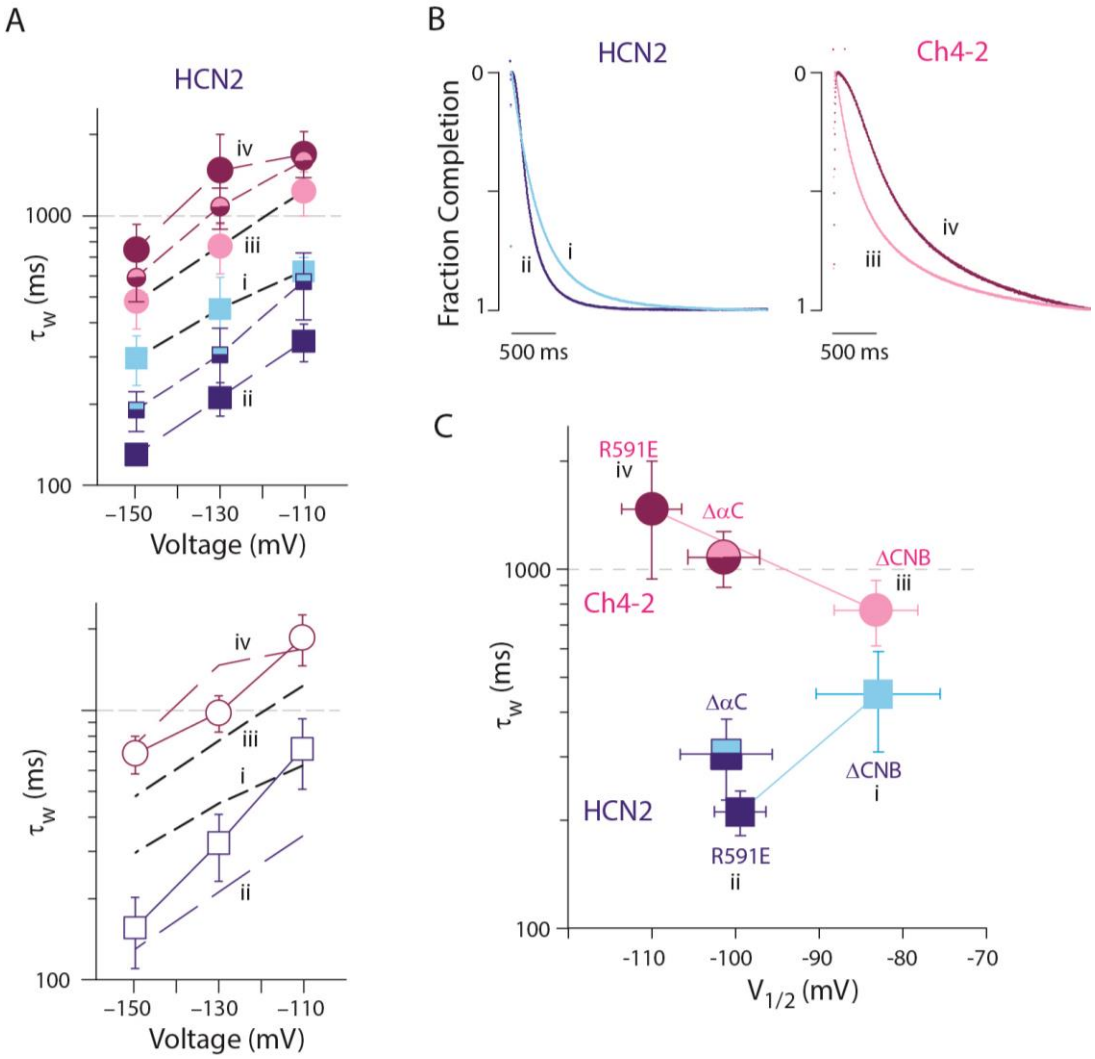

Figure 2-6: Effect of augmented autoinhibition on activation kinetics

A, Mean τ_w values with error bars showing SD, with ≥ 6 recordings for each channel; for some channels the bars are drawn wider for clarity. Selected datasets are labelled with roman numerals for reference in *panels B and C*. In *upper panels,* datasets are plotted for channels lacking cAMP potentiation: HCN2 ΔCNB, light solid squares, label *i*; HCN2 R591E, dark solid squares, label *ii*; HCN2 ΔαC, half-shaded squares; Ch4-2 ΔCNB, light solid circles, label *iii*; Ch4-2 R591E, dark solid circles, label *iv*; Ch4-2 ΔαC, half-shaded circles. In *lower panels* datasets for channels with cAMP potentiation are plotted*:* HCN2, open squares; Ch4-2, open circles. For reference, datasets are repeated from *upper panels* for corresponding ΔCNB and R591E channels (*dashed lines*, *labels i through iv*). **B***,* Representative activation currents at −130 mV, each normalized to total decay amplitude in the 3-s activation epoch. Roman numeral labels refer to channels in panel *A*. HCN2 R591E (labeled *ii*) exhibits Quick-Activation whereas Ch4-2 R591E (labeled *iv*) exhibits autoinhibition. For these example traces, the lag (d) and τ_w values are as follows: HCN2 ΔCNB (label *i*), d = 120 ms and τ_w = 380 ms; HCN2 R591E (label *ii*), d = 150 ms and τ_w = 190 ms; Ch4-2 ΔCNB (label *iii*), d = 60 ms and τ_w = 680 ms; Ch4-2 R591E (label *iv*), d = 410 ms and τ_w = 1340 ms. Note the lack of sigmoidicity in ΔCNB channels indicated by smaller d values.**C**, Correlation plot of activation τ_w (-130 mV, from *panel A*) vs. $V_{1/2}$ (from *Fig. 2-3C*). Point symbols and roman numeral labels are as in *panel A*. For each of the HCN2 and Ch4-2 groups of derivatives, the datapoints for ΔCNB and R591E channels are connected by a straight line.

Table 2-1: Mean gating parameters

	G-V			Deactivation (+20 mV)		Activation (-130 mV)		
Construct	**$V_{1/2}$ (mV**	**s (mV)**	**N**	**$t_{1/2}$ (ms)**	**N**	**d (ms)**	**τw (ms)**	**N**
HCN2	−83.4 ± 5.0	14.4 ± 2.6	49	243 ± 51	49	103 ± 28	322 ± 90.	49
Ch4-2	−93.2 ± 3.2	18.9 ± 1.4	8	410 ± 160	8	186 ± 35	980 ± 150	8
HCN2 R591E	−99.4 ± 3.1	10.7 ± 1.8	10	118 ± 14	10	153 ± 25	211 ± 30.	10
Ch4-2 R591E	−107.9 ± 5.0	13.5 ± 0.6	16	223 ± 33	16	450 ± 100	1470 ± 530	16
HCN2 ΔCNB	−82.9 ± 7.4	19.6 ± 1.4	6	139.6 ± 5.5	6	142 ± 93	450 ± 140	6
Ch4-2 ΔCNB	−82.9 ± 5.2	19.0 ± 3.7	11	620 ± 180	11	48 ± 19	770 ± 160	11
HCN2 ΔαC	−101.13 ± 5.5	8.5 ± 3.1	10	151 ± 13	10	221 ± 32	305 ± 78	10
Ch4-2 ΔαC	−101.2 ± 4.5	14.9 ± 1.5	7	309 ± 54	11	314 ± 72	1080 ± 190	7

Mean gating parameters for HCN2 and Ch4-2 derivatives.

Table 2-2: Activation fit parameters

Construct	τ_{early}	n	τ_{late}	n	f_{early}	n	τ_W	n	D	n
HCN2	144 ± 31	49	960 ± 270	48	0.79 ± 0.06	49	322 ± 90.	49	103 ± 28	49
Ch4-2	254 ± 31	8	1480 ± 210	8	0.41 ± 0.03	8	980 ± 150	8	186 ± 35	8
HCN2 R591E	137 ± 30.	10	360 ± 140	10	0.62 ± 0.16	10	211 ± 30.	10	153 ± 25	10
Ch4-2 R591E	430 ± 100	16	2170 ± 800	16	0.40 ± 0.05	16	1470 ± 530	16	450 ± 100	16
HCN2 ΔCNB	323 ± 70.	6	1300 ± 1100	5	0.83 ± 0.10	6	450 ± 140	6	142 ± 93	6
Ch4-2 ΔCNB	228 ± 64	11	1240 ± 240	11	0.47 ± 0.04	11	770 ± 160	11	48 ± 19	11
HCN2 ΔαC	231 ± 58	10	630 ± 290	8	0.73 ± 0.29	10	305 ± 78	10	221 ± 32	10
Ch4-2 ΔαC	315 ± 61	7	1560 ± 250	7	0.40 ± 0.03	7	1080 ± 190	7	314 ± 72	7

Average activation exponential fit parameters (±SD) for all HCN2 and Ch4-2 constructs analyzed. Parameters were calculated at -130 mV. F_{early} was calculated using the formula: $f_{early} = A_{early} / (A_{early} + A_{late})$ (see Methods). τ_w was calculated using the formula: $\tau_w = (\tau_{early} * f_{early}) + (\tau_{late} * (1 - f_{early}))$ (see Methods). τ_{early}, τ_{late}, τ_w and D are given in ms.

2.4. Discussion

2.4.1. Augmentation of autoinhibition

Autoinhibition of HCN channels is mediated by the cytoplasmic CNB fold, but this study shows for the first time that the magnitude of this autoinhibition is not solely determined by the sequence of the C-terminal region; rather, autoinhibition magnitude can also be strongly altered by substitution of the TM region. We analyzed autoinhibition magnitude separately from cAMP potentiation magnitude to determine the effect of TM-replacement on each one. This approach revealed that while HCN2 exemplified conventional autoinhibition, HCN4 TM-replacement in full-length HCN2 channels introduced an additional mechanism that augmented autoinhibition to produce a substantial (10 mV) negative shift of $V_{1/2}$. While augmented autoinhibition originated from the HCN4 TM region, it also relied on structures in the C-terminal region since it was abolished by truncation within the CNB fold after the beta-roll. This is strong evidence that a functional interaction between the TM and C-terminal regions was required for augmented autoinhibition.

Our finding of augmented autoinhibition differs from a report by Stieber *et al*. where HCN4 TM-replacement did not significantly change the $V_{1/2}$ in either full-length or truncated HCN2 sequence backgrounds (Stieber et al., 2003b). One experimental difference is that Stieber *et al.* used human HCN2 and HCN4 sequence whereas we used mouse HCN2 and HCN4 sequences, but the orthologue divergence (mouse vs. human, <3%) is far less than the paralogue divergence (HCN2 vs. HCN4, >11% in TM region) (Ludwig et al., 1998, 1999; Santoro et al., 1998). A more prominent experimental difference is that Stieber *et al*. expressed channels in HEK293 cells and tested them in the whole-cell patch configuration, whereas we expressed channels in intact *X. laevis* oocytes and tested them in the two-electrode voltage-clamp configuration. The whole-cell patch configuration applied to mammalian cells exchanges the cytoplasmic contents with pipette solution; consequent loss of intracellular factors such as PIP_2 leads to HCN channel "rundown" as evidenced by $V_{1/2}$ values being generally more hyperpolarized than in the intact oocyte (Pian et al., 2006, 2007; Zolles et al., 2006). In contrast, the intact-oocyte configuration retains cytoplasmic contents; this enables observation of regulation mechanisms reliant on intracellular factors, such as the previously reported Quick-Activation mechanism that governs kinetics of unliganded HCN2 channels (Magee

et al., 2015). Possibly the augmentation of autoinhibition is another example of a mechanism reliant on intracellular factors to help determine $V_{1/2}$.

We found further evidence for augmentation of autoinhibition in deactivation kinetics, which Stieber et al. did not characterize. As a general rule, HCN4 TM-replacement slowed deactivation kinetics in either full-length or truncated HCN2 sequence backgrounds. But in full-length channels, HCN4 TM-replacement additionally augmented autoinhibition to significantly speed deactivation (relative to the ΔCNB truncated channel). Augmentation of autoinhibition was so strong that the open-state trapping mechanism of HCN2 was disrupted; autoinhibition hence became the dominant mechanism contributed by the C-terminal region to determine deactivation kinetics. As was found for $V_{1/2}$, the effect of augmented autoinhibition on deactivation kinetics originated with the HCN4 TM region but relied on structures in the C-terminal region. Therefore, functional interaction between TM and C-terminal regions determines how much autoinhibition speeds deactivation and how much open-state trapping slows deactivation.

We further found that, as a general rule, HCN4 TM-replacement slows activation kinetics in either full-length or truncated HCN2 sequence backgrounds. In our intact-oocyte experiments with low concentrations of endogenous cAMP, closed channels with an intact CNB fold are predominantly in the unliganded state and bind cAMP only during the course of the activation epoch (Wang et al., 2001). Consequently, our conclusions about activation kinetics are limited to channels without cAMP potentiation. For activation of full length, unliganded HCN2, the increases in τ_w we observed were similar in extent to those observed by Stieber *et al.* (approximately 3-fold increase in tau at -140 mV). However, because we additionally determined autoinhibition magnitude of our full-length channels by comparison with ΔCNB channels, we were able to test for the Quick-Activation mechanism which appears in the intact oocyte but not in cell-free excised-patch conditions (Magee et al., 2015). HCN4 TM-replacement augmented autoinhibition so much that the Quick-Activation mechanism of HCN2 was disrupted; autoinhibition hence became the dominant mechanism contributed by the C-terminal region to determine activation kinetics. Therefore, functional interaction between TM and C-terminal regions determines how much autoinhibition slows activation and how much Quick-Activation speeds activation. A summary of these reported findings can be found in Figure 2-7.

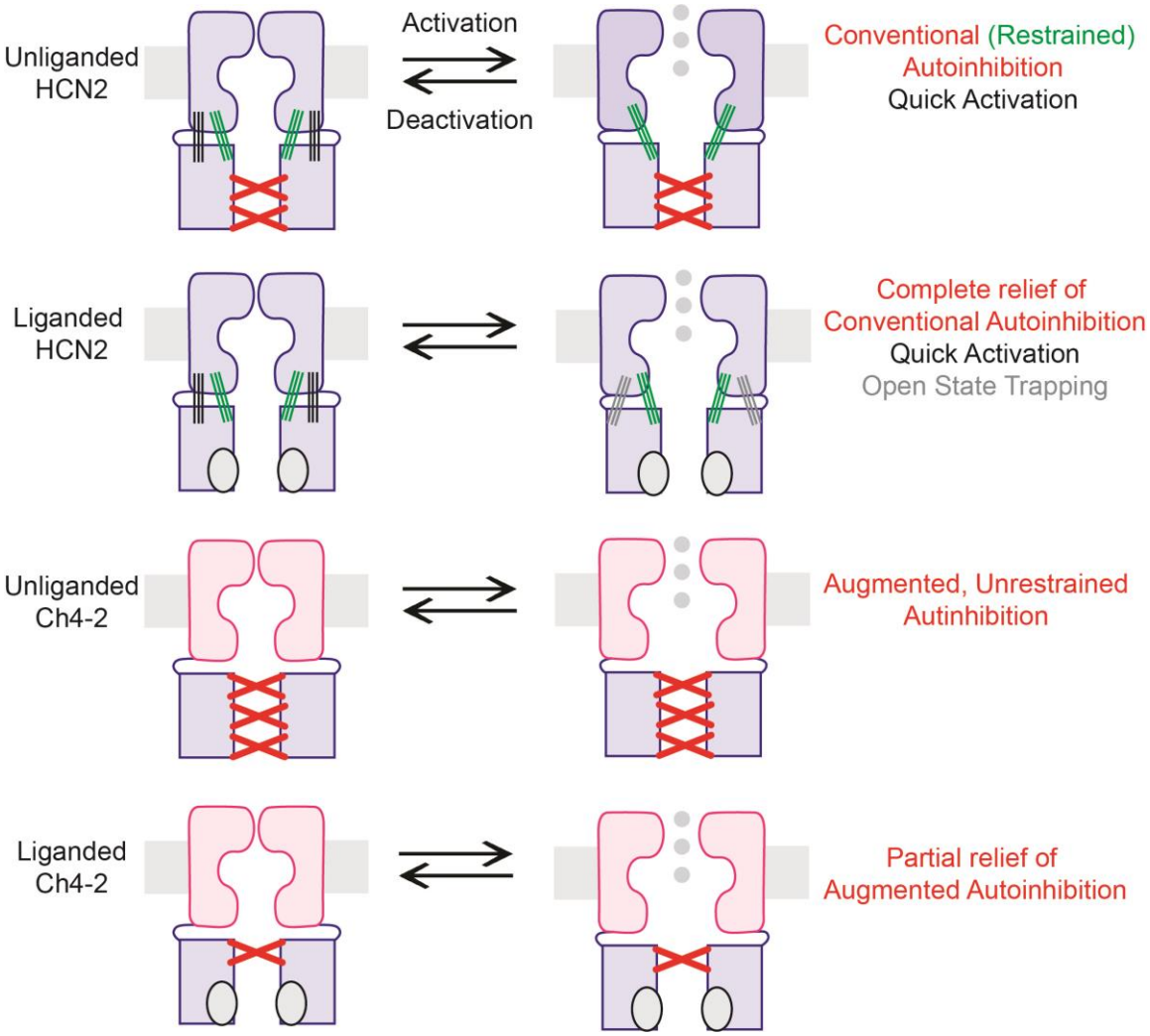

Figure 2-7: Schematic summarizing effects of HCN4 TM-replacement on Autoinhibition, Open-State Trapping and Quick-Activation

Schematic of the different C-terminally mediated mechanisms present in mHCN2 and Ch4-2 channels. In unliganded mHCN2 channels autoinhibition (red crosses) regulates $V_{1/2}$ in a limited or restrained fashion (restraint on autoinhibition indicated with green lines) and deactivation kinetics, while Quick-Activation regulates activation kinetics (indicated with black lines). In liganded mHCN2 channels autoinhibition has been relived (red crosses removed), Quick-Activation regulates activation kinetics (black lines), and the Open-State Trapping mechanism regulates deactivation kinetics (grey lines). In Ch4-2 channels the Quick-Activation and Open-State Trapping mechanisms have been disrupted (black and grey lines removed), resulting in Autoinhibition regulating activation and deactivation kinetics. Additionally, the restraint or limit on autoinhibition has been removed (indicated by removal of green lines and addition of another red cross), resulting in augmentation of autoinhibition. Magnitude of relief of autoinhibition by cAMP binding in Ch4-2 channels is the same as in HCN2 channels, resulting in some degree of autoinhibition remaining (single red cross remains).

2.4.2. Separate effects on kinetics and $V_{1/2}$

A positively shifted $V_{1/2}$ generally reflects preferential stabilization of the open state in thermodynamic terms. As discussed previously, the autoinhibition model follows a simple conception of gating that we could call "parallel stabilization", where preferential thermodynamic stabilization of the open state is accompanied by kinetic destabilization of the closed state (faster activation) and kinetic stabilization of the open state (slower deactivation). Another example of parallel stabilization is observed with the well-known cAMP potentiation of HCN channels, where cAMP binding leads to a positive shift of $V_{1/2}$, speeding of activation, and slowing of deactivation (DiFrancesco and Tortora, 1991; Ludwig et al., 1998, 1999; Santoro et al., 1998). This was confirmed in our tests of cAMP potentiation in intact oocytes: the elimination of cAMP binding using the R591E mutation resulted in parallel destabilization of the open state, with a negative shift of $V_{1/2}$ and speeding of deactivation (activation kinetics of liganded channels are excluded from consideration in intact oocytes, as stated in the previous paragraph). Additionally, if Ch4-2 R591E has its augmented autoinhibition removed by C-terminal truncation, this results in parallel stabilization of the open state, with Ch4-2 ΔCNB exhibiting positively shifted $V_{1/2}$, faster activation, and slower deactivation compared to Ch4-2 R591E.

However, parallel stabilization will not necessarily hold in a mechanism with multiple reaction steps or a channel with multiple mechanisms present (e.g. HCN2). Previous studies on various HCN channel derivatives have reported cases where truncation or sequence replacement altered gating kinetics but did not change $V_{1/2}$ (Magee et al., 2015; Wicks et al., 2009, 2011; Xu et al., 2010). And in the notable case of the Quick-Activation mechanism in HCN2, truncation of the C-terminal region positively shifts $V_{1/2}$ (thermodynamically destabilizing the closed state) but slows activation kinetics (kinetically stabilizing the closed state) (Magee et al., 2015). In this work, HCN4 TM-replacement was associated with slowing of deactivation in general (an effect intrinsic to the HCN4 TM region) but this kinetic stabilization of the open state was not accompanied by a positive shift in $V_{1/2}$. Rather, there was no detectable $V_{1/2}$ shift in HCN2 ΔCNB and ΔαC, and even a negative $V_{1/2}$ shift in HCN2 R591E. Our results help confirm that channel activation and deactivation speeds should be examined in addition to $V_{1/2}$ trends to fully understand HCN channel behavior.

The $V_{1/2}$ parameter gives an incomplete assessment of thermodynamics in HCN channels because the gating mechanism is believed to involve separate steps for voltage-dependent S4 movement and voltage-independent pore opening (Chen et al., 2007; Craven and Zagotta, 2004). This means the pore-opening step might have an unfavorable equilibrium such that the maximum open probability at saturating hyperpolarization (Pmax) is significantly less than 100%. In this scenario, a shift in the pore-opening equilibrium due to autoinhibition might decrease Pmax without shifting $V_{1/2}$ (Craven and Zagotta, 2004). Our work implicitly assumes that the autoinhibition-free channels Ch4-2 ΔCNB and HCN2 ΔCNB have Pmax sufficiently close to 100% so that the shift in the pore-opening equilibrium due to autoinhibition causes a negative shift in $V_{1/2}$; this would be in addition to any shift in $V_{1/2}$ caused by the effect of autoinhibition on S4 movement steps. This limitation does not apply to our evaluation of kinetics, such as our conclusion that HCN4 TM replacement augments the autoinhibition effect on deactivation kinetics.

2.4.3. Possible domain interactions

The structural basis of conventional autoinhibition in HCN channels is proposed to be interactions between C-linker regions in adjacent subunits of the tetramer (Craven and Zagotta, 2004; Zhou et al., 2004). Such interactions are observable in the crystallographic and cryoEM structures of the unliganded isolated C-terminal region and full-length channel (Lee and MacKinnon, 2017; Taraska et al., 2009). The inhibitory interaction between C-linkers is believed to be disrupted when the conformation of the C-linker is altered upon cAMP binding the CNB fold (autoinhibition relief) or upon truncation of the CNB fold (autoinhibition removal). Our work shows that this autoinhibition can be augmented by HCN4 TM-replacement, and we suggest that since this augmentation utilizes TM residues specific to HCN4, it has a different structural basis than conventional autoinhibition. We propose that most likely the augmentation is facilitated by a direct interaction between the C-linker and the TM region, although we cannot rule out that the interaction may be an indirect interaction through a network of bonds going through the HCN domain in the N-terminal region. Complete deletion of the CNB fold alters C-linker conformation to eliminate all forms of autoinhibition. However, a less drastic truncation of the CNB fold after the beta-roll would alter the C-linker conformation in an intermediate fashion, such that the C-linker – TM interaction required

for augmentation of autoinhibition is lost, but the C-linker – C-linker interaction required for conventional autoinhibition is retained. In contrast, binding cAMP in an intact CNB fold would disrupt the C-linker – C-linker interaction (conventional autoinhibition) but retain the C-linker – TM interaction (augmentation of autoinhibition). Notably, we are not suggesting that HCN2 does not have any C-linker – TM interactions. In fact, we propose that HCN2 uses C-linker – TM interactions to impose a limit on how much autoinhibition can stabilize the closed state, which enables Quick-Activation and (when cAMP-liganded) open-state trapping. When these C-linker – TM interactions are altered through HCN4 TM-replacement, the limit to closed state stability is lost, so that Quick-Activation and open-state trapping are disrupted and augmented autoinhibition is observed.

Within the C-linker, the A' helix is most likely to be involved with functional TM region interaction. The A' helix immediately follows S6, and is observed in proximity to cytoplasmic portions of the TM region in the cryo-EM structure of the closed HCN channel (Lee and MacKinnon, 2017). Previous studies have implicated interactions of the A' helix with the TM region in determining open-state stability and $V_{1/2}$ (Chen et al., 2001a; Decher et al., 2004; Kwan et al., 2012). The recently obtained structure of the hHCN1 channel showed extensive interactions of the C-linker, specifically the A’ helix, with the TM region, which were proposed to help stabilize the channel in the observed closed state (Lee and MacKinnon, 2017). They also suggested that cAMP potentiation is partially due to a conformational change in the C-linker, which would subsequently change the interdomain interactions between the C-linker and TM region. We would suggest that in addition to the proposed functions of the A’ helix, it can also interact with HCN4 TM region structures to augment autoinhibition by thermodynamically and kinetically stabilizing the closed state in full-length channels.

HCN4 co-assembles in vivo with HCN2 or HCN1 to form heterotetramers (Much et al., 2003; Ye and Nerbonne, 2009). Our studies were performed on homomeric channels, but the augmented autoinhibition derived from the HCN4 TM region might still operate in a heteromer due to conservation between C-terminal region sequences; for instance, the A' helix is fully conserved in all HCN subtypes. Therefore, since truncations of the CNB fold in HCN4 have been found in patients with idiopathic sinus node dysfunction (Schulze-Bahr et al., 2003; Schweizer et al., 2010), the relief of

autoinhibition caused by such truncations may be larger than predicted from in vitro studies on homomers of truncated HCN2 (Magee et al., 2015; Wainger et al., 2001).

Chapter 3.

Characterization of an interdomain interaction in HCN channels: E457 interacts with the transmembrane region to stabilize the open state and regulate the autoinhibition mechanism

Chapter 3 is composed of unpublished work with the intent of composing a manuscript for publication in the future. I was responsible for the experimental design and initial mutagenesis. Further subcloning of mutants, data acquisition, and data analysis was performed by either myself or undergraduate students (Jessica Li, Matt Jung and Allaa Ela-Alim) whom I trained and supervised. I was responsible for all remaining work including generating the figures and text of this chapter. I also presented a poster based on parts of this work at the Biophysical Society Meeting (2016).

Page D.A., Young, E.C. A charged residue in the HCN channel C-linker stabilizes the open state. Poster presented at Biophysical Society's Annual Meeting, March 2016.

3.1. Introduction

HCN channels play an important physiological role in regulating electrical activity in excitable cells of the heart and nervous system (Wahl-Schott and Biel, 2009). Historically HCN channel research has focused on activation voltage-dependence and kinetics, leaving the deactivation reaction pathway relatively unstudied. However, HCN channel deactivation plays an important role in regulating HCN channel activity. For example, the fast deactivation of HCN channels is required for the role of HCN channels in dendritic integration in neurons (Magee, 2000). Additionally, C-terminal functions like autoinhibition, cAMP-relief of autoinhibition, and Open-State Trapping affect deactivation rates of HCN channels (DiFrancesco and Tortora, 1991; Magee et al., 2015; Wainger et al., 2001; Wicks et al., 2011). Overall, the molecular mechanisms for how HCN channel deactivation is regulated are not well understood.

As summarized in Ch. 1.4 interdomain interactions are predicted to occur between the TM and C-terminal regions, specifically the cytoplasmic ends of the S4 and S5 helices interacting with the A' helix which lies parallel to the membrane (Lee and MacKinnon, 2017). These interactions have been hypothesized to modify channel activity in a variety of ways, including changing the relative thermodynamic stability of either the open or closed states, or changing gating kinetics (Chen et al., 2001a; Decher et al., 2004; Kwan et al., 2012; Lee and MacKinnon, 2017; Prole and Yellen, 2006). In general, however, there is poor understanding of what specific CNB fold-mediated mechanisms these interdomain interactions are involved in. My work in Ch. 2 successfully uncovered evidence for functional interdomain interactions controlling Autoinhibition and Open-State Trapping which are two possible mechanisms governing the deactivation pathway. However, Ch. 2 provided simply a general demonstration of the interaction existence and did not attempt to focus on any individual residue that might participate in interdomain interaction.

Di-sulfide cross-linking experiments suggest that the A' helix has at least two different conformations, one for the open state and one for the closed state (Kwan et al., 2012; Prole and Yellen, 2006). These same experiments suggest that some A' helix residues would only interact with the TM region in a state-dependent manner (i.e. only in the open state or only in the closed state (Kwan et al., 2012). An interdomain interaction formed only in the open state would as a consequence most prominently affect the

kinetics of channel deactivation. Moreover, if this interdomain interaction were rearranged during cAMP binding to the CNB fold, it could provide an explanation for the effect of cAMP binding on deactivation speed. In this Chapter, I found functional evidence for a charged residue in the A' helix (E457) forming an interdomain interaction with the TM region, that stabilized the channel's open state. A charge reversal mutation here (E457R) resulted in speeding of deactivation in several channels with a varying degree of autoinhibition vs. autoinhibition relief. Analysis of the gating parameters suggests that the E457R mutation has two distinct effects on the autoinhibition mechanism: suppression of the magnitude of thermodynamic autoinhibition, and augmentation of the magnitude of kinetic autoinhibition. I also found that with one full length form of the autoinhibitory C-terminal region, the E457R mutation had a reversed phenotype (slowing rather than speeding deactivation), suggesting an alternative conformation of A' helix which may be dependent on a cellular factor.

3.2. Methods

3.2.1. Construct Composition

As described in Chapter 2 the Ch4-2 constructs are composed of the N-terminal region (M1-G130) of mouse HCN2 fused to the transmembrane region (M214-D521) of mouse HCN4 (Santoro and Tibbs, 1999). This invariant sequence was then fused to various portions of the C-terminal region derived from mouse HCN2: for Ch4-2 ΔXC, S444-H645, see Chapter 2 for composition of previously characterized Ch4-2 channels (Magee et al., 2015). Note the specifically named residue "K381" in the HCN4 TM region within CH4-2 is named according to its mouse HCN4 sequence number, whereas "E457" and "R591E" in the HCN2 C-terminal region within Ch4-2 are named according to their mouse HCN2 sequence numbering. The Ch4-2 K381E ΔXC channel is identical to the Ch4-2 ΔXC channel with the exception of the K381E mutation (Wicks et al., 2009, 2011). Initial introduction of the E457 point mutations (E457R, E457Q, E457C) in Ch4-2 ΔXC and Ch4-2 K381E ΔXC constructs was done through site-directed mutagenesis using type IIs restriction enzymes (Ko and Ma, 2005). Introduction of E457R mutation into other Ch4-2 construct backgrounds was completed using subcloning. Sequence of mutant constructs was verified by dideoxy sequencing (Eurofins Operon). All constructs

were subcloned into the pGEM-HE vector for high expression in *Xenopus laevis* oocytes as previously reported (Magee et al., 2015).

3.2.2. Electrophysiology

All channels were expressed as homomers from in vitro transcribed RNA injected into *X. laevis* oocytes, obtained using established procedures through ovariectomies following guidelines from the Canadian Council on Animal care (Magee et al., 2015). Two-electrode voltage clamp (TEVC) recordings for each construct or condition were obtained as described in Chapter 2 unless stated otherwise.

The isochronal activation protocol was as described in Chapter 2 using a 3-s activation epoch. The isochronal deactivation protocol stepped from the holding voltage to −130 mV for a 4-s activation epoch (as in Chapter 2), followed by a step to a larger number of voltages than in Chapter 2: between −120 mV and +40 mV (Δ20 mV) for a 4-s deactivation epoch (Figure 3-1), or for slow closing channels (i.e. CNB-fold truncations and channels with the K381E mutation) an 8-s deactivation epoch. The deactivation epoch was followed by a tail epoch at −120 mV and a second deactivation epoch at 0 mV for 5 s. This second deactivation epoch was performed to ensure all channels are in the closed state before returning to the holding voltage. Channel behaviour was typically stable over at least 10 minutes, as verified with a control protocol which was identical to the deactivation protocol except for it containing just a single sweep with a step from the activation epoch to 0 mV for the deactivation epoch. Oocytes were excluded from analysis if absolute tail currents differed by more than 100 nA in control protocols before and after the deactivation protocol.

Inside-out patch clamping recordings were obtained using solutions and procedures as described previously (Wicks et al., 2009, 2011). The isochronal deactivation protocol stepped from the holding voltage of −40 mV to −140 mV for a 4-s activation epoch followed by a step to voltages between −60 and −20 mV (Δ20 mV) for a 4-s deactivation epoch before returning to the holding voltage. Intracellular bath solution used was supplemented when needed with 5 µM cAMP. Cell-attached recordings were made during the course of the inside-out patch clamp procedure, after formation of seal and before excision of the patch.

3.2.3. Analysis

For kinetics, $t_{1/2}$ for deactivation and weighted-average time constant ($\tau_{weighted}$) for activation (following delay d) were determined as in Chapter 2. For conductance−voltage relations, the voltage giving 50% of maximal activity in an isochronal activation protocol is in this Chapter called Vact,but is identical to the "$V_{1/2}$" parameter described in Chapter 2. Vact was determined as in Chapter 2 using a 3-s activation epoch. In this Chapter I added a new parameter of interest for conductance−voltage relations: Vdeact, the voltage giving 50% of maximal activity in an isochronal deactivation protocol. For determining Vdeact, tail current values at −120 mV from the deactivation protocol (4-s or 8-s deactivation epoch) were fit to a four-parameter Boltzmann equation:

$$I = y_0 + \frac{a}{(1 + e^{-(V - V_{deact})/s})}.$$

The parameters (described previously in Ch. 2 and Magee et al, 2015) were *a* (maximum time-dependent HCN current amplitude), *s* (reciprocal slope factor), *Vdeact* (midpoint deactivation voltage), and y_0 (total maximum current).

I considered whether a 4-s deactivation epoch was sufficient to reach a steady state value of Vdeact. This was tested by calculating the relative conductance and hence Vdeact at various earlier time points across the deactivation epoch (see next paragraph), and finding that the Vdeact value did not change between 3-s and 4-s

Estimation of relative conductance at earlier time points during the deactivation epoch exploited our observation that in intact oocytes expressing HCN channels, the reversal potential for time-dependent HCN channel current was similar to the reversal potential for time-independent leak current, so that they could be approximated by a single value Erev. For each oocyte tested, the "initial current" ($I_{Initial}$) was measured at the initial time point of the deactivation epoch after capacitance clearance (usually <25 ms), and plotted against voltage (IV graph, Figure 3-1A, C). The $I_{Initial}$ datapoints were fit to a linear equation, and the Erev was the X-intercept of the linear fit (Figure 3-1C). This Erev value was then used to calculate total conductance ($g_{tot,t}$) from the observed current (I_t) at the various time points (t) at each deactivation epoch voltage (V):

$$g_{tot,t}(V) = \frac{I_t}{(V - E_{rev})}.$$

The deactivation epoch with V = −40 mV was omitted from $g_{tot,t}$ calculation due to Erev being typically between −30 mV and −40 mV producing large uncertainty in (V − Erev). Each $g_{tot,t}$ conductance was then leak corrected by subtracting the $g_{tot,t}$ conductance value at the end of the deactivation epoch at +20 mV in the same recording (g_{leak}, corresponding to HCN channels all closed)

$$g_{corr,t}(V) = g_{tot,t}(V) - g_{leak}.$$

This leak-corrected conductance was then normalized to the leak-corrected ($g_{corr,t}$) conductance value at the end of the deactivation epoch at −120 mV in the same recording (g_{HCNmax}, corresponding to HCN channels maximally open)

$$g_{Norm,t}(V) = g_{corr,t}(V) / g_{HCNmax.}$$

The final normalized ($g_{Norm,t}$) conductances were plotted against deactivation voltage and used to determine Vdeact (by Boltzmann fitting as for Vact) for the various time points t (e.g. 1, 2, 3 and 4 s).

The Vdeact value for 4 s matched the conventional Vdeact value derived from the tail epoch (I_{tail}). For example, for fast closing Ch4-2 channels, the normalized conductances and Boltzmann fits at 3 s and 4 s overlap almost completely proving that the conductance−voltage relation for Vdeact has reached steady state after a 4 s deactivation epoch (Figure 3-1B). For the slower closing Ch4-2 channels (i.e. CNB-fold truncations and channels with the K381E mutation) this protocol was repeated, however these channels did not reach steady state after a 4 s deactivation epoch. After the time of deactivation was increased to 8 s, the same protocol for determining normalized conductance at various time points was repeated and I was able to conclude that the slower closing Ch4-2 channels reached steady state after an 8 s deactivation epoch.

The Vdeact parameter reaching steady state is an important distinction from the isochronal Vact when it comes to examining thermodynamics of HCN channels. HCN channels undergo multiple transitions after activation (closed to open pore transition) epochs into different open states in intact oocytes. This includes the transition from Mode I to Mode II and the transition from unliganded to liganded channels. HCN channel activation kinetics are so slow that at weaker voltages (i.e. −90 mV) some of these open states of the channel are kinetically inaccessible over the three second

activation epoch in the activation protocol (see Figure 3-1D). Thus, the Vact fails to measure the true thermodynamics of the HCN channels. In contrast, given the stronger driving force of activation in the deactivation protocol (−130 mV for 4-s), I can assume that the HCN channels have been allowed to sample all available open states. Additionally, due to the faster kinetics of HCN deactivation, I can assume that the HCN channels have kinetic access to other thermodynamic states like CII that HCN channels are unable to sample during the activation protocol. Thus, Vdeact gives a more accurate reflection of the thermodynamics of HCN channels than Vact (Figure 3-1).

3.2.4. Structural superimpositions

A structural superimposition of the liganded hHCN1 structure (PDB accession number: 5U6P; Lee and MacKinnon, 2017) and liganded *C. elegans* eukaryotic CNG channel TAX4 (PDB accession number: 5H3O; Li et al., 2017) was done on PyMOL using the *align* command (The PyMOL molecular Graphics System, Version 2.3.2 Schrodinger, LLC.) to suggest possible conformational changes in the A' helix after liganded HCN channels open. Sequence alignment of human HCN1, mouse HCN2 and TAX4 was done using BLAST software (Altschul et al., 1990).

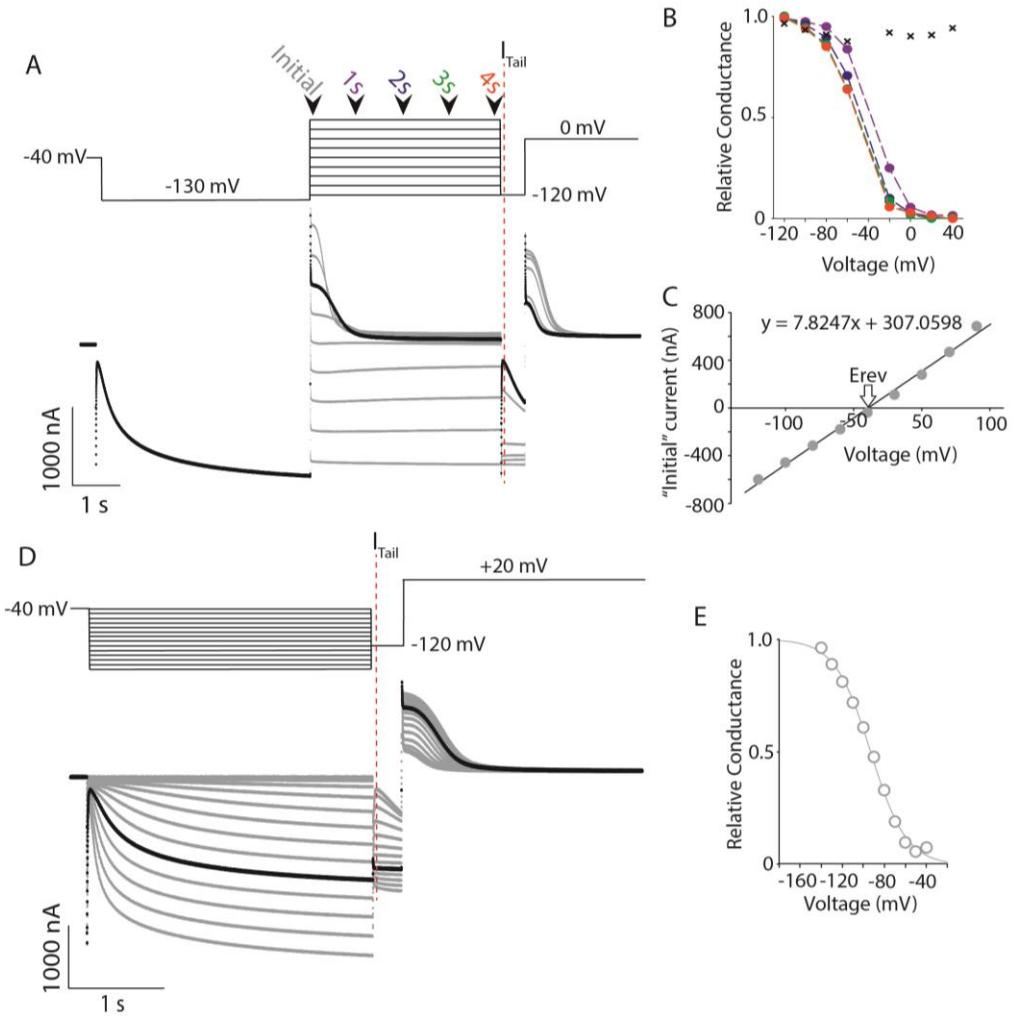

Figure 3-1: HCN channels have reached steady state for Vdeact measurements

A, *Top panel,* Voltage-clamp deactivation protocol for TEVC experiments. Different time points in the 4-s deactivation epoch shown with black arrowheads. The location of I_{Tail} measurement indicated with red dashed line. *Bottom panel,* Representative current of Ch4-2 channel during the deactivation protocol, current in gray except for the current from the 0 mV deactivation trace colored in black. Currents at the initial time point (gray) was used to calculate Erev (see Methods). Current at the 1 – 4 s time points were subsequently converted into relative conductance (see Methods). Tail current (I_{Tail}; red line) at −120 mV was used to calculate Vdeact in the conventional manner. **B,** Relative conductance values after 1-s (purple), 2-s (blue), 3-s (green), and 4-s (orange), calculated as described in Methods. Note that data points from 3-s (green) and 4-s (orange) overlap, suggesting that Vdeact is measured after the channels reach a steady state. Relative conductances ($g_{Norm,t}$) derived from the initial time point ($I_{initial}$) are shown as black crosses: if the conductance calculations were done correctly these values should be close to 1.0. **C,** Representative I−V graph of current ($I_{initial}$, from "initial" time point shown in panel *A*), fit to a linear equation. The X-intercept, calculated from the linear equation, is the Erev. **D,** *Top panel,* Voltage-clamp activation protocol for TEVC experiments. The location of I_{Tail} measurement indicated with red dashed line. *Bottom panel,* Representative current of Ch4-2 channels during the activation protocol, current in gray except for the current from the −130 mV activation trace colored in black. Tail current (I_{Tail}; red line) at −120 mV was used to calculate Vact. **E,** Activation conductance−voltage relationship for Ch4-2 I_{Tail} values from panel *D.*

3.3. Results

3.3.1. Rationale for Experimental Design

I hypothesized that interdomain interactions between the C-linker and the TM region facilitate the autoinhibition mechanism. There were multiple residues of interest in the A' helix of the C-linker that I could have targeted for mutagenesis. I first prioritized charged residues that were proposed to be in proximity with the TM region. This left a pool of residues that included D443, R446, R447, E451, K454, and E457. Of these D443 is already known to form a salt-bridge with R339 in the S4-S5 linker, and the D553N mutation in HCN4 channels can result in heart dysrhythmias like bradycardia (Decher et al., 2004; Netter et al., 2012; Ueda et al., 2004). Additionally, R447 and K454 form a potential binding site for $PIP_{2,}$ based on research in the spHCN channel (Flynn and Zagotta, 2011). I chose to prioritize residues that did not have a known functional role in HCN channel regulation, thus leaving R446 E451 and E457 as potential mutagenic targets. Of these residues, E457 was of particular interest to me, as it was found to be in close proximity to the TM region only in the open state, meaning it could regulate mechanisms involved in deactivation, which tends to be less researched historically (Kwan et al., 2012). Thus, I first chose to mutate the E457 residue in Ch4-2 channels. I predicted that the E457 residue in the C-linker would form an interaction with the transmembrane region, which could stabilize the open state of the channel.

Our previous results (see Chapter 2) showed that in intact oocytes there are multiple possible mechanisms for regulating gating kinetics in HCN channels, not just autoinhibition. In order to examine the effect of E457 mutation on the autoinhibition mechanism alone, I chose to use the Ch4-2 channel background. As shown in Chapter 2, this channel has OST and Quick-Activation disrupted, and therefore is only regulated by the autoinhibition mechanism. In the later part of this Chapter, I will present results from a derivative of Ch4-2 (Wicks et al., 2011) where deactivation kinetics are regulated only by the OST mechanism rather than autoinhibition.

Due to hysteresis in HCN channels caused by factors such as Mode Shift (see Chapter 1), conventional conductance−voltage relations and $V_{1/2}$ based on activation protocols are typically negatively shifted compared to the conductance−voltage relations and $V_{1/2}$ based on deactivation protocols. In this Chapter, I measured both types of $V_{1/2}$ values

which I distinguish by Vact (from an isochronal activation protocol, as in Chapter 2) and Vdeact (from an isochronal deactivation protocol). Importantly, I found that Vdeact reaches a steady state value within the deactivation epoch times used (4 to 8 s, see Methods section for details) in contrast to isochronal (3-s) Vact values. Thus, Vdeact is likely to give a more accurate reflection of the thermodynamics of HCN channels, and the measured Vact values are expected to be typically significantly more negative than the true activation midpoint (Figure 3-1). Notably, Vdeact can be used in replacement of Vact in correlation plots with deactivation $t_{1/2}$ to show that the Ch4-2 family of channels from Chapter 2 only display the autoinhibition mechanism, as OST and QA are disrupted (Figure 3-2, compare with Figure 2-4B). As discussed in Chapter 2, the concentration of endogenous cAMP in intact-oocyte experiments is high enough that Ch4-2 channels are assumed to be liganded during deactivation. I characterized an additional member of the Ch4-2 family, with a deletion of the extreme C-terminal region: Ch4-2 ΔXC. This channel deactivated faster and exhibited more negative Vdeact compared to full length Ch4-2 channels; this is consistent with the expectation (Zagotta et al., 2003) that the truncation of the extreme C-terminal region decreased cAMP binding, leading to decreased magnitude of autoinhibition relief by endogenous cAMP. The autoinhibition status of the Ch4-2 family members can be summarized as follows: Ch4-2 ΔCNB channels are autoinhibition- and augmented autoinhibition-free, Ch4-2 liganded channels are autoinhibition-relieved with augmented autoinhibition present, Ch4-2 ΔXC channels are partially autoinhibition-relieved with augmented autoinhibition present, Ch4-2 ΔαC are autoinhibited with augmented autoinhibition disrupted, and Ch4-2 R591E channels are autoinhibited with augmented autoinhibition present.

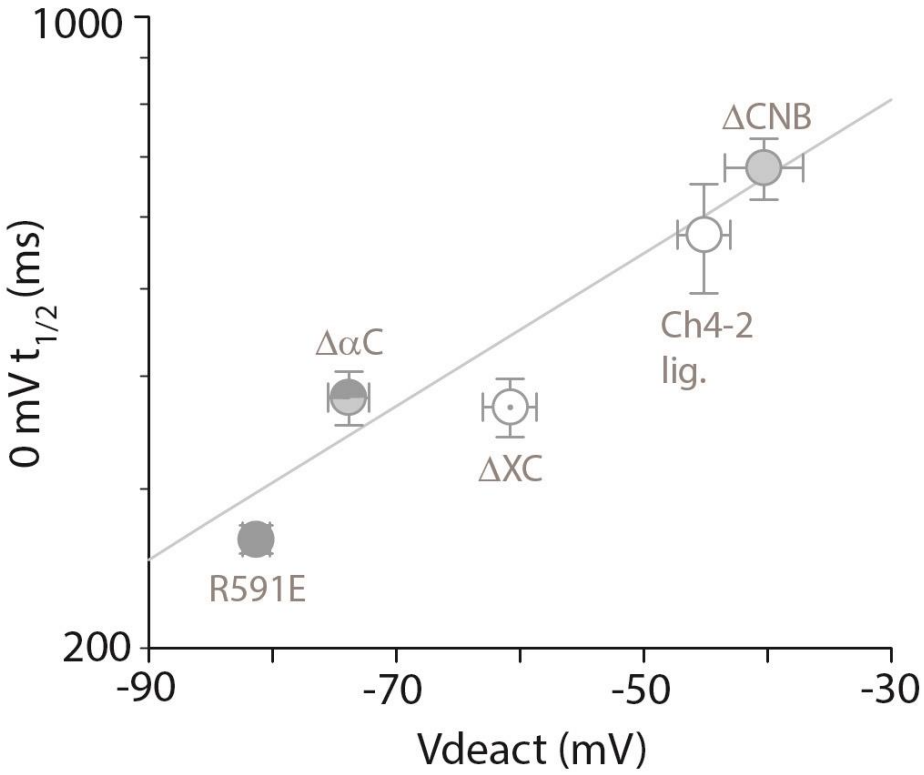

Figure 3-2: Ch4-2 family follows the autoinhibition mechanism during deactivation

Correlation plot of deactivation $t_{1/2}$ (0 mV) vs Vdeact, for the Ch4-2 family of channels (error bars shown are SEM). This figure is similar to Figure 2-5C except using Vdeact instead of Vact. The liganded Ch4-2 channel is represented by a grey empty circle, Ch4-2 R591E by dark gray circle, Ch4-2 ΔCNB by lightly filled grey circle, Ch4-2 ΔXC by grey dotted circle, and Ch4-2 ΔαC by grey half shaded circle. The datapoints are fit to an two parameter exponential decay equation ($t_{1/2}$ = a*exp(−b*Vdeact) representing autoinhibition, where the upper right portion of the fit (largest $t_{1/2}$ and most depolarized Vdeact) represents autoinhibition relief (open state stabilization) and the bottom left portion of the fit (smallest $t_{1/2}$ and most hyperpolarized Vdeact) represents autoinhibition (open state destabilization). Note that with Vdeact instead of Vact the Ch4-2 family still follows autoinhibition (as shown in Figure 2-5C), with the new channel Ch4-2 ΔXC more inhibited than Ch4-2 liganded channels as expected because extreme C-terminal deletion decreases the cAMP binding affinity of the CNB-fold (Zagotta et al., 2003).

3.3.2. A charge reversal mutation at E457 in A' helix speeds deactivation

To test if E457 generally helps stabilize the open state, I performed a charge reversal mutation of E457 in a full-length channel that can bind to cAMP (Ch4-2 E457R, Figure 3-3A) Under a simple conception of gating that we could call "parallel stabilization", if an E457R mutation resulted in thermodynamic destabilization of the open state then this should not only result in more negative Vdeact but should also be accompanied by kinetic destabilization of the open state (faster deactivation), and also kinetic stabilization of the closed state (slower activation).

I determined deactivation t1/2 values over a wide range of deactivation voltages (−80 mV to +40 mV). the E457R mutation resulted in kinetic destabilization of the open state, i.e. speeding of channel deactivation (Figure 3-3B, Table 3-2). The largest magnitude change was at −20 mV where the E457R mutation sped deactivation by 2.1-fold ($p < 0.0001$) (Figure 3-3B). The E457R mutation also resulted in a negative shift in the Vdeact by 26.0 ± 2.6 mV ($p<0.0001$) (Figure 3-3C; Table 3-1). This parallels our $t_{1/2}$ results, suggesting that the E457R mutation results in general destabilization of the open state.

Contrary to the notion of parallel stabilization, the E457R mutation did not affect activation kinetics in parallel with deactivation kinetics. Weighted-average time constants (τ_w) for activation (following delay d) were determined over a range of voltages for both Ch4-2 and Ch4-2 E457R but showed no significant difference ($p>0.2$; Table 3-2) (Figure 3-3D). Moreover, the Vact of Ch4-2-E457R (−93.9 ± 2.9 mV, n = 6) and Ch4-2 (−93.2 ± 3.2 mV, n = 8) were not significantly different ($p > 0.7$) (Figure 3-3E; Table 3-1). The lack of effect in Vact while Vdeact shows a large effect can be attributed to the distortions that are present in the isochronal Vact parameter that were discussed previously. However, the lack of effect in activation kinetics is not subject to this distortion. Combined this data suggests that glutamate 457 is forming an interaction that stabilizes the open state, and that the E457R mutation is disrupting this interaction, resulting in destabilization of the open state with a prominent effect on deactivation kinetics.

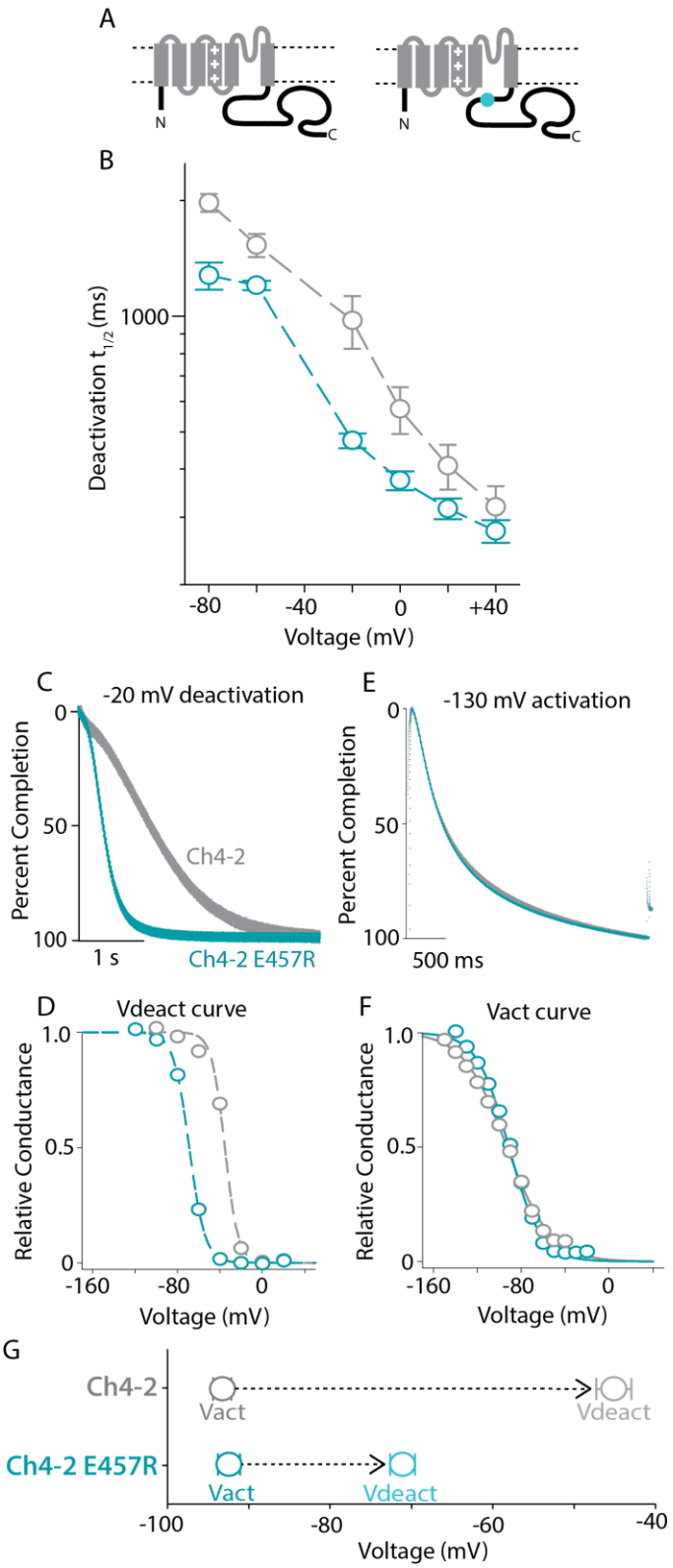

Figure 3-3: Effect of E457R mutation on Ch4-2 channels

A, Schematics of Ch4-2 channels, rectangles represent TM-helices, HCN2 sequence in black, HCN4 sequence in gray, teal circle indicating the E457R mutation **B**, Mean $t_{1/2}$ values with error

bars showing SEM, with ≥ 6 recordings for each channel: Ch4-2, gray empty circles; Ch4-2 E457R, teal empty circles. **C**, Representative deactivation currents at −20 mV, each normalized to total decay amplitude. Coloring as in panel *B*. For these example traces, the $t_{1/2}$ are as follows: Ch4-2, $t_{1/2}$ = 1028 ms; Ch4-2 E457R, $t_{1/2}$ = 431 ms. **D**, Deactivation conductance−voltage relationships for Ch4-2 and Ch4-2 E457R, coloring as in panel *B.* Boltzmann fit parameters of the representative curves are as follows: Ch4-2, −46.3 mV, s = 7.9 mV; Ch4-2 E457R, −68.8 mV, s = 7.4 mV. **E**, Representative activation currents at −130 mV, each normalized to total decay amplitude in the 3-s activation epoch. Coloring as in panel *B.* For these example traces, the lag (d) and τ_w values are as follows: Ch4-2 (gray), d = 230 ms and τ_w = 960 ms; Ch4-2 E457R (teal), d = 180 ms and τ_w = 880 ms. Note the lack of sigmoidicity in ΔCNB channels indicated by smaller d values. **F**, Activation conductance−voltage relationships for Ch4-2 and Ch4-2 E457R, coloring as in panel *B.* Boltzmann fit parameters of the representative curves are as follows: Ch4-2, −93.3 mV, s = 19.8 mV; Ch4-2 E457R, −91.3 mV, s = 14.5. **G**, Plot of mean Vact (darker color) and Vdeact (lighter color) values with error bars showing SEM, for Ch4-2 (grey) and Ch4-2 E457R (teal) channels. The hysteresis (difference between activation and deactivation voltage dependence) is represented by a dashed black arrow. Note the shift in Vdeact for Ch4-2 E457R channels decreases the size of the hysteresis.

I repeated the E457R point mutation in the Ch4-2 ΔXC channel with a lesser amount of cAMP-dependent autoinhibition relief. In this background, the E457R mutation (Ch4-2 E457R ΔXC) kinetically destabilized the open state, resulting in speeding of deactivation (Figure 3-4A), agreeing with the results from the full length Ch4-2 channel. The largest difference seen was at −20 mV, where Ch4-2 E457R ΔXC closed 1.5-fold faster than Ch4-2 ΔXC (Figure 3-4B). The Vdeact was also negatively shifted by 17.5 ± 3.4 mV (Figure 3-4C). Furthermore, activation Vact and activation kinetics showed no significant difference after introduction of the E457R mutation. From this I can conclude that the formation of the E457 interaction that stabilizes the open state is not dependent on the extreme C-terminal region.

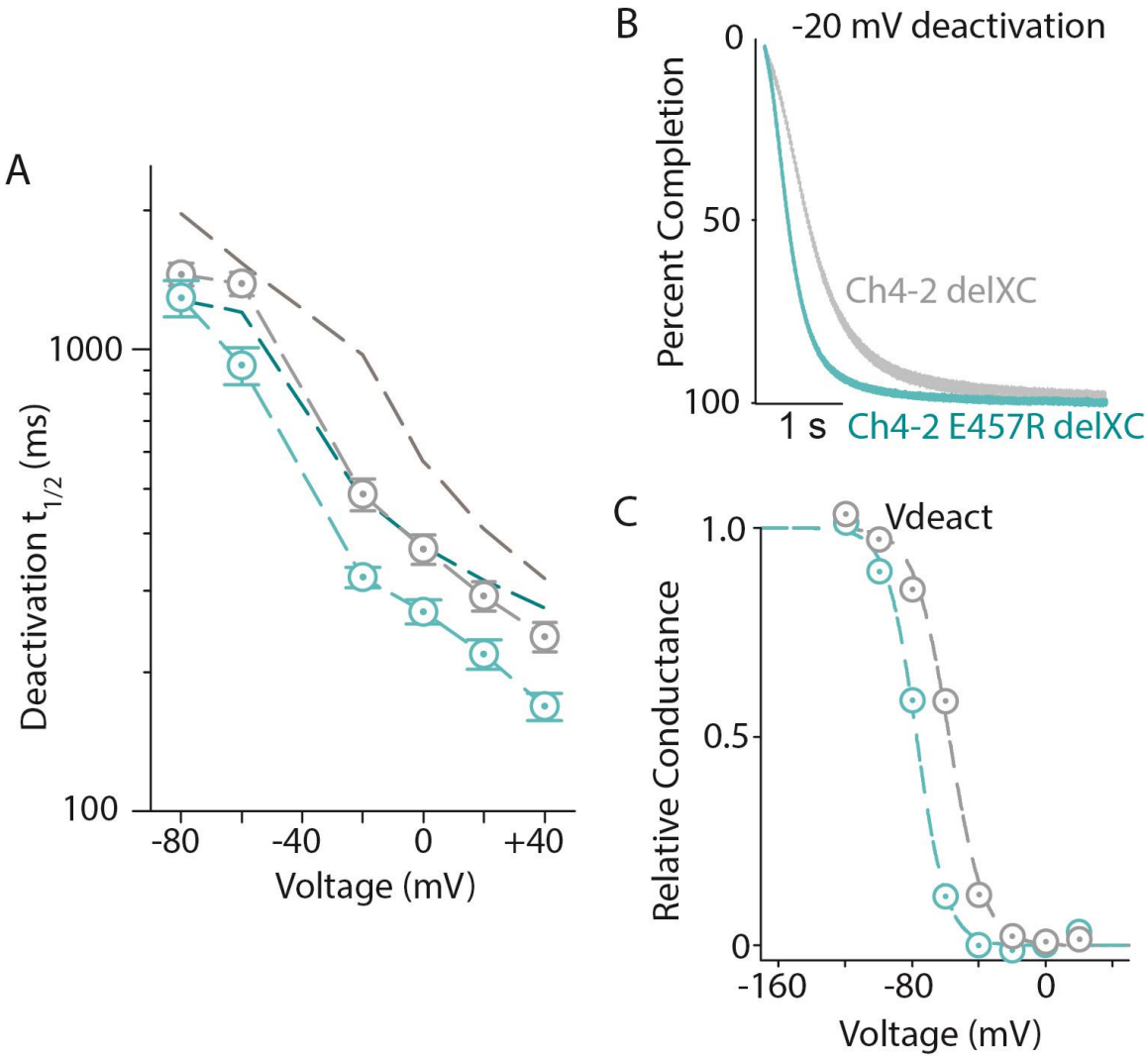

Figure 3-4: Effect of E457R is conserved in Ch4-2 ΔXC channels

A, Mean $t_{1/2}$ values with error bars showing SEM, with ≥ 6 recordings for each channel: Ch4-2 ΔXC, gray dotted circles; Ch4-2 E457R ΔXC, teal dotted circles. Dashed reference lines are shown representing the mean $t_{1/2}$ for full length Ch4-2 (dark gray) and Ch4-2 E457R (dark teal). Note that deletion of the extreme C-terminal region results in faster deactivation (dark gray line to gray data points) suggesting a decrease in cAMP binding as expected. **B,** Representative deactivation currents at −20 mV, each normalized to total decay amplitude. Coloring as in panel *A*. For these example traces, the $t_{1/2}$ are as follows: Ch4-2 ΔXC, $t_{1/2}$ = 500 ms; Ch4-2 E457R ΔXC, $t_{1/2}$ = 350 ms. **C,** Deactivation conductance−voltage relationship for Ch4-2 ΔXC and Ch4-2 E457R ΔXC, coloring as in panel *A*. Boltzmann fit parameters of the representative curves are as follows: Ch4-2 ΔXC, −57.7 mV, s = 10.1; Ch4-2 E457R ΔXC, −77.2 mV, s = 8.9 mV.

3.3.3. Open-state stabilization by E457 depends on interdomain interaction with HCN4 transmembrane region

Based on both structural and functional evidence (Kwan et al., 2012; Lee and MacKinnon, 2017) I had hypothesized that the E457-interaction is formed with a transmembrane region residue. To test this, I made the E457R mutation in an HCN2 ΔXC background, equivalent to replacing the transmembrane region of Ch4-2 E457R ΔXC with the transmembrane region of HCN2 (Figure 3-5A). The ΔXC channel was chosen instead of the full-length channel because the deletion of the extreme C-terminal region makes cloning of these channels substantially easier. Additionally, as discussed previously, the only known physiological effect of extreme C-terminal deletion is decreasing cAMP affinity, with no effect on the E457R phenotype. Notably, the introduction of the E457R mutation in HCN2 ΔXC channels had no effect on deactivation kinetics. The $t_{1/2}$ values of the HCN2 ΔXC channels with and without the E457R mutation are not significantly different (Figure 3-5A, B), and the Vdeact was negatively shifted only 4.4 ± 1.6 mV (Figure 3-5C; Table 3-1). These results suggested that the E457-interaction that stabilizes the open state in Ch4-2 channels had been disrupted by the HCN2 TM-replacement and consequently, I concluded that this interaction is formed with and dependent on structures of the HCN4 TM region.

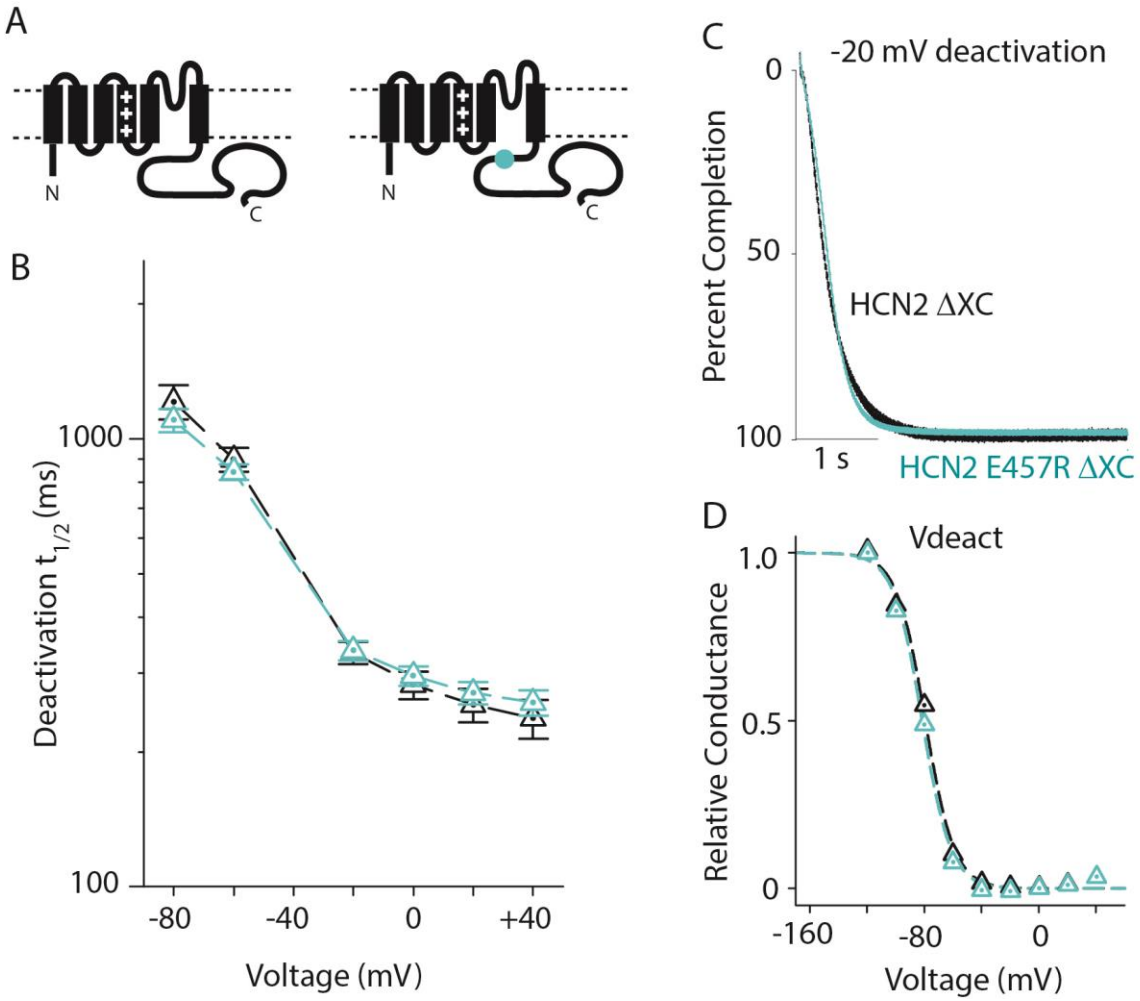

Figure 3-5: E457 forms an interaction with the TM region

A, Schematics of HCN2 ΔXC channels, rectangles represent TM-helices, HCN2 sequence in black, teal circle indicating the E457R mutation **B,** Mean $t_{1/2}$ values with error bars showing SEM, with ≥ 6 recordings for each channel: HCN2 ΔXC, black dotted triangles; HCN2 E457R ΔXC, teal dotted triangles. **C,** Representative deactivation currents at −20 mV, each normalized to total decay amplitude. Coloring as in panel *B*. For these example traces, the $t_{1/2}$ are as follows: HCN2 ΔXC, $t_{1/2}$ = 310 ms; HCN2 E457R ΔXC, $t_{1/2}$ = 310 ms. **D,** Deactivation conductance-voltage relationship for HCN2 ΔXC and HCN2 E457R ΔXC, coloring as in panel *B.* Boltzmann fit parameters of the representative curves are as follows: HCN2 ΔXC, −86.7 mV, s = 9.1; Ch4-2 E457R ΔXC, −84.1 mV, s = 12.1 mV.

3.3.4. E457-interaction stabilizes open state in autoinhibition-free channels

Based on the previous results I can imagine two potential models for the activity of the E457 interaction that stabilizes the open state in Ch4-2. I should note that, while I suggest that this interaction is a direct interaction between the E457 residue and the TM region, I cannot rule out that the E457-interaction actually occurs indirectly through a network of bonds, possibly including the HCN domain in the N-terminal region. In one model, the E457 interaction forms in all channels lacking autoinhibition. The alternative model would be that the E457 interaction only forms in full length, liganded channels. Under the first model, the E457R mutation would kinetically destabilize the open state of a channel with the CNB fold deleted, whereas no such effect would be observed under the second model.

I found that, as with Ch4-2 and Ch4-2ΔXC, the E457 residue stabilizes the open state of the Ch4-2 ΔCNB channel. The introduction of the E457R mutation resulted in kinetic destabilization of the open state, as deactivation $t_{1/2}$ values for Ch4-2 E457R ΔCNB were at least 1.2-fold smaller than Ch4-2 ΔCNB at depolarized voltages (i.e. 0 to +40 mV) (Figure 3-6A; Table 3-2). Due to the absence of autoinhibition, the ΔCNB constructs have slower deactivation kinetics and require an 8-s deactivation epoch to reach steady state Vdeact values. Although a full dataset with 8-s deactivation epochs was obtained for Ch4-2 E457R ΔCNB (n = 4 from two different frogs), the dataset for Ch4-2 ΔCNB is incomplete. Therefore Fig. 3-6A presents only the depolarized voltages from 4-s deactivation protocols where t1/2 values are significantly shorter than 4 s. Introduction of the E457R mutation resulted in a very significant negative shift in Vdeact of 30 ± 3.7 mV ($p<0.0001$) similar in magnitude to the shift in Vdeact resulting from the E457R mutation in the full length Ch4-2 channel (Figure 3-6B; Table 3-1). The measured Vdeact for Ch4-2 ΔCNB is expected to be more positive than the true steady-state Vdeact value due to the 4-s deactivation epoch. However, this error in Vdeact is expected to be limited (< 5 mV) because the steady-state value of Vdeact for Ch4-2 ΔCNB is unlikely to be more negative than that of Ch4-2 which has substantial autoinhibition relief through cAMP binding. Overall, the effect of the E457R mutation in autoinhibition-free Ch4-2 ΔCNB channels is comparable to what was seen in autoinhibition-relieved channels (full length Ch4-2). This is consistent with a model

where the E457-interaction stabilizes the open state by a similar mechanism in both autoinhibition-relieved and autoinhibition-free channels.

Another interesting observation of the Ch4-2 E457R ΔCNB channel is that this channel also displays kinetic stabilization of the closed state during activation, in parallel to the kinetic destabilization of the open state during deactivation. Activation $\tau_{weighted}$ values of Ch4-2 E457R ΔCNB were at least 1.5-fold larger ($p<0.001$) than those of Ch4-2 ΔCNB (Table 3-2). Additionally, the Vact of Ch4-2 ΔCNB was previously found to be −82.9 ± 5.2 mV (n = 11) (see Chapter 2), while the Vact of Ch4-2 E457R ΔCNB was −109.3 ±1.7 (n = 4), a significant negative shift of −26.3 ±1.8 mV ($p<0.0001$) (Table 3-1), although this difference may be due to a distortion from the slow activation kinetics. Notably, this result suggests that the introduction of the E457R mutation in the Ch4-2 ΔCNB channel reconstitutes the Quick-Activation mechanism that was disrupted by the HCN4 TM-replacement (see Figure 2-6). Introduction of the Quick-Activation mechanism did not affect the destabilization of the open state by the E457R mutation and understanding the additional effects of the E457R mutation on HCN channel activation will require further examination.

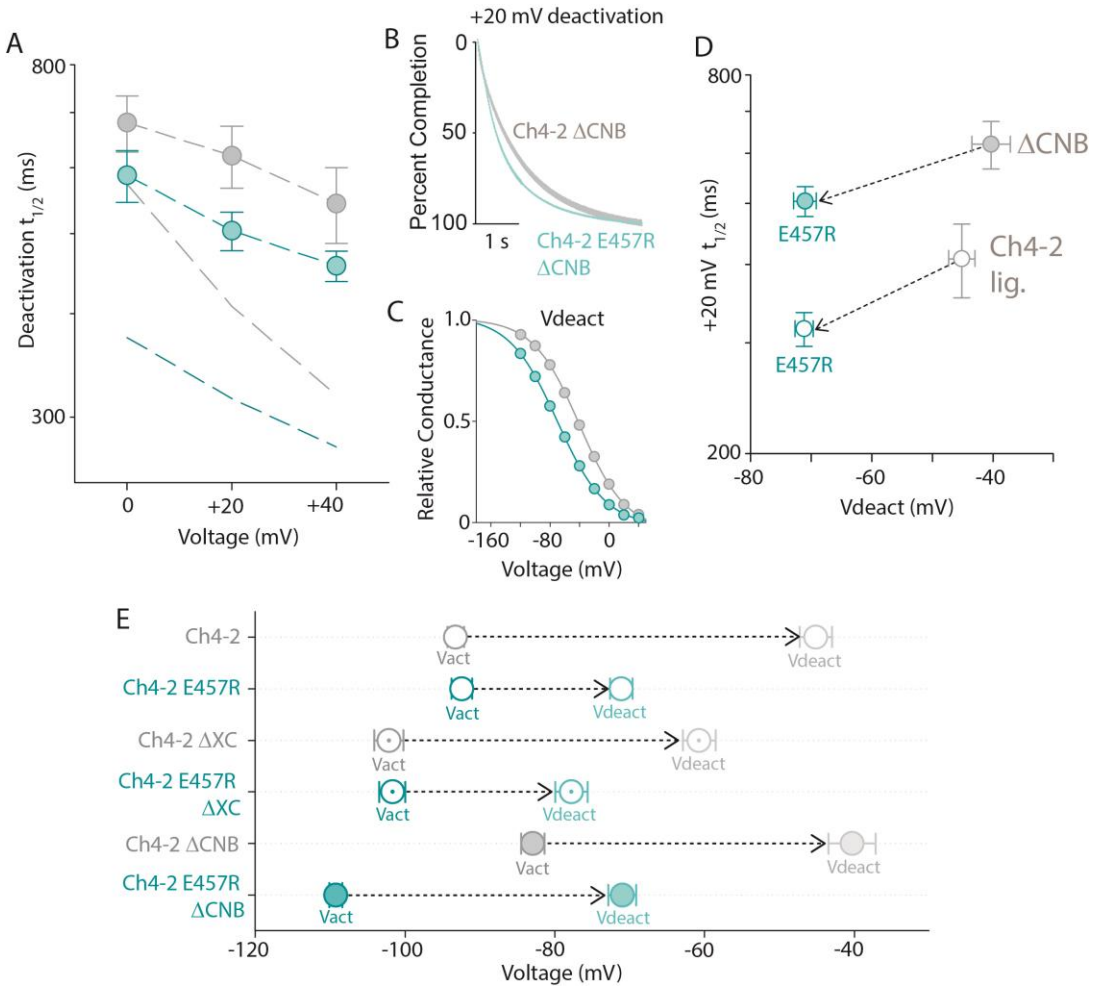

Figure 3-6: E457-interaction forms in autoinhibition-free channels

A, Mean $t_{1/2}$ values with error bars showing SEM, with ≥ 6 recordings for each channel: Ch4-2 ΔCNB, gray lightly shaded circles; Ch4-2 E457R ΔCNB, teal lightly shaded circles. Dashed reference lines are shown representing the mean $t_{1/2}$ for full length Ch4-2 (dark gray) and Ch4-2 E457R (dark teal). **B,** Representative deactivation currents at +20 mV, each normalized to total decay amplitude. Coloring as in panel *A*. For these example traces, the $t_{1/2}$ are as follows: Ch4-2 ΔCNB, $t_{1/2}$ = 675 ms; Ch4-2 E457R ΔCNB, $t_{1/2}$ = 606 ms. **C,** Deactivation conductance-voltage relationships for Ch4-2 ΔCNB and Ch4-2 E457R ΔCNB, coloring as in panel *A.* Boltzmann fit parameters of the representative curves are as follows: Ch4-2 ΔCNB, Vdeact = −45.0 mV, s = 30.1 mV; Ch4-2 E457R ΔCNB, Vdeact = −70.0 mV, s = 32.7 mV. **D,** Correlation plot of deactivation $t_{1/2}$ (0 mV, from panel *A*) vs Vdeact demonstrating the overall effect of the E457R mutation on the deactivation pathway. Lightly shaded symbols are for the ΔCNB channels, while empty circles are for the liganded (Ch4-2) channels. The datapoints for 457E (wild-type at 457, gray) and 457R (mutant, teal) are connected by a gray dashed arrow, showing the effect of the E457R mutation.**E,** Plot of mean Vact (darker color) and Vdeact (lighter color) values with error bars showing SEM of the following channels: Ch4-2 (grey, empty circle) and Ch4-2 E457R (teal, empty circle), Ch4-2 ΔXC (grey, dotted circle), Ch4-2 E457R ΔXC (teal, dotted circle), Ch4-2 ΔCNB (grey, lightly shaded circle), Ch4-2 E457R ΔCNB (teal, lightly shaded circle). Hysteresis is indicated by black dashed arrows.

3.3.5. E457-interaction stabilizes the open state in ΔαC autoinhibited channels but not in full length autoinhibited channels

A common presumption in the field is that the A' helix should change conformation between liganded (autoinhibition-relieved) and unliganded (autoinhibited) channels. Therefore, it seems reasonable that the E457 residue would change conformation in the unliganded, autoinhibited channel to destabilize the open state and enable autoinhibition. Based on this, I hypothesized that the contribution of the E457-interaction to open state stability would be removed in autoinhibited channels, leading to destabilization of the open state. The alternative hypothesis would be that the E457 interaction forms in the same way regardless of the autoinhibition status. If the formation of the E457 interaction that stabilizes the open state is dependent on autoinhibition being relieved I would expect that introduction of the E457R mutation would not affect the kinetic or thermodynamic stability of the open state in autoinhibited channels. If the E457 interaction forms in all Ch4-2 channels regardless of the autoinhibition status the E457R mutation will have the same effect on channel open states as in full length liganded channels (i.e. kinetic and thermodynamic destabilization of the open state).

As discussed in Chapter 2, Ch4-2 channels are cAMP-liganded during the deactivation epoch in intact oocyte experiments, but there are two derivatives available with autoinhibition imposed: (Chen et al., 2001b; Magee et al., 2015; Tibbs et al., 1998; Wainger et al., 2001; Wang et al., 2002):

(1) A channel with an intact CNB fold and the R591E mutation preventing cAMP binding, and

(2) A channel with the C-helix deleted (CNB fold is not intact).

Notably, the Ch4-2 R591E channel has augmented autoinhibition while Ch4-2 ΔαC does not, however I introduced the E457R mutation into both types of autoinhibited channels in order to investigate the E457 interaction that stabilizes the open state in autoinhibited channels with and without an intact CNB fold.

Surprisingly, I found that the introduction of the E457R mutation kinetically stabilized the open state of Ch4-2 R591E channel but kinetically destabilized the open state of Ch4-2 ΔαC. In Ch4-2 E457R R591E the $t_{1/2}$ over a range of voltages (−60 to +40 mV) was at least 1.6-fold larger and Vdeact was positively shifted by 12.8 ± 3.6 mV,

in comparison with Ch4-2 R591E (Figure 3-7A). In contrast, in Ch4-2 E457R ΔαC the $t_{1/2}$ was at least 1.5-fold smaller, and Vdeact was negatively shifted by 9.7 ± 3.1 mV, in comparison with Ch4-2 ΔαC and (Figure 3-7B). Combined, these results suggest that the E457 interaction that stabilizes the open state can form in ΔαC channels, but not in full-length R591E channels. A summary of the $t_{1/2}$ results from introducing the E457R mutation into the different channels is shown in Figure 3-7E. While introduction of the E457R mutation into the HCN2 ΔXC had no effect (black line), introduction of the E457R mutation into most Ch4-2 channels sped deactivation (grey line). In contrast, introduction of the E457R mutation into the full-length autoinhibited Ch4-2 R591E channel slowed deactivation (red line). I will examine the anomalous results of the Ch4-2 E457R R591E channel later, but first I will examine how the E457R mutation affects the autoinhibition mechanism in Ch4-2 ΔαC.

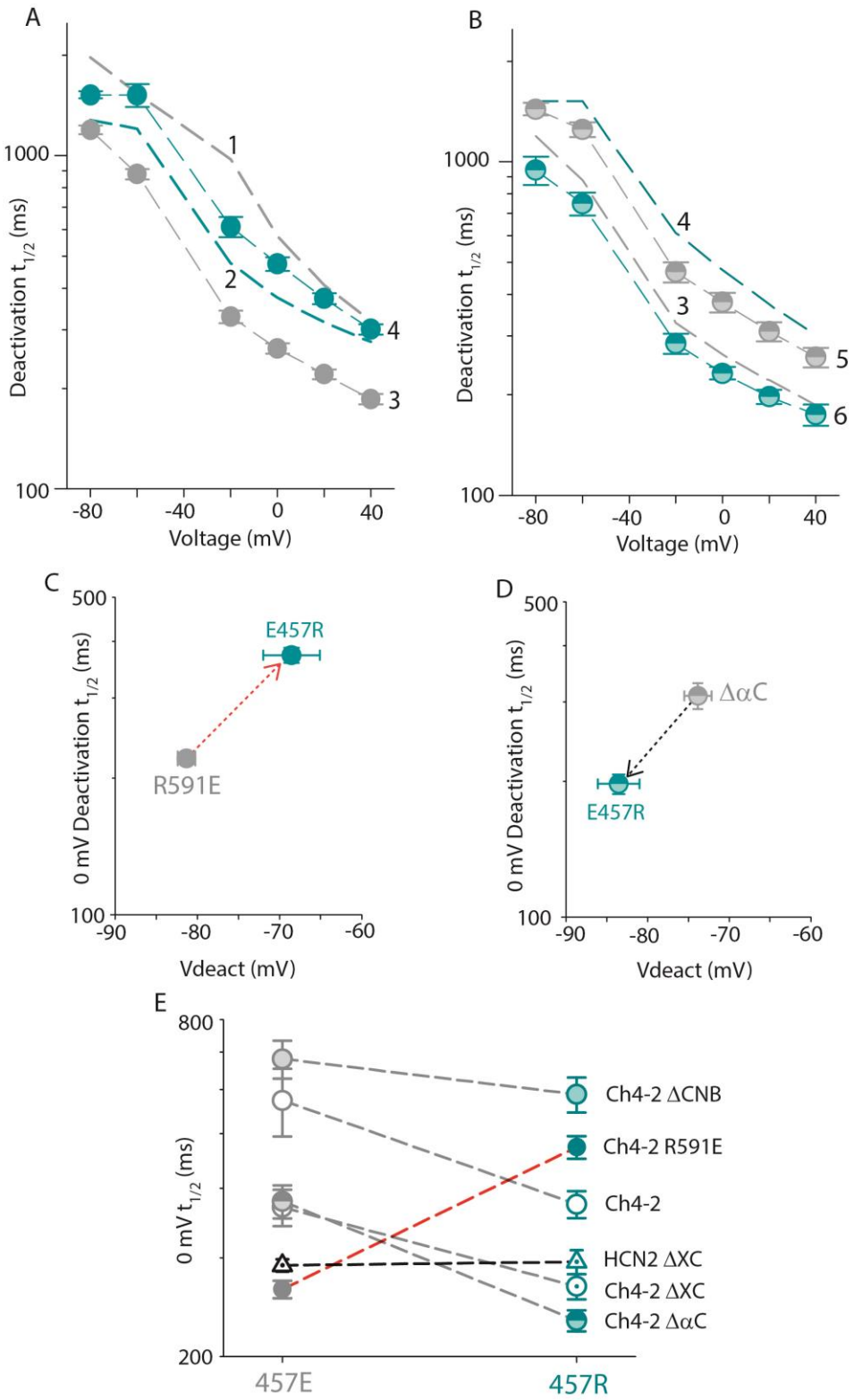

Figure 3-7: E457 changes conformation in autoinhibited channels

A, Mean $t_{1/2}$ values with error bars showing SEM, with ≥ 6 recordings for each channel autoinhibited channel: Ch4-2 R591E, gray filled circles (labelled 3); Ch4-2 E457R R591E, teal

filled circles (labelled 4). Dashed reference lines are shown representing the mean $t_{1/2}$ for full length Ch4-2 (dark gray; labelled 1) and Ch4-2 E457R (dark teal; labelled 2). **B,** Mean $t_{1/2}$ values with error bars showing SEM, with ≥ 6 recordings for each channel autoinhibited channel: Ch4-2 ΔαC, gray half-shaded circles (labelled 5); Ch4-2 E457R ΔαC, teal half-shaded circles (labelled 6). Dashed reference lines are shown representing the mean $t_{1/2}$ for the other autoinhibited channels: Ch4-2 R591E (dark gray; labelled 3) and Ch4-2 E457R R591E (dark teal; labelled 4). **C and D,** Correlation plot of deactivation $t_{1/2}$ (0 mV, from panel *A*) vs Vdeact demonstrating the overall effect of the E457R mutation on the deactivation pathway in autoinhibited channels. Labelling as in panel *B.* Half-shaded symbols are for the ΔαC channels, while filled circles are for the full-length Ch4-2 R591E channels. E457R mutants are in teal, while E457 (wild type) channels are in gray. The datapoints for Ch4-2 R591E and Ch4-2 E457R R591E are connected by a red dashed line, corresponding to the E457R mutation stabilizing the channel open state. The datapoints for Ch4-2 ΔαC and Ch4-2 E457R ΔαC are connected by a gray dashed line, corresponding to the E457R mutation destabilizing the channel open state. Note the length and slope of the gray and red dashed lines are almost identical, suggesting truncation after the beta-roll completely reverses the alternative E457R-phenotype displayed in Ch4-2 R591E channels. **E,** Mean $t_{1/2}$ at 0 mV, error bars show SEM (n ≥ 6 for all constructs), of all 457E and 457R channels, with dashed lines connecting corresponding channel backgrounds which are named at the right side. The typical or "classical" E457R phenotype, observed in channels with autoinhibition relieved or autoinhibition removed, is shown with gray dotted line. The alternative E457R effect in R591E channels is shown with red dotted line. No effect is shown with HCN2 channels shown with black dotted line.

3.3.6. The E457R mutation has opposite effects on the magnitudes of thermodynamic autoinhibition and kinetic autoinhibition

In order to examine the effect of the E457R mutation on the autoinhibition mechanism I added the E457R family to the correlation plot of deactivation $t_{1/2}$ vs Vdeact (Figure 3-2). I then fit the E457R data points (excluding Ch4-2 E457R R591E) to a straight line (exponential relation, on semilog plot) (Figure 3-8), as was done previously (Figure 3-2). As with the Ch4-2 family (Figure 3-2) the top right portion of the fit represents autoinhibition-relieved channels, while the bottom left portion of the fit represents autoinhibited channels. After introduction of the E457R mutation, the Vdeact values are not only shifted negatively but are notably limited to a narrower range of voltages. The range of Vdeact values within one family derives from the differences in thermodynamic autoinhibition within that family. Thus, I concluded that the autoinhibition mechanism has a decreased effect on thermodynamics after the introduction of the E457R mutation (Figure 3-8).

Recall that autoinhibited channels have faster deactivation (i.e. decrease in $t_{1/2}$ values) than to the autoinhibition-free channel (Ch4-2 ΔCNB). After introduction of the E457R mutation, the $t_{1/2}$ values are not only generally faster but are notably spread over to a wider range of times (on log axis). The range of $t_{1/2}$ values within one family derives from the differences in kinetic autoinhibition within that family. Therefore, introduction of

the E457R mutation magnifies or augments the effect of autoinhibition on deactivation kinetics. Thus, for instance, the E457R mutation in the autoinhibited ΔαC channel resulted in a larger decrease in $t_{1/2}$ compared to the E457R mutation in autoinhibition-free channel (Figure 3-8). In summary, the E457R mutation supresses the thermodynamic effect but augments the kinetic effect of the autoinhibition mechanism during deactivation.

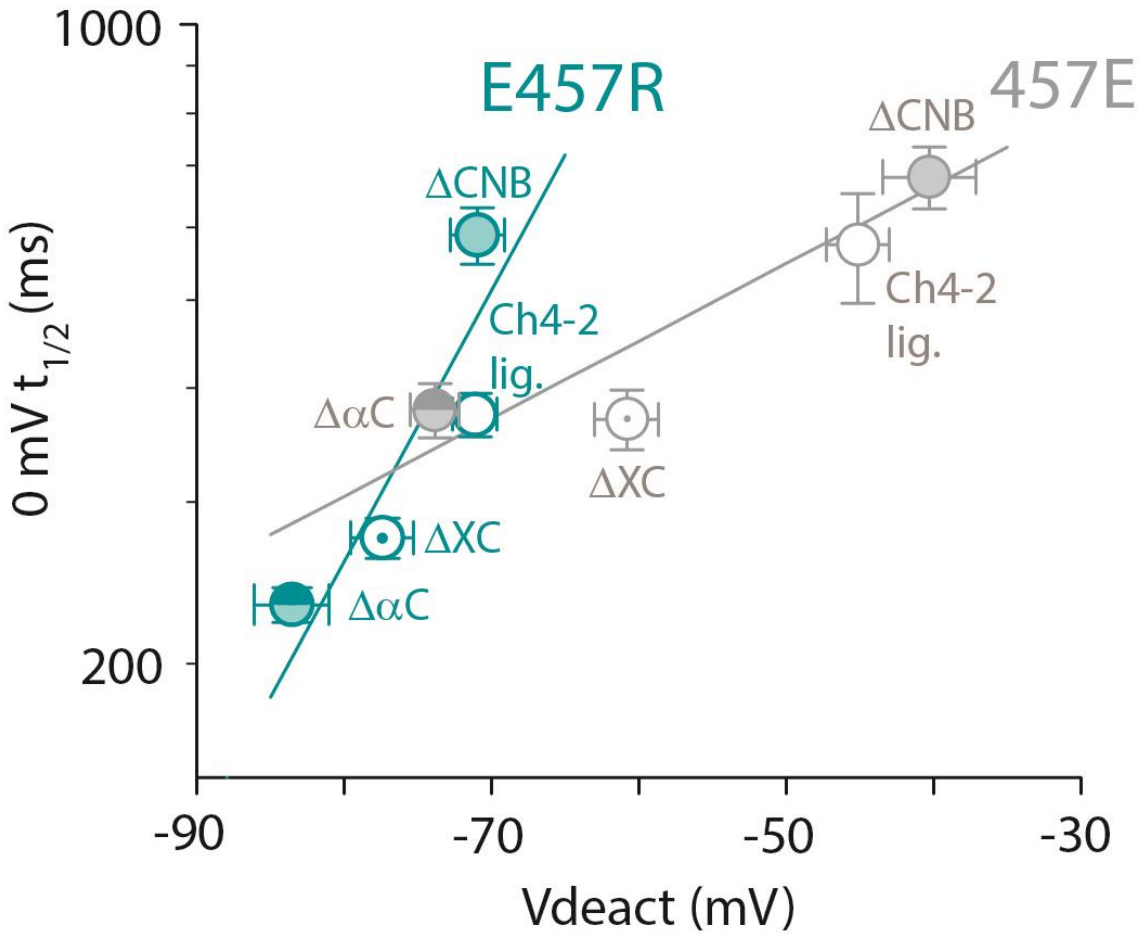

Figure 3-8: Introduction of the E457R mutation limits thermodynamic effects of autoinhibition while also disrupting autoinhibition in Ch4-2 R591E channels

Correlation plot of deactivation $t_{1/2}$ (0 mV) vs Vdeact, for the Ch4-2 family of channels before and after introduction of the E457R mutation (error bars shown are SEM). The liganded full-length constructs are represented by an empty circle, ΔCNB constructs by lightly filled grey circle, ΔXC constructs by grey dotted circle, and ΔαC constructs by grey half shaded circle. Datapoints for the R591E constructs are not included in panel *A.* Channels with the 457E residue are colored grey, while channels with the E457R mutation are shown in teal. The fit of the 457E family of channels from Figure 3-2 is shown again in grey. The datapoints from the E457R (teal) constructs (excluding R591E) are fit to an two parameter exponential equation ($t_{1/2}$ = a*exp(-b*Vdeact) representing autoinhibition, where the upper right portion of the fit (largest $t_{1/2}$ and most depolarized Vdeact) represents autoinhibition relief (open state stabilization) and the bottom left portion of the fit (smallest $t_{1/2}$ and most hyperpolarized Vdeact) represents autoinhibition (open state destabilization).

To quantify these results, I calculated the magnitude of thermodynamic autoinhibition during deactivation for the 457E and 457R families:

$$Thermodynamic\ autoinhibition\ =\ Vdeact\ (channel)\ -\ Vdeact\ (\Delta CNB)$$

The magnitude of thermodynamic autoinhibition after introduction of the E457R mutation was decreased by at least 2.8-fold in all channels (with the notable exception of Ch4-2 R591E) (Figure 3-9A). This suggests that the E457 interaction that stabilizes the open state plays an important role in the thermodynamics of the autoinhibition mechanism. Additionally, I calculated the magnitude of kinetic autoinhibition at 0 mV during deactivation for the 457E and 457R families

$$Kinetic\ autoinhibition\ =\ log\left[{t1/2\ (channel)}\Big/{t1/2\ (\Delta CNB)}\right]$$

The magnitude of kinetic autoinhibition after introduction of the E457R mutation was augmented by at least −0.1 in all channels, (with the notable exception of Ch4-2 R591E) (Figure 3-9B). This suggests that the E457 interaction also plays an important role in the kinetics of the autoinhibition mechanism. Combined these results suggest that the E457 residue normally augments the autoinhibition mechanism thermodynamically while simultaneously limiting the autoinhibition mechanism kinetically. Moreover, I can conclude that the E457 interaction that stabilizes the open state does not have parallel effects on the thermodynamics and kinetics of the autoinhibition mechanism.

In summary, I can conclude that there are various components contributing to the deactivation speed of the Ch4-2 E457R channel. Moreover, the $t_{1/2}$ at 0 mV for the cAMP-liganded Ch4-2 E457R channel in intact oocytes can be explained by the following: cAMP-relief of autoinhibition increases $t_{1/2}$ (kinetically stabilizing the open state) by 1.6-fold compared to the autoinhibited Ch4-2 ΔαC channel. This is a similar amount of cAMP-relief as occurs in Ch4-2 channels (1.5-fold compared to Ch4-2 ΔαC), suggesting that the amount of cAMP-relief is not affected by introduction of the E457R mutation. In addition, the E457R mutation decreases $t_{1/2}$ (kinetically stabilizing the open state) through two distinct mechanisms. First, there is the intrinsic speeding of deactivation that is the result of the E457R mutation by 1.2-fold (assumed based on the effect of the E457R mutation in Ch4-2 ΔCNB). Second, there is the augmentation of kinetic autoinhibition by -0.2, which corresponds to speeding by an additional 1.6-fold

compared to Ch4-2 ΔCNB (Figure 3-9B). I have not included the Ch4-2 E457R R591E construct in this analysis of the autoinhibition mechanism, and instead have considered the Ch4-2 E457R ΔαC channel as the autoinhibited channel. Although the Ch4-2 ΔαC channel has a smaller magnitude of thermodynamic autoinhibition than the full-length channel (Ch4-2 R591E thermodynamic autoinhibition = −41.0 ± 3.3 mV), the C-helix deletion still inhibits the Ch4-2 channel by −33.6 ± 3.6 mV.

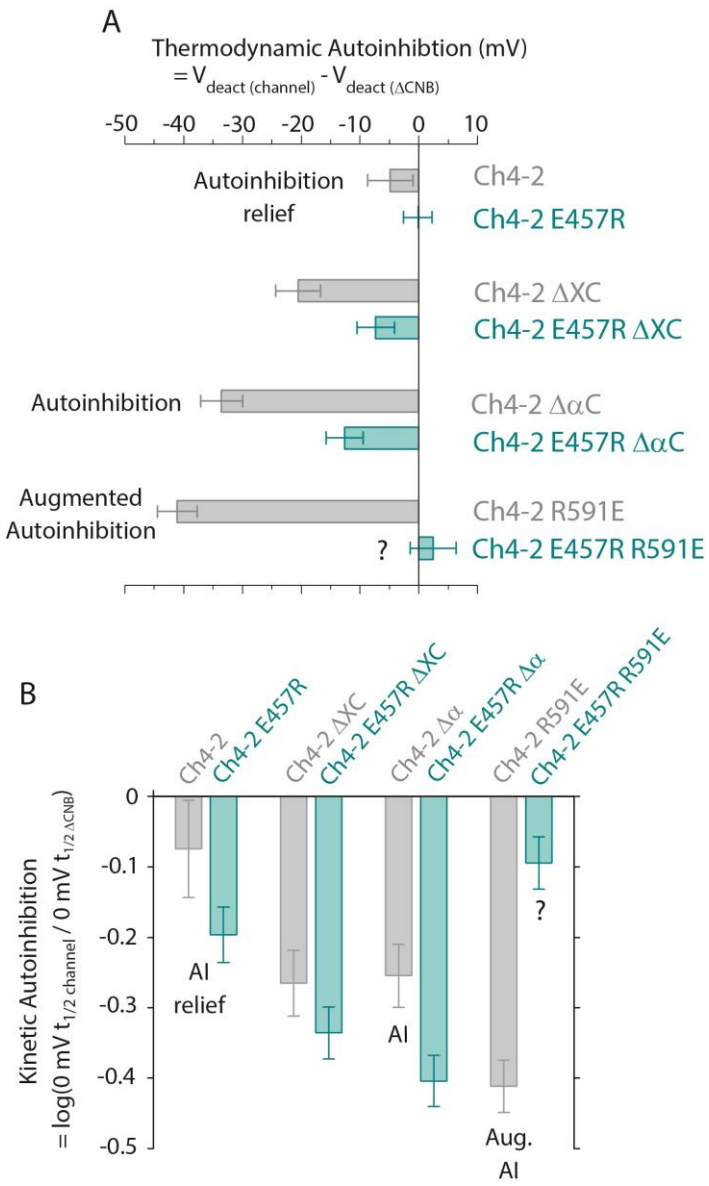

Figure 3-9: E457R mutation does follow parallelism with the thermodynamic and kinetic effects of autoinhibition

A, The magnitude of thermodynamic autoinhibition for each channel was calculated from that channel's mean Vdeact after subtracting the mean Vdeact of the corresponding ΔCNB channel (i.e. only sequence difference being 457E or E457R mutation). *Error bars* show uncertainties from error propagation using SEM as uncertainty of individual mean $V_{1/2}$ values. Channels with the 457E residue are colored grey while channels with the E457R mutation are colored teal. The state of autoinhibition for different constructs is indicated on the left. The question mark "?" is used to represent the possible disruption of autoinhibition in Ch4-2 E457R R591E constructs. **B,** The magnitude of kinetic autoinhibition for each channel was calculated from the log of the ratio of that channel's mean $t_{1/2}$ at 0 mV divided by the mean $t_{1/2}$ at 0 mV of the corresponding ΔCNB channel. *Error bars* show uncertainties from error propagation using SEM as uncertainty of individual mean $V_{1/2}$ values. Coloring as in panel *A.* The abbreviation "AI" (e.g. AI relief) represents autoinhibition, while the abbreviation "Aug." represents the word augmented. The question mark "?" is used to represent the possible disruption of autoinhibition in Ch4-2 E457R R591E constructs

3.3.7. The E457-interaction that stabilizes the open state forms in a channel with the open-state trapping mechanism

I examined whether the functional role of the E457 interaction would be affected by introducing a different gating mechanism controlling deactivation kinetics, such as open-state trapping (OST). As discussed in Chapter 1 & 2, in an autoinhibition model, channels with an intact CNB fold have a kinetically destabilized open state and hence faster deactivation compared to channels lacking the CNB fold (e.g. ΔCNB). The opposite is true in an OST model, so that channels with an intact CNB fold have slower deactivation compared to channels lacking the CNB fold (Wicks et al., 2011). Notably, cAMP-liganded HCN2 channels exhibit OST, so if the E457 interaction stabilizing the open state was incompatible with operation of OST, this could explain why the E457R mutation had no effect on deactivation kinetics of HCN2 ΔXC channels.

Although I showed in Chapter 2 that the open-state trapping (OST) mechanism is not detectable in Ch4-2 channels, previous work has shown that OST is the dominant factor controlling deactivation kinetics in Ch4-2 ΔXC channels that have a charge reversal mutation in the S4 voltage sensor, K381E (Wicks et al., 2011). Thus, liganded channels deactivated slower than unliganded channels, but both liganded and unliganded channels deactivated slower than channels with the C-terminal region deleted (ΔC), indicating that kinetic autoinhibition was not operating.

To test whether operation of the OST mechanism would change the functional role of E457, I determined the effect of E457R mutation in Ch4-2 K381E ΔXC. Previous studies of OST in Ch4-2 K381E ΔXC were in the inside-out excised patch configuration (Wicks et al., 2009, 2011), so this is the first characterization of this channel in intact oocytes. Compared to Ch4-2 ΔXC, introduction of the K381E mutation resulted in marked slowing of deactivation, for instance with 10-fold increase in $t_{1/2}$ at 0 mV (Table 3-2), similar to the phenotype previously observed in inside-out patch clamp. (Figure 3-10A). Within this sequence background, the introduction of the E457R mutation in Ch4-2 K381E ΔXC channels decreased $t_{1/2}$ by at least 1.8-fold over a range of voltages (-20 to +40 mV), and negatively shifted Vdeact by 43.3 ± 2.9 mV (Figure 3-10A-C; Table 3-1, 3-2). The E457 residue still exerts its most prominent effects on the deactivation pathway, as tau-weighted values were not significantly different after introduction of the E457R mutation in Ch4-2 K381E ΔXC (Table 3-1, 3-2). Combined, this data suggests

that even when the OST mechanism is present, E457 can still function to stabilize the open state of the channel. The lack of phenotype for E457R in HCN2 ΔXC possessing OST is not simply due to a lack of autoinhibition; rather it is due to some key residues lacking in the HCN2 TM region but present in the HCN4 TM region.

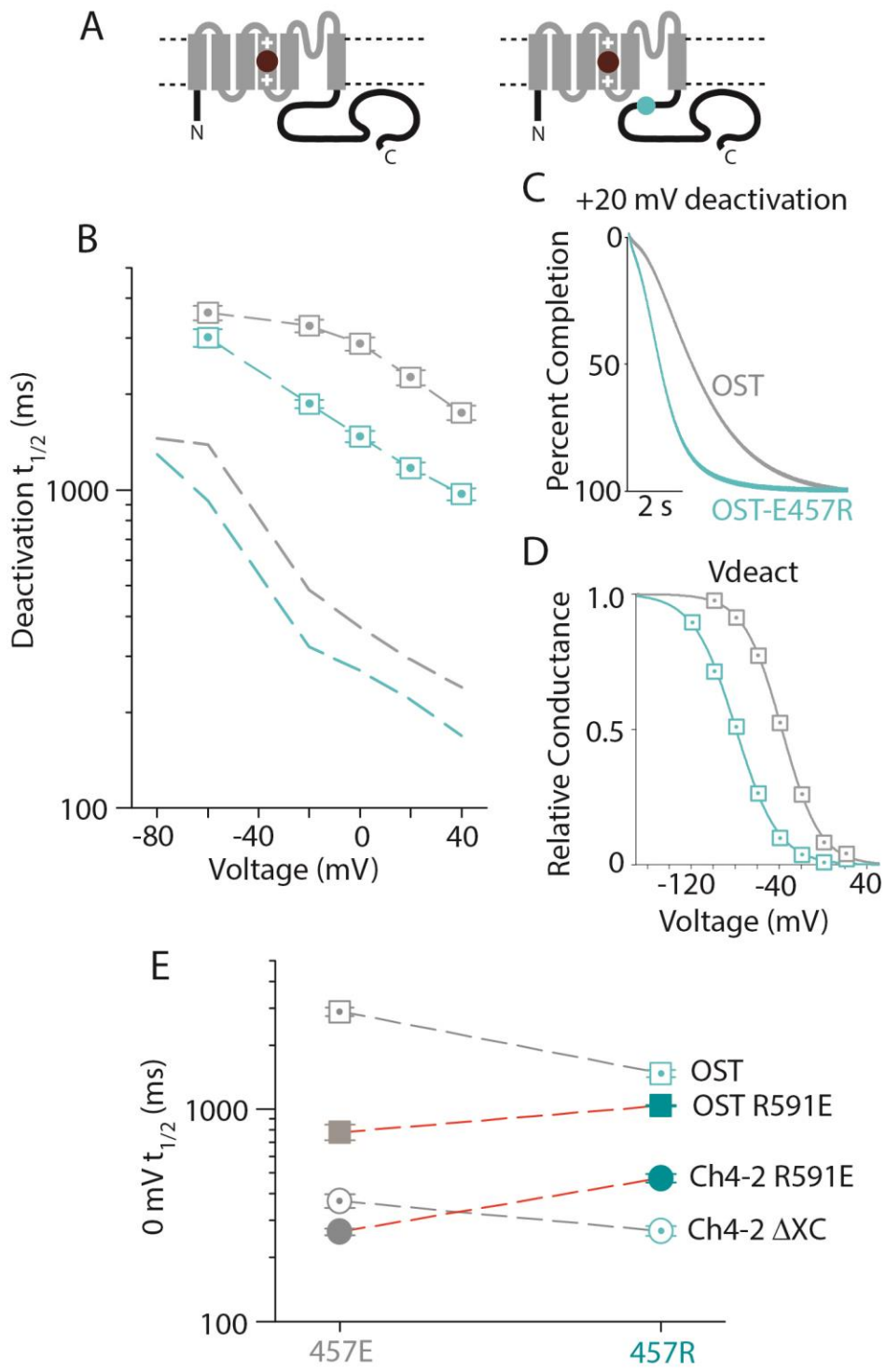

Figure 3-10: Addition of the OST mechanism does not change the effect of E457R and Mutation series suggest E457-interaction is a salt bridge

A, Schematics of Ch4-2 K381E ΔXC channels, rectangles represent TM-helices, HCN2 sequence in black, HCN4 sequence in gray, teal circle indicating the E457R mutation and red circle indicating the K381E mutation. **B,** Mean $t_{1/2}$ values with error bars showing SEM, with ≥ 6 recordings for each channel: Ch4-2 K381E ΔXC, gray dotted circles; Ch4-2 K381E E457R ΔXC,

teal dotted circles. Dashed reference lines are shown representing the mean $t_{1/2}$ for Ch4-2 ΔXC (dark gray) and Ch4-2 E457R ΔXC (dark teal) to show the successful addition of the OST mechanism to Ch4-2 channels. **C,** Representative deactivation currents at −20 mV, each normalized to total decay amplitude. Coloring as in panel *A*. For these example traces, the $t_{1/2}$ are as follows: Ch4-2 K381E ΔXC (labelled OST), $t_{1/2}$ = 2210 ms; Ch4-2 K381E E457R ΔXC (labelled OST-E457R), $t_{1/2}$ = 1150 ms. **D,** Deactivation conductance-voltage relationship for Ch4-2 K381E ΔXC and Ch4-2 K381E E457R ΔXC, coloring as in panel *B.* Boltzmann fit parameters of the representative curves are as follows: Ch4-2 K381E ΔXC, −38.4 mV, s = 17.3 mV; Ch4-2 K381E E457R ΔXC, −80.2 mV, s = 19.3 mV. **E,** Mean $t_{1/2}$ at 0 mV, error bars show SEM (n ≥ 6 for all constructs), of all 457E (gray) and 457R (teal) channels, with dashed lines connecting corresponding channel backgrounds. Ch4-2 channel symbols are circles and channels with the OST mechanism (K381E mutation) are squares. Extreme C-terminal deletion channels are dotted symbols and full length unliganded channels are filled symbols. The autoinhibition-relieved E457R effect is shown with gray dotted line, and the autoinhibited E457R effect is shown with red dotted line.

3.3.8. Mutation series in a channel with the Open-State Trapping mechanism suggests that the E457-interaction that stabilizes the open state is a salt-bridge

Due to the fact that the E457 residue is negatively charged I hypothesized that the E457-interaction that stabilizes the open state is a salt-bridge. To test this, I made a mutation series in the Ch4-2 K381E channels (E457Q and E457C). If the E457-interaction that stabilizes the open state relies on the charge of E457 then I would expect that the conserved E457Q mutation will have an intermediate deactivation speed compared to E457 and E457R. I exploited the fact that Ch4-2 K381E channels deactivate extremely slowly so that small changes in deactivation speed will be more easily observable than if I used the Ch4-2 background. In agreement with predictions I found that the introduction of the E457Q mutation sped deactivation by an intermediate amount: $t_{1/2}$ was decreased by at least 1.2-fold, compared to the E457R mutation which decreased $t_{1/2}$ by at least 1.8-fold. Similarly, introduction of the E457Q mutation negatively shifted Vdeact by 18.3 ± 3.4 mV, compared to introduction of the E457R mutation which negatively shifted Vdeact by 43.3 ± 2.9 mV (Figure 3-11A-C; Table 3-1, 3-2).

I further considered whether the size or shape of the E457 residue is important for formation of the E457 interaction that stabilizes the open state. Introduction of an E457C mutation into the Ch4-2 K381E ΔXC channel further sped deactivation kinetics compared to E457Q. The $t_{1/2}$ values were decreased by at least 1.5-fold, whereas E457Q sped deactivation by only 1.2-fold. Additionally, Vdeact was negatively shifted 13.8 ± 3.5 mV compared to Ch4-2 K381E ΔXC (Figure 3-11C). These results imply that

there is also a size or shape component to the E457 residue that is important, as the smaller cysteine mutation further sped deactivation from the glutamine mutation. Therefore, it is possible that surrounding residues may contribute to the overall effect of E457R. Taken together, this suggests that E457 is forming a salt bridge with a positively charged partner residue in the TM region. Moreover, I can conclude that complete disruption of the E457 interaction (both charge and shape) speeds deactivation by 1.5-fold, and the further speeding of deactivation seen after introduction of E457R is due to repulsion with the E457 partner residue.

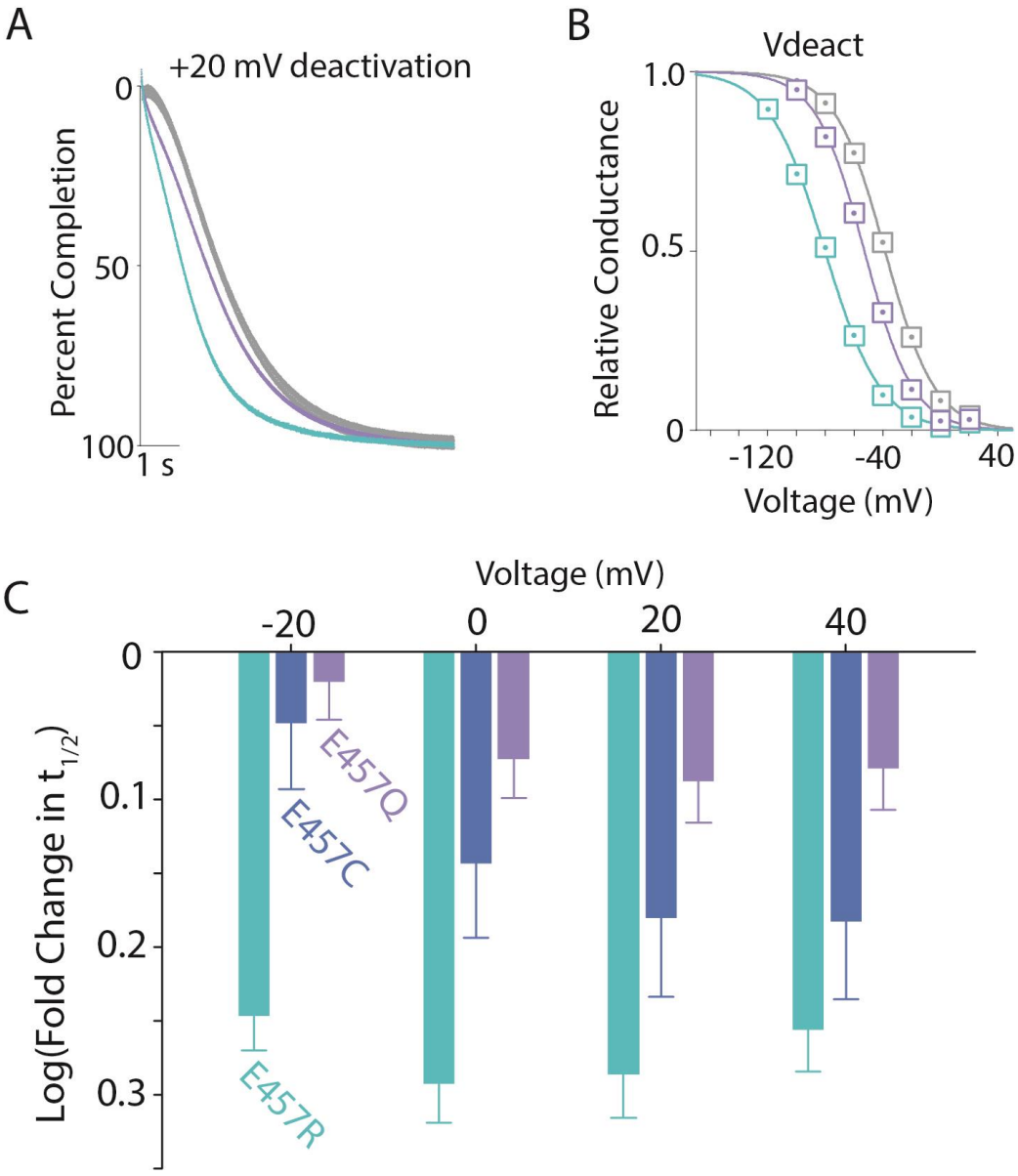

Figure 3-11: Mutation series shows charge is important for the E457 interaction

A, Representative deactivation currents at +20 mV, each normalized to total decay amplitude. The deactivation transient for the E457C mutation is not included for clarity. The Ch4-2 K381E ΔXC channel is shown in grey, while the E457R mutant is shown in teal and the E457Q mutant is shown in purple. For these example traces, the $t_{1/2}$ are as follows: Ch4-2 K381E ΔXC, $t_{1/2}$ = 2210 ms; Ch4-2 K381E E457R ΔXC, $t_{1/2}$ = 1061 ms; Ch4-2 K381E E457Q ΔXC, $t_{1/2}$ = 1813 ms. **B,** Deactivation conductance-voltage relationship for Ch4-2 K381E ΔXC, Ch4-2 K381E E457R ΔXC and Ch4-2 K381E E457Q ΔXC, coloring as in panel *A*. The deactivation conductance-voltage relationship for the E457C mutation is not included for clarity. Boltzmann fit parameters of the representative curves are as follows: Ch4-2 K381E ΔXC, −38.4 mV, s = 17.3; Ch4-2 E457R ΔXC, −80.2 mV, s = 19.3 mV; Ch4-2 E457Q ΔXC, −52.8 mV, s = 16.9 mV. **C,** Fold change and error in deactivation $t_{1/2}$ in Ch4-2 K381E ΔXC channels after introduction of the E457R (teal), E457C (blue) or E457Q (purple) mutation. Mean $t_{1/2}$ of each mutant was divided by mean $t_{1/2}$ of Ch4-2 K381E ΔXC at each voltage (-20 to +40 mV), and the logarithm of this ratio was subsequently calculated and graphed with the corresponding error values (calculated from SEM).

3.3.9. Proposal for conformation of an open, liganded HCN channel based on the CNG channel from *C.* elegans: TAX4

The proposed interaction of E457 should occur in the open state in order to achieve kinetic stabilization of this state, Unfortunately, while the recent structure of the HCN1 channel (Lee and MacKinnon, 2017) did identify multiple interactions between the TM region and the A' helix, the structure was only determined in the closed state. To examine potential TM region residues that E457 could interact with in the open state, I used the C-terminal region of a recent structure of the liganded CNG channel (Li et al., 2017) to propose a conformation for the A' helix in an open, liganded HCN channel.

CNG channels are related to HCN channels having both a putative voltage sensor, pore, C-linker and CNB-fold, but these channels do not respond to voltage and instead open only in the presence of cyclic nucleotides (Craven and Zagotta, 2006). I assumed that CNG channels have an S4 segment which is constitutively positioned in the "IN" conformation that would be formed by HCN channels during hyperpolarization. I used a recent cryoEM structure of a liganded, and therefore open CNG channel (*C. elegans* TAX4) (Li et al., 2017) to compare by superimposition with the closed human HCN1 channel. Sequence alignments of mouse HCN1 and TAX4 C-terminal regions (Lee and MacKinnon, 2017; Li et al., 2017) show that while the E457 residue is not conserved in the TAX4 channels, the sequences of the S6 and C-linker align without gaps. The TAX4 residue K415 is homologous to E415 in hHCN1 and E457 in mouse HCN2. In the open TAX4 channel, K415 of one subunit is in position to interact with the S4-S5 linker of the adjacent subunit and the S2-S3 linker of the neighbouring subunit's transmembrane region (Figure 3-12).

I then compared the conformation of the A' helix in the open-state TAX4 structure and the closed-state HCN1 structure. Upon opening, the A' helix swings outwards away from the center of the pore and upwards towards the TM region. In fact, TAX4 K415 is much closer to the TM region, specifically the C-terminal region of the S4 helix from the adjacent subunit, which contains positively charged residues. The C-terminal region of S4 has been found to inhibit the pore domain and is important for voltage response in spHCN channels (Flynn and Zagotta, 2018). While this region of S4 is conserved in all HCN subtypes, E457 could possibly interact with other TM region structures like the S2-S3 linker of the transverse subunit since the TAX4 K415 is also closer to the S2-S3

linker of the neighbouring subunit. Importantly, this linker contains multiple charged residues that differ in mouse HCN2 and HCN4 sequences.

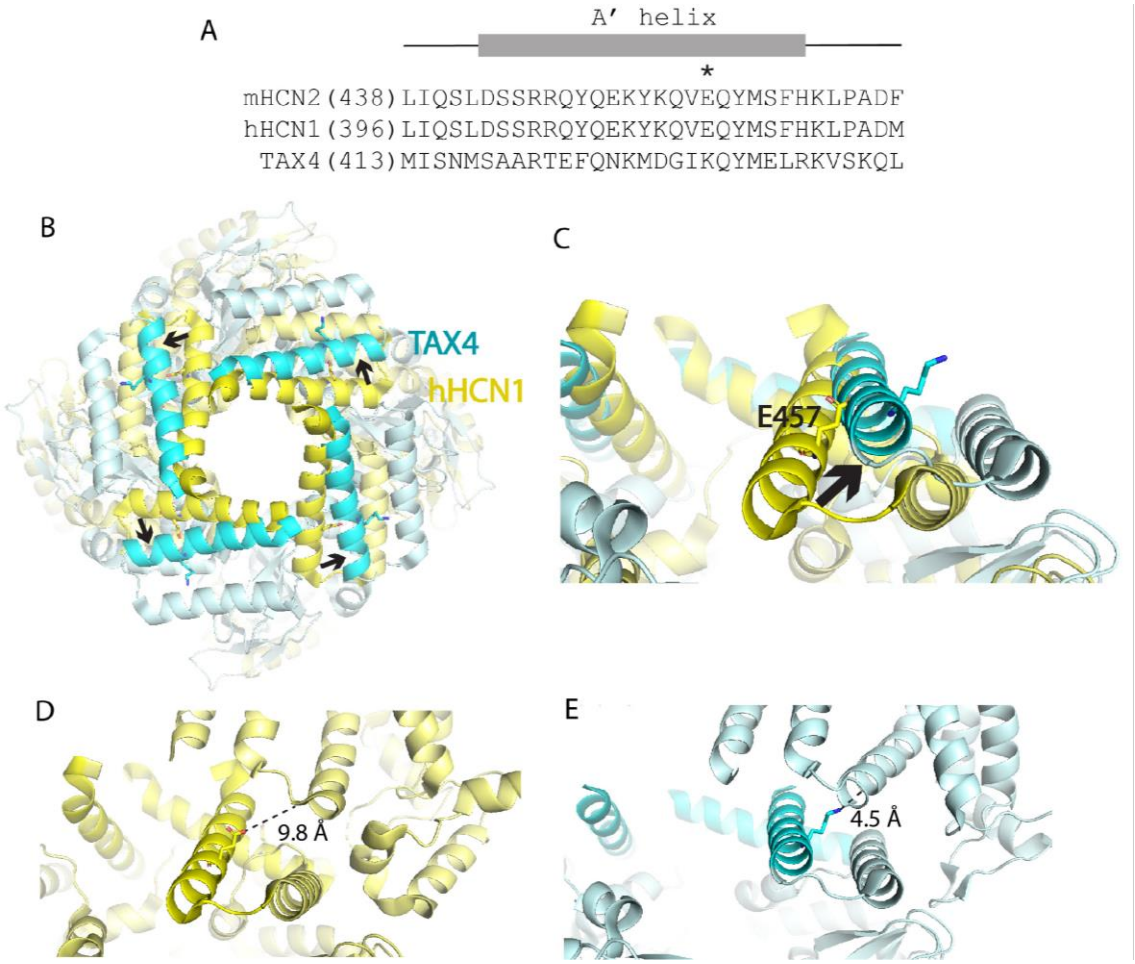

Figure 3-12: Structural superimposition of an open HCN channel using the TAX4 cGMP bound structure

A, Sequence of the mouse HCN2 (mHCN2) region proximal to the A' helix aligned to the sequence of the human HCN1 (hHCN1) channel and the sequence of the CNG channel TAX4. The A' helix is indicated above with a grey box and the 457E residue that was mutated in this work is indicated with a star. The hHCN1 and TAX4 channels have cryoEM structures published (Lee and MacKinnon, 2017; Li et al., 2017). **B,** Top down view of the C-terminal regions of the liganded hHCN1 and liganded TAX4 aligned structures. The hHCN1 structure is shown in yellow, TAX structure is shown in blue. The structure of the 457E residue (starred residue from panel *A*) is shown. This structural superimposition suggests that the A' helix moves outward away from the center axis when the channel opens (indicated with a black arrow). **C,** Side view of superimposition from panel *B,* centered on a single A' helix. Coloring as in panel *B.* Structure of the 457E residue starred from panel *A* shown and labelled. The structural superimposition suggests that not only does the A' helix move outward but it also moves upwards towards the membrane and TM helices (indicated with a black arrow). **D and E,** Individual structure of hHCN1 (panel *D*) and TAX4 (panel *E*) centered on the A' helix. Structure of 457E residue starred from panel *A* shown. Dashed black line demonstrates the distance between the 457E residue and the S4 helix in the TM region. Note that in the A' helix is closer to the TM region in the TAX4 structure (i.e. the structural superimposition for an open liganded HCN channel) than in the closed liganded hHCN1 structure.

3.3.10. Investigating the anomalous results from introducing the E457R mutation in full length R591E channels

Intact oocyte investigations

Recall that introduction of the E457R mutation into the Ch4-2 R591E channel resulted in unexpected stabilization of the open state. This was the only instance of the E457R mutation not destabilizing the open state in Ch4-2 channels. There are multiple potential models that could explain this anomalous result:

(1) The Ch4-2 E457R R591E channel is properly folded and all other channels in the Ch4-2 E457R family are either misfolded compared to the Ch4-2 family or have had cAMP potentiation disrupted.

(2) The Ch4-2 E457R R591E channel has undergone a conformational change in E457R, compared to the classical conformation of E457R found in the liganded Ch4-2 E457R channel. This alternative conformation results in the E457R mutation forming a reproducible interaction to stabilize the open state.

(3) The Ch4-2 E457R R591E channel displays the classical conformation of the E457R residue, but is misfolded in a different way, resulting in stabilization of the open state.

(4) The Ch4-2 E457R R591E channel is misfolded, resulting in the anomalous stabilization of the open state.

Notably, in the presence of the E457R mutation cAMP-bound channels close slower than unliganded channels, not faster as would be predicted by cAMP-dependent relief of autoinhibition (Figure 3-13). This is an unprecedented result that could suggest that model (1) is correct and cAMP potentiation has been disrupted in some way. However, Ch4-2 E457R ΔXC channels were more autoinhibited than Ch4-2 E457R, which would be as expected if Ch4-2 E457R ΔXC channels are a mixture of liganded (autoinhibition-relieved) and unliganded (autoinhibited) channels. To confirm that cAMP potentiation has not been disrupted in Ch4-2 E457R channels I can examine them under an IOPC configuration with and without cAMP in the bath solution. In order to verify this, I will have to change experimental configurations to inside-out patch clamping (IOPC). IOPC will allow me to control the concentration of cAMP in the bath solution, so that I can definitively show if the addition of cAMP to the bath potentiates the Ch4-2 E457R channel.

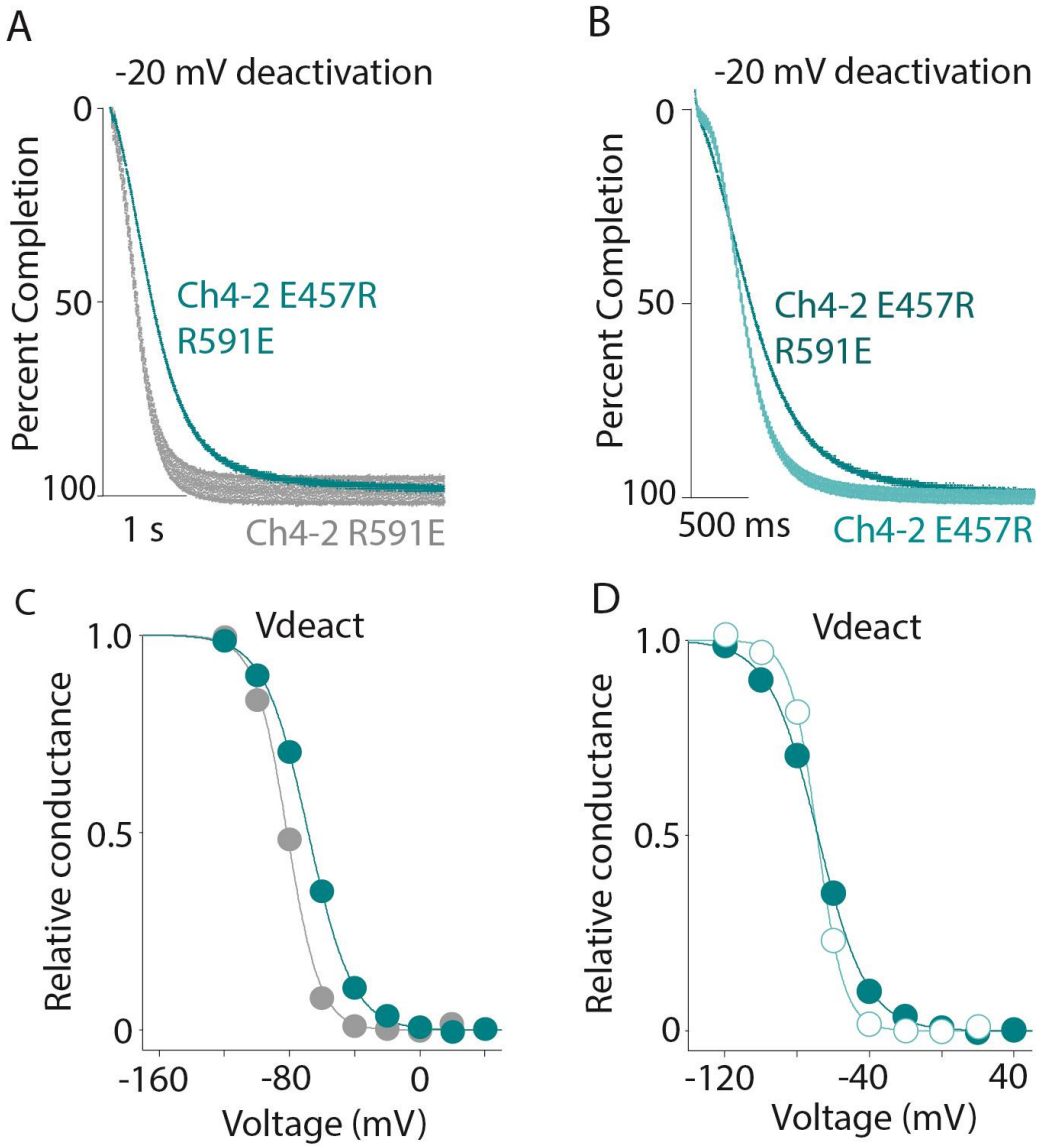

Figure 3-13: Ch4-2 E457R R591E channels close slower than Ch4-2 E457R

A, Representative deactivation currents at −20 mV, each normalized to total decay amplitude. Coloring as in panel *A*. For these example traces, the $t_{1/2}$ are as follows: Ch4-2 R591E, $t_{1/2}$ = 330 ms; Ch4-2 E457R R591E, $t_{1/2}$ = 670 ms. **B,** Representative deactivation currents at −20 mV, each normalized to total decay amplitude for Ch4-2 E457R R591E from panel *A* (dark teal) and Ch4-2 E457R (light teal). For these example traces, the $t_{1/2}$ of Ch4-2 E457R is $t_{1/2}$ = 431 ms. **C,** Deactivation conductance-voltage relationships for Ch4-2 E457R and Ch4-2 E457R R591E, coloring as in panel *A.* Boltzmann fit parameters of the representative curves are as follows: Ch4-2 R591E, −80.2 mV, s = 10.0 mV; Ch4-2 E457R R591E, −68.5 mV, s = 11.5 mV. **D,** Deactivation conductance-voltage relationships for Ch4-2 E457R R591E from panel *B* and Ch4-2 E457R (light teal), coloring as in panel *B.* Boltzmann fit parameters for Ch4-2 E457R R591E, −67.2 mV, s = 7.3 mV.

To further examine model (1) I chose to visualize the E457R phenotype in the context of the rest of the Ch4-2 family. To that end I added the R591E channels to the Ch4-2 family correlation plots of Fig. 3-8 (Figure 3-14). The Ch4-2 R591E channel is the most autoinhibited of the 457E family, and thus is located at the bottom left quadrant of the graph. In contrast, the Ch4-2 E457R R591E channel is located close to Ch4-2 E457R ΔCNB at the upper left quadrant of the graph, whereas Ch4-2 R591E is located close to the other autoinhibited channel Ch4-2 ΔαC in the bottom left quadrant of the graph (Ch4-2 ΔαC). This plot suggests the unlikely idea that the rest of the Ch4-2 E457R family of channels (except Ch4-2 E457R ΔCNB) are all more autoinhibited than the Ch4-2 E457R R591E channel, especially since all the rest of the Ch4-2 family of channels follow normal predictions for autoinhibition.

I did not consider the Ch4-2 E457R R591E channel as an autoinhibited channel in Chapter 3.3.6 (Figure 3-9) due to the anomalous result of the introduction of the E457R mutation slowing deactivation by at least 1.6-fold and positively shifting Vdeact by 12.8 ± 3.6 mV. When the magnitudes of thermodynamic and kinetic autoinhibition were calculated (i.e. Vdeact and $t_{1/2}$ compared to the respective parameters from the Ch4-2 E457R ΔCNB channel) the Vdeact and $t_{1/2}$ values of Ch4-2 E457R R591E channel suggest that the autoinhibition mechanism has been attenuated (Figure 3-14, Figure 3-9A, B). The magnitude of thermodynamic autoinhibition is approximately 0 mV (Figure 3-9A), while the magnitude of kinetic autoinhibition is decreased such that it is similar to that of the autoinhibition-relieved Ch4-2 channel (around −0.1; Figure 3-10B). Consequently, I can conclude that in Ch4-2 E457R R591E the effect of the autoinhibition mechanism on thermodynamics has been disrupted while the effect of the autoinhibition mechanism on kinetics has been attenuated. However, some kinetic autoinhibition is still detectable which distinguishes Ch4-2 E457R R591E from Ch4-2 E457R ΔCNB. Combined, these results lead me to propose that model (1) does not successfully explain the anomalous result. Additionally, these results argue against a scenario where the C-terminal region of Ch4-2 E457R R591E is unfolded in a random structure.

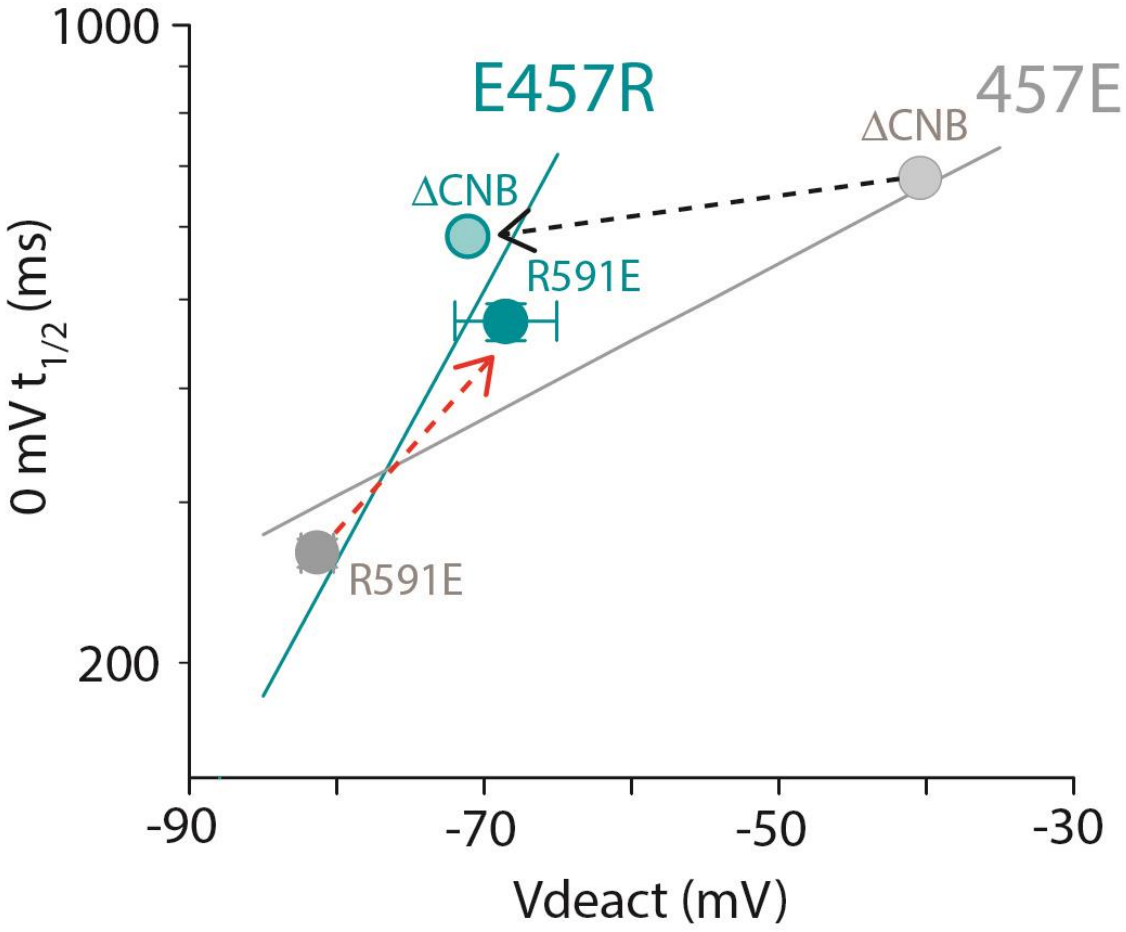

Figure 3-14: E457R mutation in Ch4-2 R591E channels disrupts autoinhibition

Correlation plot of deactivation $t_{1/2}$ (0 mV) vs Vdeact with the fit lines from panel *A.* The R591E constructs are shown as filled circles. The datapoints for ΔCNB constructs are shown for reference. Channels with the 457E residue are colored grey while channels with the E457R mutation are colored teal. Black dashed arrow shows the effect of introducing the E457R mutation to the Ch4-2 ΔCNB channel, while the red dashed arrow shows the effect of introducing the E457R mutation to the Ch4-2 R591E channel. Note how the directionality of the effect of introducing the E457R mutation in the Ch4-2 R591E channel is reversed compared to Ch4-2 ΔCNB.

In order to further examine the validity and reproducibility of the proposed alternative conformation of E457 in full length, unliganded channels (model 2) I introduced the E457R mutation into a second full length, unliganded channel: Ch4-2 K381E R591E. The introduction of the K381E mutation in unliganded channels was previously shown to partially disrupt the OST mechanism since unliganded channels closed slower than the C-terminal deletion construct, a result that is not predicted by the autoinhibition mechanism (Wicks et al., 2009, 2011). As expected, the Ch4-2 K381E R591E channel closed at least 3.3-fold faster than Ch4-2 K381E, indicating that Ch4-2 K381E R591E is unliganded (Figure 3-11E, Table 3-2). The addition of the E457R mutation to this unliganded channel slowed deactivation by at least 1.3-fold (Figure 3-11E, Table 3-2), although this did not result in a shift in Vdeact (Table 3-1). These deactivation results are in agreement with my previous findings that in full length, unliganded channels introduction of the E457R mutation slows deactivation, although the thermodynamic stabilization of the open state may be affected by the addition of the OST mechanism. Moreover, these results further suggest that model (4) is incorrect and that the C-terminal region of Ch4-2 E457R R591E is not unfolded in a random structure because this is a reproducible phenotype in multiple channel backgrounds.

The remaining two models (model (2) and (3)) are difficult to differentiate, however I prefer model (2) which conforms with the assumption from literature that the A' helix conformation changes between the liganded and unliganded states. Model (2) proposes that in Ch4-2 E457R R591E channels the mutant residue undergoes a conformational change out of the classical conformation and into an alternative conformation. Notably, when you compare the effect of introducing the E457R mutation in the two autoinhibited channels (Ch4-2 R591E and Ch4-2 ΔαC) you can see that truncation after the beta-roll has completely disrupted the alternative conformation of E457, allowing E457 to return to the classical conformation (Figure 3-7C, D). Combined with the results of the Ch4-2 E457R ΔXC channel these results suggest a model where the classical conformation of the E457 residue is such that it can form the TM-interaction which stabilizes the open state. However, when the full-length channel is unliganded the E457 residue is forced into an alternative conformation, which results in destabilization of the open state. The ability of the autoinhibited channel to change the E457 conformation is dependent on an intact extreme C-terminal region, as truncation after

the β-roll (ΔαC) and after the CNB fold (ΔXC) allows the E457 residue to change back into the classical conformation. Confirmation of model (2) will require further study.

Excised patch-clamp investigations

I used inside-out excised patch-clamp experiments to verify that Ch4-2 E457R can bind cAMP as predicted and to examine if the unliganded Ch4-2 E457R channel (analogous to the Ch4-2 E457R R591E channel) also undergoes a conformational change of the E457R residue compared to the liganded channel. Historically, cAMP binding is known to have multiple effects on HCN channels when using an IOPC configuration. In addition to slowing deactivation speed, cAMP binding is also expected to increase the maximum open probability (Pmax) of the channel, speed channel activation, and positively shift V1/2 (DiFrancesco and Tortora, 1991; Ludwig et al., 1998, 1999; Santoro et al., 1998). Based on the results from intact oocytes, in an IOPC configuration I would predict that Ch4-2 E457R channels should close slower in cAMP-free bath than in bath with a saturating concentration of cAMP (5μM), similar to how Ch4-2 E457R R591E closes slower than Ch4-2 E457R in intact-oocytes. At the same time, if Ch4-2 E457R is properly binding cAMP I would also expect that in the presence of a saturating concentration of cAMP the maximum open probability (Pmax) should increase, activation should be faster, and V1/2 should be positively shifted. If the Pmax has not increased, activation has not become faster and V1/2 has not been positively shifted then I would have to conclude that the Ch4-2 E457R channel is unable to bind cAMP, possibly due to a misfolded C-terminal region. However, if the previously stated predictions are correct then I could conclude that the E457R mutation not only disrupts but actually reverses the effect of cAMP potentiation. The last possible outcome is that Ch4-2 E457R does not follow predictions based on results from intact-oocytes, and instead deactivation would be slower in the presence of saturating cAMP concentrations than in the cAMP-free bath as predicted by normal cAMP potentiation. If this were true then I would conclude that the Ch4-2 E457R R591E deactivation results are anomalous, or possibly dependent on cellular factors.

Preliminary IOPC data with Ch4-2 E457R suggests that this channel can bind cAMP, since Pmax has increased, and activation is faster (Figure 3-1). However, deactivation speeds of Ch4-2 E457R were faster in cAMP-free bath and slower in the presence of saturating cAMP concentrations (Figure 3-15). This was not predicted

based on intact-oocyte results and suggests that Ch4-2 E457R R591E results are possibly dependent on cellular factors. In other words, if model (2) is correct then the conformational change of E457R to the alternative conformation requires a cellular factor, the activity of which is disrupted by truncation of the extreme C-terminal region.

There are various cellular factors that have been previously found to bind to HCN channels, any of which could facilitate the Ch4-2 E457R R591E phenotype. For example, the lipids PIP2 and cholesterol are known to bind all HCN subtypes, although the exact binding sites in the transmembrane region have not been identified, one PIP2 binding site has been identified in the C-linker. Additionally, a caveolin binding domain that is conserved in all HCN subtypes has been identified in the N-terminal region. Lastly, different scaffold proteins have been implicated in binding to the extreme C-terminal region and the accessory protein TRIP8b binds to a region around the C-helix.

To test if the Ch4-2 E457R R591E conformational change from the classical conformation to the alternative conformation is dependent on cellular factors, I plan to perform both cell-attached and inside-out patch clamp configurations on Ch4-2 E457R R591E. I would predict that Ch4-2 E457R R591E would have slower deactivation during cell-attached recordings than after membrane excision has occurred, and that after membrane excision Ch4-2 E457R R591E will close at a similar speed as excised Ch4-2 E457R in cAMP-free bath. Preliminary cell-attached recordings of Ch4-2 E457R R591E do display slower deactivation than after excision (Figure 3-15). This slowing of deactivation was not dependent on PIP2, as deactivation became faster immediately upon excision and the rundown of PIP2 concentrations over time (Pian et al., 2006, 2007; Zolles et al., 2006) did not affect deactivation speed (Figure 3-15). It is possible that this speeding could occur due to binding of PIP2 and a second PIP2-binding site which has a much faster, or immediate off-rate due to dissociation not hydrolysis. If this is true, applying exogenous PIP2 to the excised patch would restore the slow deactivation phenotype that was observed in cell-attached recordings. This suggests that the alternative conformation of E457R is dependent on cellular factors that are disrupted by excision from the membrane, like scaffolding proteins.

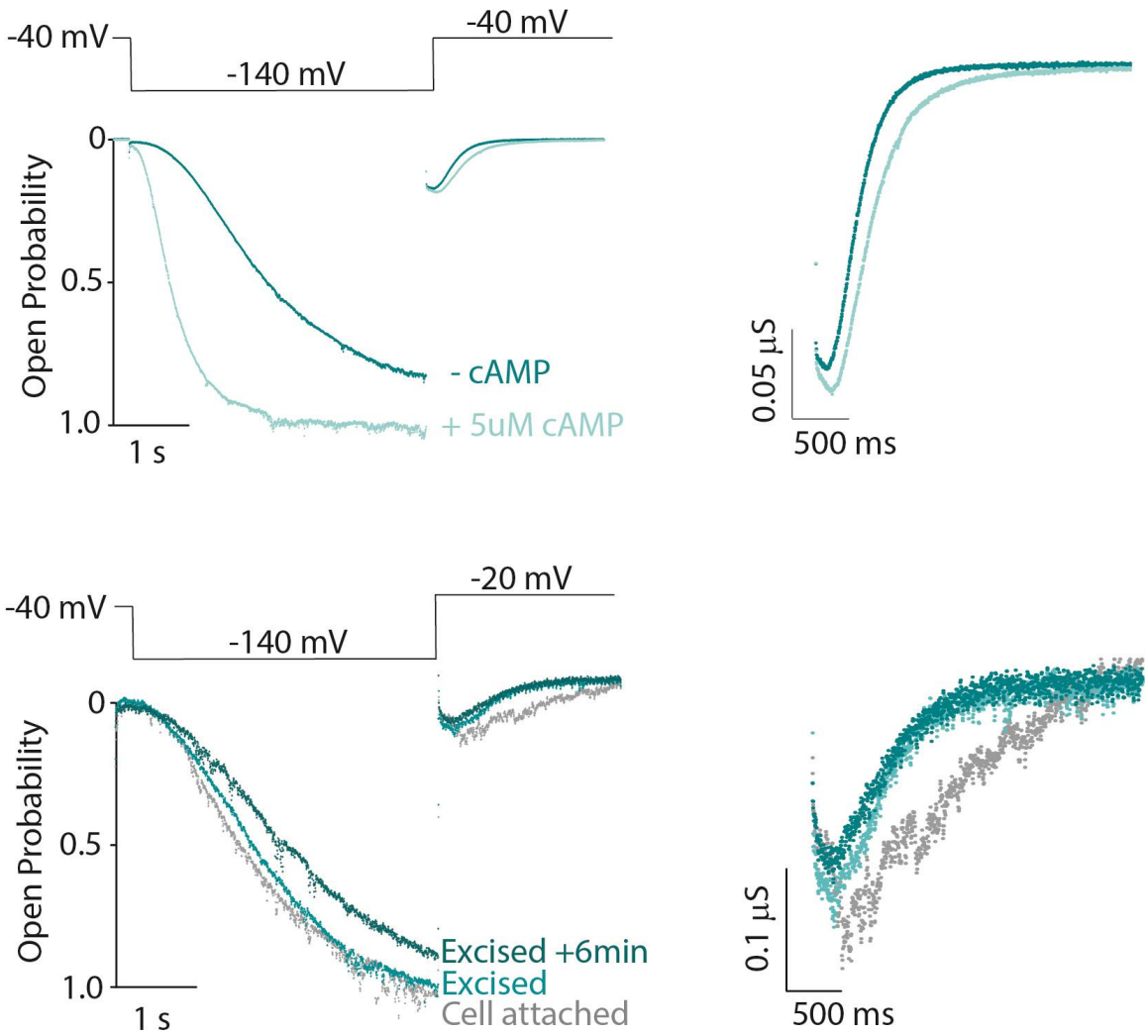

Figure 3-15: Effect of E457R mutation using the inside out patch clamp configuration

A, *Top panel,* Voltage-clamp protocol for IOPC showing the deactivation epoch of only one voltage: −40 mV. *Bottom panel,* Representative normalized current of Ch4-2 E457R in an excised membrane patch after 6 min to allow for rundown to occur. Current from representative excised membrane patch was normalized to maximal conductance in the 4-s activation epoch. Dark teal corresponds to recordings with a bath solution without cAMP, while light teal corresponds to recordings with a bath solution supplemented with 5µM cAMP. Note that cAMP appears to bind properly to Ch4-2 E457R as the open probability and activation speed of the channel have increased. **B,** Deactivation epoch from panel *A* at −40 mV, coloring as in panel *A.* Note that Ch4-2 E457R deactivation is slower when the bath is supplemented with saturating cAMP concentrations (light teal). **C,** *Top panel,* Voltage-clamp protocol for IOPC showing the deactivation epoch of only one voltage: −20mV. *Bottom panel,* Representative normalized current of Ch4-2 E457R R591E in both a cell-attached patch (gray, labelled *Cell attached*) and an excised patch both immediately after excision (teal, labelled *Excised*), and after 6 min to allow for rundown to occur (dark teal, labelled *Excised +6 min*). **D,** Deactivation epoch from panel *C* at −20 mV, coloring as in panel *C.* Note that Ch4-2 E457 R591E deactivation is slower in the cell-attached patch (gray) than after excision (light teal), and rundown of PIP2 does not affect deactivation speed (dark teal).

Since the activity of the cellular factor is disrupted by C-helix deletion, I propose limiting possible cellular factors to those that interact with the cytosolic domains, which would allow direct interaction with the extreme C-terminal region. Multiple cellular factors in addition to cyclic nucleotides bind to the cytosolic regions of HCN channels, any of which could potentially be facilitating the forced conformational change in unliganded Ch4-2 channels (i.e. Ch4-2 R591E). The brain-specific accessory protein TRIP8b is known to bind HCN2 channels around the C-helix, although TRIP8b is not normally expressed in *X. laevis* oocytes, it is conceivable that a homologous accessory protein could bind there in intact oocytes (Santoro et al., 2004; Saponaro et al., 2014). The scaffolding protein caveolin binds to the caveolin binding domain (CBD) is in the N-terminal region (Barbuti et al., 2004, 2012). This N-terminal region, also called the "HCN domain," interacts with the beta-roll of the C-terminal region and consequently caveolin binding could be disrupted by truncation after the beta-roll (Lee and MacKinnon, 2017). Additionally, other scaffolding proteins like filamin A, Mint2, S-SCAM, and tamalin are predicted to bind to the extreme C-terminal region, any of which could be disrupted by a C-helix deletion or an extreme C-terminal region deletions (Gravante et al., 2004; Kimura et al., 2004). Scaffolding proteins interact with many ion channels, not just HCN, including $Na_{V,}$ L-type and T-type calcium channels, the sodium-calcium exchanger (NCX), KCNQ1 and multiple K_{IR} channels (Vaidyanathan and Makielski, 2014). Disrupting ion channel – scaffolding protein interactions alters ion channel function which can result in diseases, for example Long QT (Vaidyanathan and Makielski, 2014). To account for these important cellular factors, I propose moving towards the perforated patch clamp configuration using mammalian cells in the future, which allows for control of cytosolic cAMP concentrations while maintaining the physiologically relevant cellular factors. I will discuss this further in Chapter 4.1.

Table 3-1: Thermodynamic fit parameters

Construct	Vact (mV)	s (mV^{-1})	n	Vdeact (mV)	s (mV^{-1})	n
Ch4-2	-93.2 ± 1.1	18.94 ± 0.53	8	-45.1 ± 2.1	8.13 ± 0.43	8
Ch4-2 E457R	-92.4 ± 1.4	16.41 ± 0.52	6	-71.1 ± 1.5	7.78 ± 0.40	6
Ch4-2 ΔXC	-102.2 ± 2.0	15.55 ± 0.58	12	-60.7 ± 2.2	11.47 ± 0.47	12
Ch4-2 E457R ΔXC	-101.7 ± 1.7	14.53 ± 0.26	6	-77.8 ± 2.2	8.96 ± 0.67	6
Ch4-2 ΔCNB	-82.9 ± 1.6	19.0 ± 1.1	11	-40.3 ± 3.2	28.8 ± 2.1	11
Ch4-2 E457R ΔCNB	-109.26 ± 0.87	15.01 ± 0.24	4	-71.0 ± 1.9	28.2 ± 1.7	4
Ch4-2 R591E	-108.2 ± 1.2	13.59 ± .014	17	-81.3 ± 1.1	10.41 ± 0.34	17
Ch4-2 E457R R591E	-104.95 ± 0.55	14.48 ± 0.80	8	-68.5 ± 3.4	12.00 ± 0.56	8
Ch4-2 ΔαC	-101.2 ± 1.7	14.93 ± 0.55	7	-73.9 ± 1.7	13.10 ± 0.86	7
Ch4-2 E457R ΔαC	-96.8 ± 2.4	14.75 ± 0.51	5	-83.6 ± 2.6	13.9 ± 1.6	5
Ch4-2 K381E ΔXC	-111.3 ± 1.8	14.36 ± 0.52	8	-36.2 ± 2.6	16.22 ± 0.51	8
Ch4-2 K381E E457R ΔXC	-112.1 ± 2.2	15.96 ± 0.35	6	-79.5 ± 1.3	16.9 ± 1.0	6
Ch4-2 K381E R591E	-113.69 ± 0.86	11.40 ± 0.92	4	-71.4 ± 2.8	13.52 ± 0.91	4
Ch4-2 K381E E457R R591E	-116.89 ± 0.62	15.00 ± 0.32	4	-73.4 ± 2.4	22.35 ± 0.51	4
Ch4-2 K381E E457Q ΔXC	-121.9 ± 2.5	14.19 ± 0.88	6	-54.5 ± 2.2	17.67 ± 0.68	6
Ch4-2 K381E E457C ΔXC	-112.1 ± 1.6	12.6 ± 1.1	4	-49.9 ± 2.3	10.79 ± 0.65	4
HCN2 ΔXC	-94.7 ± 1.8	14.45 ± 0.26	4	-81.2 ± 2.4	10.81 ± 0.57	4
HCN2 E457R ΔXC	-93.7 ± 1.6	12.6 ± 1.1	6	-87.0 ± 1.2	10.50 ± 0.48	6

Vact and Vdeact with the corresponding reciprocal slope factors (s), (mean ± SEM).

Table 3-2: Kinetic parameters

Construct	0 mV $t_{1/2}$ (ms)	n	-130 mV $\tau_{weighted}$ (ms)	d (ms)	n
Ch4-2	574 ± 79	8	978 ± 51	186 ± 13	8
Ch4-2 E457R	374 ± 21	6	937 ± 47	195 ± 12	6
Ch4-2 ΔXC	370 ± 28	12	1340 ± 150	340 ± 33	12
Ch4-2 E457R ΔXC	274 ± 14	6	1156 ± 77	389 ± 25	6
Ch4-2 ΔCNB	681 ± 53	11	775 ± 47	48.2 ± 5.6	11
Ch4-2 E457R ΔCNB	588 ± 42	4	1940 ± 210	316 ± 58	4
Ch4-2 R591E	263.8 ± 9.5	17	1470 ± 130	449 ± 25	16
Ch4-2 E457R R591E	473 ± 22	8	1140 ± 100	343 ± 26	8
Ch4-2 ΔαC	379 ± 26	7	1076 ± 72	314 ± 27	7
Ch4-2 E457R ΔαC	232 ± 10	5	637 ± 59	236 ± 17	5
Ch4-2 K381E ΔXC	2880 ± 140	8	846 ± 61	131 ± 24	8
Ch4-2 K381E E457R ΔXC	1472 ± 60	6	876 ± 78	117 ± 26	6
Ch4-2 K381E R591E	778 ± 65	4	903 ± 44	194 ± 27	4
Ch4-2 K381E E457R R591E	1039.3 ± 8.4	4	918 ± 47	178 ± 12	4
Ch4-2 K381E E457Q ΔXC	2442 ± 98	6	1530 ± 300	290 ± 80	6
Ch4-2 K381E E457C ΔXC	2080 ± 220	4	987 ± 65	194 ± 10	4
HCN2 ΔXC	282 ± 20	6	340 ± 140	97.0 ± 6.0	4
HCN2 E457R ΔXC	295 ± 15	6	282 ± 47	130 ± 14	6

Average $t_{1/2}$ at 0 mV and $\tau_{weighted}$ at −130 mV (±SEM) for all constructs including the lag (d) for the activation fit (see Methods).

3.4. Discussion

In summary, I was able to find functional evidence for an interdomain interaction between the E457 residue in the A' helix and the HCN4 TM region. The E457-interaction contributes to stabilization of the open state in autoinhibition relieved channels (full length liganded channels or partially liganded ΔXC channels), autoinhibition-free channels (ΔCNB), and autoinhibited channels without an intact CNB fold (ΔαC). Notably, the E457R mutation effected the autoinhibition mechanism in two distinct, non-parallel ways: suppression of thermodynamics and augmentation of kinetics. The introduction of a second CNB fold-mechanism that controls deactivation kinetics (OST) did not change the ability of the E457-interaction to form. Furthermore, using OST channels I was able to show that in autoinhibition relieved channels E457 is forming a salt bridge with the TM region. However, in the full length autoinhibited channel (with and without the K381E mutation) the E457 residue appears to destabilize the open state, suggesting a conformational change in the A' helix that moves E457 from its classical conformation into an alternative conformation. In this alternative conformation, the E457R residue attenuated both the thermodynamic and kinetic effects of the autoinhibition mechanism. Moreover, I believe that this conformational change in E457 is dependent on cellular factors, whose activity requires the extreme C-terminal region.

The autoinhibition model and cAMP relief of autoinhibition rely on the idea that conformational changes upon cAMP binding in the CNB fold are translated into conformational changes in the C-linker (see Figures 1-3 and 1-4). However, when the first unliganded CNB fold crystal structure was published, the C-linker did not display the large conformational changes that were predicted (Taraska et al., 2009). This result was also found in the full length hHCN1 cryoEM structure (Lee and MacKinnon, 2017). Notably, the results presented here act as proof of concept that a small conformational change in a single residue (E457) when cAMP binds can dramatically modify HCN channel activity. Introduction of the charge reversal mutation (E457R) in unliganded channels slowed deactivation by at least 1.7-fold over a range of voltages (-60 to +20 mV). In contrast, introduction of the E457R mutation in liganded channels resulted in a speeding of deactivation by at least 1.3-fold over the same range of voltages. This not only suggests that the E457 residue changes conformation upon cAMP binding in full

length channels, but that this conformational change can have a large effect on the autoinhibition mechanism and cAMP-relief of autoinhibition.

While I have been able to determine that the autoinhibition-relieved E457-interaction is an electrostatic interaction with the TM region of HCN4 channels, I have not completed similar studies of the full-length autoinhibited E457-interaction. To determine whether E457 forms a repulsive interaction in the alternative conformation I plan to make the same mutation series (E457C and E457Q) in the Ch4-2 R591E background. I would expect that, as with the autoinhibition-relieved channels the E457Q and E457C mutations in Ch4-2 R591E will have an intermediate effect on deactivation compared to both Ch4-2 R591E and Ch4-2 E457R R591E channels. In other words, the Ch4-2 R591E channel will have the fastest deactivation followed by the E457Q mutant, the E457C mutant and finally I would expect that the E457R mutant would have the slowest deactivation of the mutation series. Additionally, I will perform the same TM-replacement as was done with the Ch4-2 E457R ΔXC channel, to introduce the HCN2 TM region into the Ch4-2 E457R R591E channel (i.e. HCN2 E457R R591E), which is akin to introducing the E457R mutation into the HCN2 R591E channel. If the deactivation of this channel is not significantly slower than HCN2 R591E than I could conclude that, as with the autoinhibition-relieved channels, the E457 residue interacts with HCN4 TM region structures. However, if introduction of the E457R mutation into HCN2 R591E channel results in slower deactivation, as was true in Ch4-2 R591E channels, I cannot conclude that the E457 interaction is not forming with TM region structures. The E457 residue could be interacting with TM region structures that are conserved between HCN2 and HCN4 channels. This means the E457 residue could be interacting with structures of the HCN2 N-terminal region, the HCN2 C-terminal region or HCN2 TM region structures that are conserved in HCN4 channels.

There have been previous studies aimed at identification of functional evidence of interdomain interactions between the A' helix and the TM region. Alanine scans of the A' helix and putative S4-S5 linker of HCN2 channels identified potential electrostatic interdomain interactions (Decher et al., 2004). While this study did not find any functional evidence for E457 forming an interdomain interaction in HCN2 channels and they did not investigate the role of A' residues in other HCN subtypes and I found that the liganded E457-interaction is dependent on the HCN4 TM region structures. Studies by the Yellen group also investigated the ability of the A' helix and putative S4-S5 linker

to form interdomain interactions (Kwan et al., 2012; Prole and Yellen, 2006). These Cd^{2+} cross linking studies were used to determine if the residues were in close proximity in either the closed or open states. This study did suggest that the E457 residue is in close proximity with putative S4-S5 linker residues in the open state. Notably, all of these studies were done before the hHCN1 cryoEM structure was published (Lee and MacKinnon, 2017), so that the S4-S5 linker was assumed to be alpha-helical in nature, as is true for classical Kv channels (Jiang et al., 2003; Long et al., 2005b, 2007). However, the hHCN1 structure showed that instead of the classical alpha-helical S4-S5 linker, HCN channels S4 and S5 helices extend into the cytosol and are linked by a short 3 residue linker that is not alpha-helical in nature. Thus, putative S4-S5 linker residues that were previously examined are now expected to be part of the N-terminal region of S5. Moreover, neither study ever examined if A' helix residues could form interactions with the C-terminal region of S4, meaning they may have missed possible interactions that the A' helix residues could form. Additionally, neither study examined the ability of the A' helix residues to form interdomain interactions in an unliganded channel or an autoinhibition-free channel with the CNB fold deleted. Thus, this study represents the first attempt to find functional evidence for interdomain interactions that effect the autoinhibition mechanism.

The results presented here represent a step forward in understanding how interdomain interactions support the autoinhibition mechanism. In addition, this study represents further proof of activation and deactivation being separate pathways. While fewer studies of HCN channel deactivation pathway exist compared to studies of the activation pathway, it is still an important area of research as deactivation of HCN channels plays important physiological roles. For example, fast deactivation of HCN channels is essential for inhibiting temporal summation in CA1 pyramidal neurons. Finally, this research provides insight into an interdomain interaction that plays an important role in the autoinhibition mechanism. Due to the complete conservation of the A' helix across the four HCN subtypes, I predict that the E457-interaction and conformational changes would be conserved in HCN4 channels.

Chapter 4.

Conclusions and Future Directions

This chapter discusses preliminary results of PIP_2 depletion on the interdomain interactions discussed in Chapters 2 and 3. Data acquisition and analysis of results after PIP_2 depletion was performed by myself or an undergraduate student (Matt Jung) whom I trained and supervised. I was responsible for all remaining work presented in this chapter including figure generation and writing the text for this chapter.

The overarching goal of this work was to explore functional evidence for interdomain interactions that facilitated the three different C-terminally mediated mechanisms for modulating HCN channel activity. To accomplish this I posed three questions (see section 1.8) which are restated here along with the answers to the questions that were found in chapters 2 and 3.

Do interdomain interactions exist that are subtype-specific?

Yes, using TM region substitution (see Chapter 2) I found functional evidence for subtype-specific interdomain interactions since performing an HCN4 TM-replacement disrupted interdomain interactions that facilitated OST and QA in HCN2 channels. This TM-replacement also removed an interdomain interaction that limited the magnitude of autoinhibition in HCN2 channels. In other words, the resultant augmented autoinhibition required HCN4 TM region structures. Additionally, I found that the effect of the E457R mutation in Ch4-2 ΔXC channels is removed in HCN2 ΔXC channels (see Chapter 3). This suggests that the formation of the classical E457 salt bridge (i.e. not the alternative conformation from Ch4-2 R591E) is dependent on HCN4 TM region structures and therefore this interdomain interaction is subtype specific.

Which C-terminal functions (OST, QA, autoinhibition, and cAMP-relief of autoinhibition) are supported by interdomain interactions?

In Chapter 2 I found that HCN4 TM-replacement in HCN2 channels disrupted the OST mechanism. Liganded HCN2 channels have the OST mechanism active since they close slower than OST-free channels (i.e. channels with a CNB fold truncation). However, after the HCN4 TM-replacement, liganded channels closed faster than OST-free channels, suggesting that the OST mechanism had been disrupted (see Figure 2-5. I concluded that this CNB fold-mediated regulatory mechanism requires HCN2 TM region structures. This implied that interdomain interactions between the C-terminal region and the HCN2 TM region facilitate the OST mechanism

In Chapter 2 I also found that HCN4 TM-replacement in HCN2 channels disrupted the Quick-Activation mechanism. Full length HCN2 channels have the Quick-Activation mechanism active since they open faster than channels without an intact CNB fold (i.e. ΔCNB or ΔαC). However, after the HCN4 TM-replacement, full length channels no longer opened faster than those channels without an intact CNB fold, suggesting that

the Quick-Activation mechanism had been disrupted (see Figure 2-6). I concluded that, as with the OST mechanism, the Quick-Activation mechanism requires HCN2 TM region structures. This implies that interdomain interactions between the C-terminal region and the HCN2 TM region facilitated the Quick-Activation mechanism.

I found functional evidence for interdomain interactions supporting autoinhibition in both Chapter 2 and Chapter 3. In Chapter 2 I found that HCN4 TM-replacement in HCN2 channels augmented autoinhibition. This augmentation shifted the Vact by 10 mV in full length channels and made the autoinhibition mechanism the dominant kinetic mechanism affecting both activation and deactivation (see Figures 2-6 and 2-5 respectively). I concluded that HCN2 TM region structures limit autoinhibition, implying that interdomain interactions between the C-terminal region and the TM region controls the magnitude of autoinhibition (see Figure 2-7). In Chapter 3 I found that an electrostatic interdomain interaction between the E457 residue and the HCN4 TM region is important for regulating the magnitude of autoinhibition. The E457R mutation had two distinct effects on the autoinhibition mechanism. This mutation limited the magnitude of thermodynamic autoinhibition while also augmenting the magnitude of kinetic autoinhibition (see Figures 3-8 and 3-9). Notably, a conformational change in the E457R mutation disrupted thermodynamic autoinhibition and attenuated the magnitude of kinetic autoinhibition. I concluded that the electrostatic interdomain interaction between the E457 residue and an unspecified partner residue in the HCN4 TM region helps facilitate the autoinhibition mechanism in Ch4-2 channels.

Lastly, I did not find any evidence for interdomain interactions supporting cAMP-relief of autoinhibition in either Chapter 2 or Chapter 3. The magnitude of cAMP relief (compared to the full length autoinhibited channels) did not depend on HCN2 TM region structures, as HCN4 TM-replacement did not affect the magnitude of cAMP relief (see Figure 2-3D). Additionally, the magnitude of cAMP relief (compared to the ΔαC autoinhibited channels) was not affected by the E457R mutation. This does not suggest that cAMP relief of autoinhibition is not facilitated by interdomain interactions, but just that they do not depend on HCN2 TM region structures or the E457 residue.

I will now discuss general conclusions and future directions based on the work presented in Chapters 2 and 3.

4.1. Different experimental configurations affect conclusions on HCN channels

The majority of the work presented in this thesis was performed using the Two Electrode Voltage Clamp (TEVC) experimental configuration. Using TEVC allows for the use of intact oocytes, complete with cytosolic factors like cAMP, PIP2 and scaffolding proteins but the concentration of cAMP in the cytosol is unknown. Unlike this work, much of the previous research on HCN channels in *X. laevis* oocytes used the Inside-Out Patch Clamp (IOPC) configuration. The IOPC configuration first requires the generation of a giga-ohm seal between the oocyte membrane and the glass electrode. Once the seal has been formed the membrane "patch" is excised from the membrane. The excision of the HCN channels allows for direct control of cAMP concentrations in the bath solution. However, the excision also results in the separation of the HCN channels in the patch from cytosolic proteins like kinases that generate PIP_2 but not the membrane-bound phosphatase that dephosphorylates PIP_2. This results in PIP_2 being slowly degraded over time, a phenomenon called rundown (Flynn and Zagotta, 2011; Pian et al., 2007; Zolles et al., 2006). Moreover, scaffolding proteins that connect the HCN channel to the cytoskeleton are also removed upon excision of the patch from the membrane.

My lab has previously described the QA mechanism which regulates activation kinetics of HCN2 channels in intact-oocytes (i.e. TEVC) (Magee et al., 2015). It was hypothesized that the QA mechanism was dependent on the activity of a cellular factor, although the researchers showed the cellular factor was not PIP_2 (Magee et al., 2015). In Chapter 3 I also found that when I used the IOPC configuration the effect of the E457R mutation was not as expected based on results acquired using the TEVC configuration (Figure 3-15A). Notably, the slowing of deactivation after introduction of the E457R mutation in unliganded channels (Ch4-2 E457R R591E) seemed to be present when I performed cell-attached recordings after formation of seal and before excision of the patch. This phenotype was removed immediately upon excision of the patch from the oocyte membrane (Figure 3-15B). This suggested that the conformational change in E457 when the Ch4-2 channel is autoinhibited was also dependent on cellular factors. I hypothesized that this cellular factor was not PIP2 since the speeding effect upon excision was evident prior to rundown occurring (see Figure 3-7).

Under physiological conditions HCN channels are expressed in intact mammalian cells, with cAMP, PIP_2 and scaffolding proteins present. Based on my work and the previous work by my lab I believe that using IOPC configurations to examine HCN channels provides an incomplete picture of HCN channel activity and regulatory mechanisms because of the removal of cellular factors. In comparison, using TEVC configurations allows for the determination of a more complete picture of HCN channel activity and regulatory mechanisms.

The downside of using the TEVC configuration on *X. laevis* oocytes is two-fold:

(i) There is an unknown concentration of cAMP in the cytosol

(ii) *X. laevis* oocytes are not mammalian cells

Therefore, in the future I would recommend moving towards using the perforated-patch clamp technique on mammalian cells, like HEK 293. The perforated patch clamp configuration involves forming a giga-ohm seal (as with IOPC), but instead of membrane excision, a chemical is used to perforate the membrane to small molecules. This allows for the flow of ions through the perforations in the cell membrane, but not cAMP or proteins. This would allow for the study of HCN channels in near-physiological conditions, where all cellular factors are present in a mammalian cell type.

4.2. Examining divergent residues in the HCN2 and HCN4 TM regions

The logical next step in the research from both Chapter 2 and Chapter 3 would be to identify the physical determinants of the proposed interdomain interactions. In Chapter 2 we found that interdomain interactions in mHCN2 channels facilitate both the Open-State Trapping and Quick-Activation mechanisms. We also concluded that an interdomain interaction in mHCN2 channels limited the magnitude of autoinhibition present in the unliganded channel. The mHCN2 and mHCN4 TM regions are somewhat conserved, with a divergence of approximately 12%. Therefore, I can conclude that the mHCN2 TM region residues responsible for the described interactions must be one of the few divergent residues from the mHCN4 TM region.

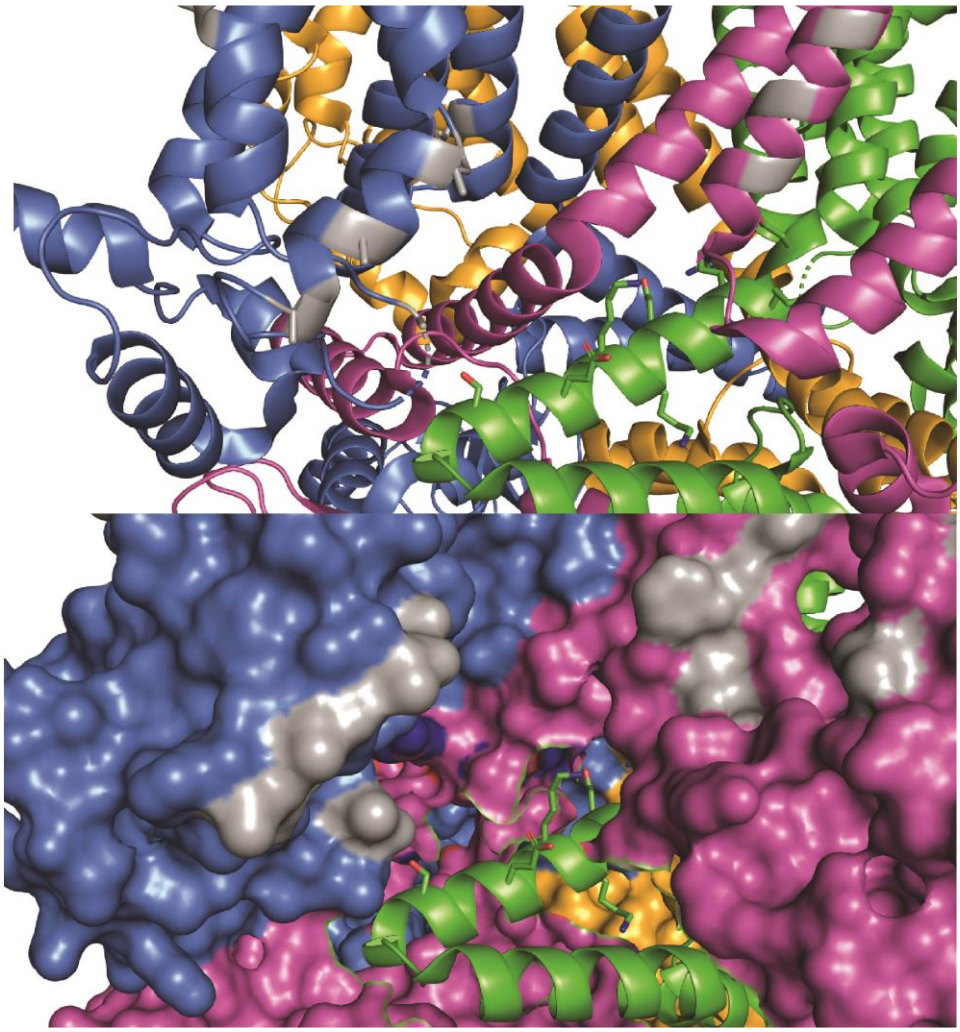

Figure 4-1: Divergent residues in HCN2 and HCN4 subtypes TM region

Divergent residues in the TM region of the mHCN2 and mHCN4 channels (grey) centered on the A" helix (green). A' helix residues and divergent residues structures shown. Note that the A' helix of one subunit (green) can contact the TM region of two other subunits (blue and pink). Upper panel shows TM region as cartoon, while lower panel shows TM region as surface structure.

To further the research from Chapter 2 I suggest performing targeted substitution in the Ch4-2 channel background to identify the specific residue or residues in the TM region that form the different interdomain interactions which facilitate OST and QA, and limit autoinhibition. Substitution of the mHCN2 residue or residues involved in, for example, facilitating OST, into the Ch4-2 background of channels would result in the channels following the OST mechanism, so that the Ch4-2 channel would close significantly slower after introduction of the mutation. Alternatively, replacement of the mHCN2 residue or residues involved in OST, with the mHCN4 residue would result in disruption of the OST mechanism, so that the HCN2 channel would close significantly faster after introduction of the mutation. Once potential residues have been identified in the full length HCN2 or Ch4-2 channels, I can confirm that these residues facilitate the different regulatory mechanisms the ΔCNB backgrounds which are free of all three different CNB fold-mediated mechanisms.

Once completed, the partner residues in the A' helix can be identified through site-directed mutagenesis or an alanine scan of full helix in the mHCN2 background. For example, I would expect that for any A' residue that facilitates OST, mutation would disrupt the OST mechanism, so that HCN2 channels closed at similar speeds as HCN2 ΔCNB channels. The identity of these residues and the proposed interactions can be verified by introducing the A' helix mutations into the TM region mutants discussed earlier. For example, the OST mechanism would be disrupted after the substitution of the HCN4 residues in the HCN2 channel, and when a second mutation to the A' helix partner residue was made, the OST mechanism would be reintroduced.

Recall from Chapter 3 I found that the E457 residue in the A' helix helped to stabilize the open state of Ch4-2 channels. This interaction was not present in an HCN2 background, suggesting that the partner residue for E457 must be one or more of the mHCN4 TM region residues that was not conserved in mHCN2 channels, most likely a positively charged residue like R254 in the S2-S3 linker. To further the research from Chapter 3 I suggest performing charge reversal mutations of these to identify the autoinhibition-relieved partner residue for E457. If, for example, E457 forms a salt-bridge with R254, then a charge reversal mutation (i.e. R254E) should result in destabilization of the open state in a Ch4-2 background, similar to what was seen after introduction of the E457R mutation in Ch4-2. The interaction can be confirmed using a double mutation (i.e. Ch4-2 R254E E457R) where the two mutant residues would be

able to re-form a salt-bridge, allowing for stabilization of the open state during deactivation in Ch4-2 channels, with similar deactivation speeds as the Ch4-2 channel.

4.3. Effect of PIP_2 on interdomain interactions and CNB fold-regulated mechanisms

In Chapters 2 and 3 I have presented functional evidence of interdomain interactions in the presence and absence of the HCN channel potentiator cAMP. However, I have not examined the evidence for interdomain interactions in the absence of PIP2, a second potentiator of HCN channels. Intact oocytes have a basal amount of PIP2 present in the membrane, therefore all of the results presented in Chapter 2 and Chapter 3 are reliant on the presence of PIP_2. But would these results change if PIP2 was not present? Two simple models for how PIP_2 could effect the results of each chapter are:

- Does augmented autoinhibition require PIP_2 or does it occur independent of PIP_2?
- Does the formation of the E457 interaction that stabilizes the open state require the binding of PIP_2 or does it occur independent of PIP_2?

HCN channels can be studied without PIP_2 present by either using IOPC and waiting for rundown to occur in the oocyte membrane, or using a chemical, like wortmannin, to deplete the amount of PIP_2 in the intact oocyte (Magee et al., 2015; Pian et al., 2007; Zolles et al., 2006). Our lab has developed a protocol to perform TEVC recordings before and after a wortmannin incubation (45µM wortmannin incubated for 45 min.) to examine the effect of PIP_2 on the HCN constructs (Magee et al., 2015). This protocol was previously used to determine that PIP_2 does not facilitate the QA mechanism in HCN2 channels (Magee et al., 2015). Using this protocol, I have aimed to determine the effect of PIP_2 on the interdomain interactions identified in Chapters 2 and 3. While this work has not been completed I will present some preliminary results here.

4.3.1. The effect of PIP_2 on Augmented Autoinhibition

Will autoinhibition be augmented when PIP_2 is depleted? Recall that in Chapter 2 the HCN4 TM-replacement in HCN2 and HCN2 R591E channels negatively shifted Vact by 10 mV, but $V_{1/2}$ was not negatively shifted after HCN4 TM-replacement in autoinhibition-free HCN2 ΔCNB channels. I concluded that HCN4 TM-replacement resulted in the formation of a new interdomain interaction that augmented autoinhibition by 10 mV compared to the HCN2 channels (see Figure 2-3D). If the formation of the interdomain interaction that augments autoinhibition is dependent on PIP_2 binding the Ch4-2 channels I would expect that PIP-depletion would result in HCN4 TM-replacement in HCN2 channels no longer negatively shifting $V_{1/2}$ by 10 mV. This would also mean that the $V_{1/2}$ of Ch4-2 would no longer be negatively shifted by 10 mV compared to Ch4-2 ΔCNB (see Figure 2-3B, C). However, if PIP_2 depletion does not change the effect of HCN4 TM-replacement in HCN2 channels on the magnitude of autoinhibition (i.e. $V_{1/2}$ is still negatively shifted by 10 mV) then I would be able to conclude that augmented autoinhibition does not require PIP_2 to be bound to the channel.

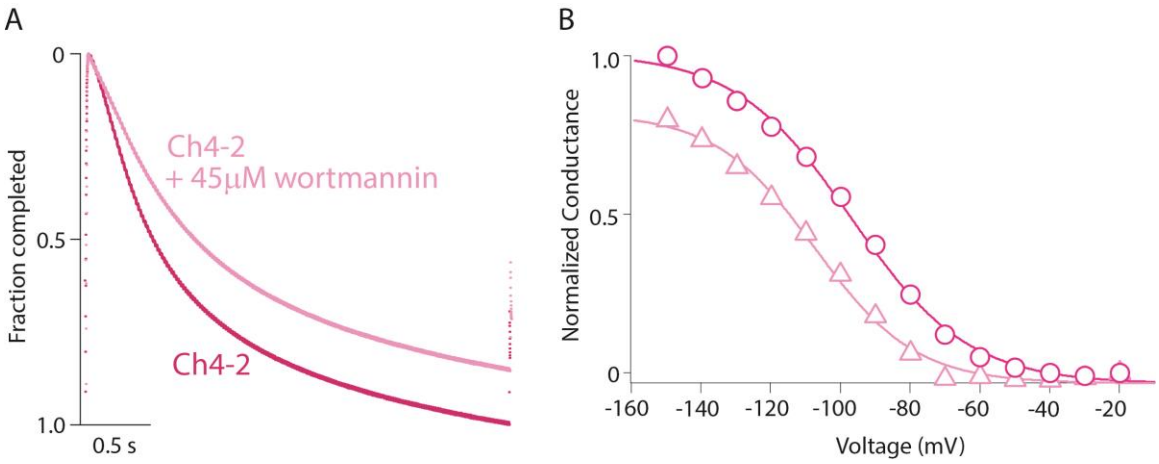

Figure 4-2: Wortmannin successfully removes PIP_2 from oocytes expressing Ch4-2 channels

A, Representative current at −130 mV of the Ch4-2 channels expressed in the same oocyte before (dark pink) and after (light pink) incubation with 45μM wortmannin, each normalized to total decay current before wortmannin. **B,** Conductance-voltage relationship for the oocyte from panel *A* where each is normalized to maximal conductance from before wortmannin (dark pink circle). Not only is the Vact negatively shifted after incubation with 45μM wortmannin (light pink triangle) but the maximal conductance is decreased. Boltzmann fit parameters of the representative curves are as follows: Ch4-2, −96.5 mV, s = 17.4 mV; Ch4-2 + 45μM wortmannin, −111.5 mV, s = 18.1 mV.

Post-wortmannin recordings of Ch4-2 constructs displayed the characteristic negative Vact shift and amplitude decrease associated with PIP_2-depletion, suggesting that the incubation of the oocytes with wortmannin was successful(Figure 4-2). On average wortmannin incubation resulted in a decrease in amplitude of Ch4-2 activation by at least 13%. Additionally, wortmannin incubation negatively shifted the Ch4-2 Vact by an average of 15.2 ± 3.2 mV. To examine if augmented autoinhibition was present in the absence of PIP_2 I compared Ch4-2 and HCN2 after incubation with wortmannin to deplete PIP_2. The $V_{1/2}$ of Ch4-2 channels after PIP_2 depletion (−104.0 ± 10.5 mV; $n = 5$) was not significantly different ($p > 0.5$) from the Vact of HCN2 channels after PIP_2 depletion (−100.9 ± 9.0 mV, $n = 11$; experiments done previously in Magee et al., 2015). Recall that the Ch4-2 ΔCNB does not have augmented autoinhibition. Therefore, I verified these results by comparing the Vact of Ch4-2 and Ch4-2 ΔCNB after PIP_2 depletion. As expected, the $V_{1/2}$ of Ch4-2 channels was not significantly different (i.e. no negative Vact shift; $p > 0.4$) than Ch4-2 ΔCNB channels (−100.3 ± 4.8 mV, $n = 7$). This suggests a model where augmented autoinhibition has been disrupted in Ch4-2 channels by PIP_2 depletion. In other words, the interdomain interaction that results in augmented autoinhibition is dependent on PIP_2 binding the Ch4-2 channel.

A simple alternative model to the one suggested above is that PIP_2 depletion disrupts the autoinhibition mechanism. In order to determine which model is correct further study of autoinhibited channels in PIP_2-depleted conditions will be needed. If PIP_2 depletion disrupts the autoinhibition mechanism, then the Vact of Ch4-2 R591E would not be significantly different from Ch4-2 channels. However, if autoinhibition remains unaffected, but the interdomain interaction that facilitates augmented autoinhibition is disrupted by PIP_2 depletion then I would expect that the Vact for Ch4-2 R591E would not be negatively shifted by 10 mV compared to HCN2 R591E. Additionally, since Ch4-2 ΔαC channels do not have augmented autoinhibition (see Figure 2-3D), I would expect that the Vact of Ch4-2 ΔαC would not be significantly different from Ch4-2 R591E after PIP_2 depletion. Moreover, I would expect that the magnitude of autoinhibition (i.e. comparison of R591E and ΔCNB channels) will be the same in HCN2 and Ch4-2 backgrounds after PIP_2 depletion.

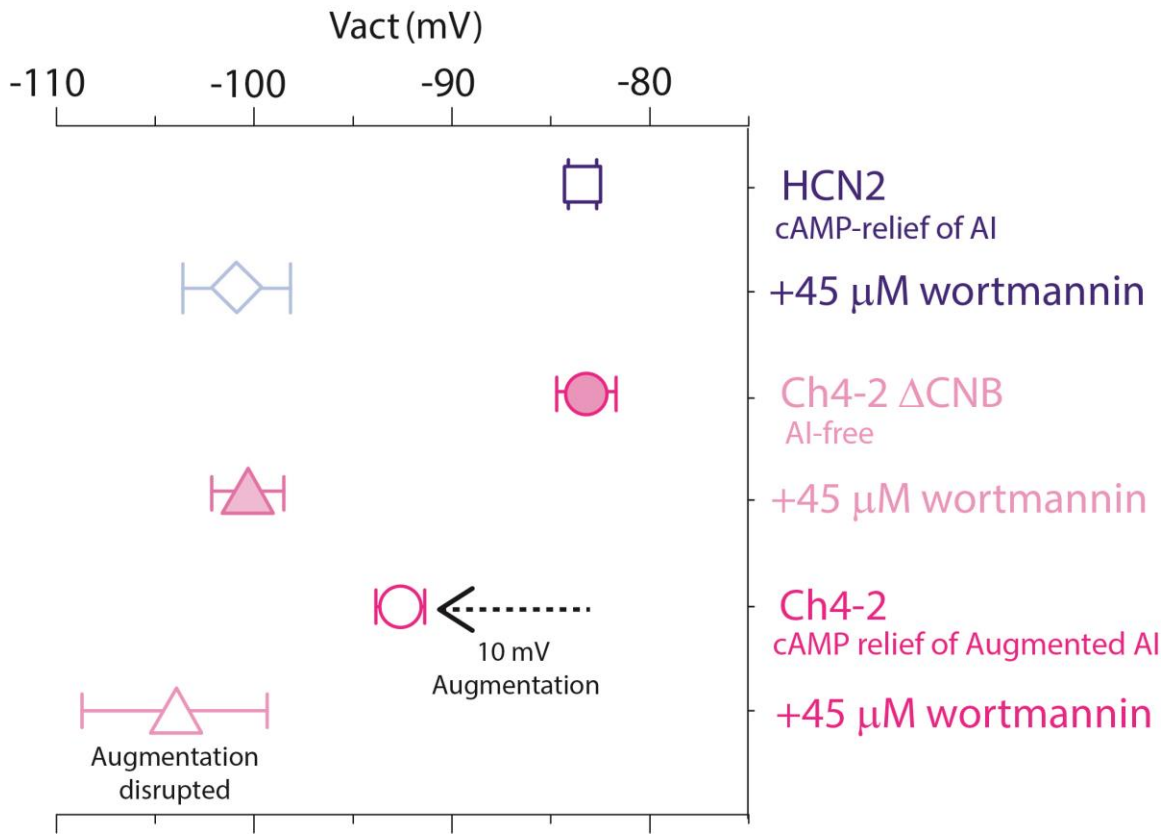

Figure 4-3: PIP_2 depletion disrupts augmented autoinhibition

Mean Vact values before (dark color) and after (light color) incubation with 45μM wortmannin. HCN2 before as blue square (n = 49), HCN2 after as light blue diamond (n = 10), Ch4-2 before as dark pink empty circle (n = 8), Ch4-2 after as light pink empty triangles (n = 4), Ch4-2 ΔCNB before as dark pink filled circle (n = 11), and Ch4-2 ΔCNB after as light pink filled triangles (n = 6) channels. *Error bars* show SEM. The augmentation of autoinhibition by 10 mV in Ch4-2 channels, as compared to both autoinhibition-relieved HCN2 channels and autoinhibition-free Ch4-2 ΔCNB, demonstrated with black dashed arrow. Note that after incubation this augmentation has been disrupted as the Vact of all channels after incubation with 45μM wortmannin shows no difference. The abbreviation "AI" stands for autoinhibition.

4.3.2. The effect of PIP_2 on the conformation of E457

PIP_2 is thought to bind to the TM region of mammalian HCN channels, but in addition to this a second PIP_2 binding site has been identified in the A' helix of the HCN channel homolog found in sea urchin (spHCN) (Flynn and Zagotta, 2011). This second PIP_2 binding site is located one helical turn upstream of the E457 residue. Based on the close proximity of this potential binding site in Ch4-2 channels, I hypothesized that the formation of the E457 interaction that stabilizes the open state might be dependent on the binding of PIP_2. Alternatively, I could imagine that this interdomain interaction does not depend on the binding of PIP_2. If the formation of this E457 interaction requires PIP_2 I would expect that the introduction of the E457R mutation into Ch4-2 or Ch4-2 ΔXC channels would not speed deactivation after PIP_2 depletion. However, if PIP_2 is not required, I would expect PIP_2 depletion to have no effect on the E457R phenotype.

Preliminary results suggest that PIP_2 depletion has no effect on the E457R phenotype (Figure 4-4). Specifically, the introduction of the E457R mutation into Ch4-2 ΔXC channels still negatively shifts Vdeact after PIP_2-depletion. This suggests that the salt-bridge formed by E457 in autoinhibition-relieved channels is not dependent on PIP_2 binding. Further examination of autoinhibition-relieved channels is required to confirm this finding. This can be done by incubating intact oocytes with wortmannin or performing voltage-clamp experiments with these channels in the IOPC configuration after rundown has occurred.

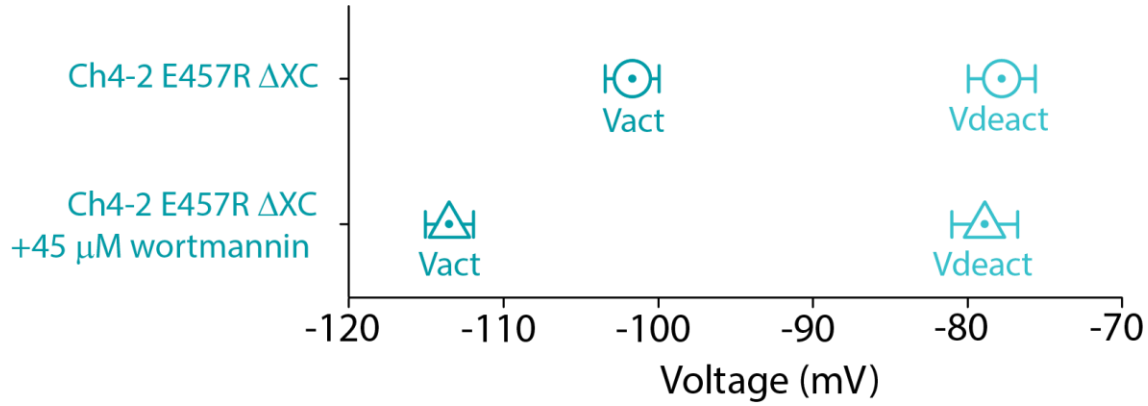

Figure 4-4: Effect of wortmannin on the Ch4-2 E457R ΔXC channels

Mean Vact (dark color) and Vdeact (light color) values before (dotted circles) and after (dotted triangles) incubation with 45μM wortmannin for Ch4-2 E457R ΔXC. *Error bars* show SEM. Note that Vact is negatively shifted but Vdeact does not change after incubation with wortmannin.

4.4. Conservation of results in mHCN4 channels

The functional evidence for interdomain interactions presented in Chapter 2 and Chapter 3 identified two new potential interdomain interactions in Ch4-2 channels:

1) The interdomain interaction that facilitates augmented autoinhibition (Chapter 2)

2) The E457 interdomain interaction that stabilizes the open state (Chapter 3)

I have hypothesized that these interactions occur between the A' helix and the HCN4 TM region. Since the A' helix is 100% conserved in all HCN subtypes, I would hypothesize that any interdomain interaction in Ch4-2 channels between HCN4 TM region structures and the A' helix would be conserved in full length mouse HCN4 channels. In the future, the work presented in Chapters 2 and 3 can be repeated in a mouse HCN4 background, including all C-terminal truncations (ΔCNB, ΔαC, ΔXC) as well as sequence permutations (R591E mutation). These new channels would allow us to determine if the two interdomain interactions are conserved in full length HCN4 channels as I suggest. This study would provide more insight into how autoinhibition is facilitated in HCN4 channels.

References

Akimoto, M., Zhang, Z., Boulton, S., Selvaratnam, R., Van Schouwen, B., Gloyd, M., Accili, E. a., Lange, O.F., and Melacini, G. (2014). A mechanism for the auto-inhibition of hyperpolarization-activated cyclic nucleotide-gated (HCN) channel opening and its relief by cAMP. J. Biol. Chem. *289*, 22205–22220.

Altschul, S., Gish, W., Miller, W., Myers, E., and Lipman, D. (1990). Basic local alignment search tool. J. Mol. Bol. *215*, 403–410.

Bal, T., and Mccormick, D.A. (1996). What Stops Synchronized Thalamocortical Oscillations? Neuron *17*, 297–308.

Barbuti, A., Gravante, B., Riolfo, M., Milanesi, R., Terragni, B., and DiFrancesco, D. (2004). Localization of pacemaker channels in lipid rafts channel kinetics. Circ. Res. *94*, 1325–1331.

Barbuti, A., Scavone, A., Mazzocchi, N., Terragni, B., Baruscotti, M., and Difrancesco, D. (2012). A caveolin-binding domain in the HCN4 channels mediates functional interaction with caveolin proteins. J. Mol. Cell. Cardiol. *53*, 187–195.

Baruscotti, M., Bucchi, A., and T, D.D. (2005). Physiology and pharmacology of the cardiac pacemaker (funny) current. Pharmacol. Ther. *107*, 59–79.

Baruscotti, M., Bottelli, G., Milanesi, R., DiFrancesco, J.C., and DiFrancesco, D. (2010). HCN-related channelopathies. Pflugers Arch. *460*, 405–415.

Bell, D.C., Yao, H., Saenger, R.C., Riley, J.H., and Siegelbaum, S. a (2004). Changes in local S4 environment provide a voltage-sensing mechanism for mammalian hyperpolarization-activated HCN channels. J. Gen. Physiol. *123*, 5–19.

Biel, M., and Wahl-Schott, C. (2009). Hyperpolarization-activated cation channels: from genes to function. Physiol. Rev. *89*, 847–885.

Brioschi, C., Micheloni, S., Tellez, J.O., Pisoni, G., Longhi, R., Moroni, P., Billeter, R., Barbuti, A., Dobrzynski, H., Boyett, M.R., et al. (2009). Distribution of the pacemaker HCN4 channel mRNA and protein in the rabbit sinoatrial node. J. Mol. Cell. Cardiol. *47*, 221–227.

Brown, H.F., DiFrancesco, D., and Noble, S.J. (1979). How does adrenaline accelerate the heart? Nature *280*, 235–236.

Chen, J., Mitcheson, J.S., Tristani-Firouzi, M., Lin, M., and Sanguinetti, M.C. (2001a). The S4-S5 linker couples voltage sensing and activation of pacemaker channels. Proc. Natl. Acad. Sci. *98*, 11277–11282.

Chen, S., Wang, J., and Siegelbaum, S. A (2001b). Properties of hyperpolarization-

activated pacemaker current defined by coassembly of HCN1 and HCN2 subunits and basal modulation by cyclic nucleotide. J. Gen. Physiol. *117*, 491–504.

Chen, S., Wang, J., Zhou, L., George, M.S., and Siegelbaum, S.A. (2007). Voltage Sensor Movement and cAMP Binding Allosterically Regulate an Inherently Voltage-independent Closed − Open Transition in HCN Channels. J. Gen. Physiol. *129*, 175–188.

Craven, K.B., and Zagotta, W.N. (2004). Salt Bridges and Gating in the COOH-terminal Region of HCN2 and CNGA1 Channels. J. Gen. Physiol. *124*, 663–677.

Craven, K.B., and Zagotta, W.N. (2006). CNG and HCN Channels: Two Peas , One Pod. Annu. Rev. Physiol. *68*, 375–401.

Dascal, N. (1987). The use of Xenopus oocytes for the study of ion channels. Crit. Rev. Biochem. *22*, 317–387.

Decher, N., Chen, J., and Sanguinetti, M.C. (2004). Voltage-dependent gating of hyperpolarization-activated, cyclic nucleotide-gated pacemaker channels: molecular coupling between the S4-S5 and C-linkers. J. Biol. Chem. *279*, 13859–13865.

DiFrancesco, D. (1981). A study of the ionic nature of the pace-maker current in calf Purkinje fibers. J. Physiol. *50*, 377–393.

DiFrancesco, D. (1984). Characterization of the pace-maker current kinetics in calf Purkinje fibres. J. Physiol. *348*, 341–367.

DiFrancesco, D. (1986). Characterization of single pacemaker channels in cardiac sino-atrial node cells. Nature *324*, 470–473.

DiFrancesco, D., and Tortora, P. (1991). Direct activation of cardiac pacemaker channels by intracellular cyclic AMP. Nature *351*, 145–147.

DiFrancesco, J.C., and DiFrancesco, D. (2015). Dysfunctional HCN ion channels in neurological diseases. Front. Cell. Neurosci. *6*, 1–10.

DiFrancesco, D., Ferroni, A., Mazzanti, M., and Tromba, C. (1986). Properties of the hyperpolarizing-activated current (if) in cells isolated from the rabbit sino-atrial node. J. Physiol. *377*, 61–88.

DiFrancesco, J.C., Barbuti, A., Milanesi, R., Coco, S., Bucchi, A., Bottelli, G., Ferrarese, C., Franceschetti, S., Terragni, B., Baruscotti, M., et al. (2011). Recessive loss-of-function mutation in the pacemaker HCN2 channel causing increased neuronal excitability in a patient with idiopathic generalized epilepsy. J. Neurosci. *31*, 17327–17337.

Doan, T.N., and Kunze, D.L. (1999). Contribution of the hyperpolarization-activated current to the resting membrane potential of rat nodose sensory neurons. J.

Neurophysiol. *514*, 125–138.

Duhme, N., Schweizer, P. a, Thomas, D., Becker, R., Schröter, J., Barends, T.R.M., Schlichting, I., Draguhn, A., Bruehl, C., Katus, H. a, et al. (2013). Altered HCN4 channel C-linker interaction is associated with familial tachycardia-bradycardia syndrome and atrial fibrillation. Eur. Heart J. *34*, 2768–2775.

Elinder, F., Männikkö, R., Pandey, S., and Larsson, H.P. (2006). Mode shifts in the voltage gating of the mouse and human HCN2 and HCN4 channels. J. Physiol. *575*, 417–431.

Flynn, G.E., and Zagotta, W.N. (2011). Molecular mechanism underlying phosphatidylinositol 4,5-bisphosphate-induced inhibition of SpIH channels. J. Biol. Chem. *286*, 15535–15542.

Flynn, G.E., and Zagotta, W.N. (2018). Insights into the molecular mechanism for hyperpolarization-dependent activation of HCN channels. Proc. Natl. Acad. Sci. *115*, E8086–E8095.

Goldschen-Ohm, M.P., Klenchin, V.A., White, D.S., Cowgill, J.B., Cui, Q., Goldsmith, R.H., and Chanda, B. (2016). Structure and dynamics underlying elementary ligand binding events in human pacemaking channels. Elife 1–23.

Gravante, B., Barbuti, A., Milanesi, R., Zappi, I., Viscomi, C., and Difrancesco, D. (2004). Interaction of the Pacemaker Channel HCN1 with Filamin A. J. Biol. Chem. *279*, 43847–43853.

Hille, B. (1992). Ionic Channels of Excitable Membranes (Sunderland, Massachusetts: Sinauer Associates Inc.).

Jiang, Y., Lee, A., Chen, J., Ruta, V., Cadene, M., Chait, B.T., and Mackinnon, R. (2003). X-ray structure of a voltage-dependent K channel. Nature *423*, 33–41.

Kimura, K., Kitano, J., Nakajima, Y., and Nakanishi, S. (2004). Hyperpolarization-activated, cyclic nucleotide-gated HCN2 cation channel forms a protein assembly with multiple neuronal scaffold proteins in distinct modes of protein – protein interaction. Genes to Cells *9*, 631–640.

Ko, J.-K., and Ma, J. (2005). A rapid and efficient PCR-based mutagenesis method applicable to cell physiology study. Am. J. Physiol. Cell Physiol. *288*, C1273-8.

Kusch, J., Biskup, C., Thon, S., Schulz, E., Nache, V., Zimmer, T., Schwede, F., and Benndorf, K. (2010). Interdependence of receptor activation and ligand binding in hcn2 pacemaker channels. Neuron *67*, 75–85.

Kwan, D.C.H., Prole, D.L., and Yellen, G. (2012). Structural changes during HCN channel gating defined by high affinity metal bridges. J. Gen. Physiol. *140*, 279–291.

Lee, C.-H.H., and MacKinnon, R. (2017). Structures of the Human HCN1 Hyperpolarization-Activated Channel. Cell *168*, 111–120.

Li, M., Zhou, X., Wang, S., Michailidis, I., Gong, Y., Su, D., Li, H., Li, X., and Yang, J. (2017). Structure of a eukaryotic cyclic-nucleotide-gated channel. Nature *542*, 60–65.

Long, S.B., Campbell, E.B., and Mackinnon, R. (2005a). Voltage sensor of Kv1.2: structural basis of electromechanical coupling. Science *309*, 903–908.

Long, S.B., Campbell, E., and MacKinnon, R. (2005b). Crystal Structure of a Mammalian Voltage-Dependent Shaker Family K+ Channel. Science *309*, 897–903.

Long, S.B., Tao, X., Campbell, E.B., and MacKinnon, R. (2007). Atomic structure of a voltage-dependent K+ channel in a lipid membrane-like environment. Nature *450*, 376–382.

Ludwig, A., Zong, X., Jeglitsch, M., Hofmann, F., and Biel, M. (1998). A family of hyperpolarization-activated mammalian cation channels. Nature *393*, 587–591.

Ludwig, A., Zong, X., Stieber, J., Hullin, R., Hofmann, F., and Biel, M. (1999). Two pacemaker channels from human heart with profoundly different activation kinetics. EMBO *18*, 2323–2329.

Ludwig, A., Budde, T., Stieber, J., Moosmang, S., Wahl, C., Holthoff, K., Langebartels, A., Wotjak, C., Munsch, T., Zong, X., et al. (2003). Absence epilepsy and sinus dysrhythmia in mice lacking the pacemaker channel HCN2. EMBO *22*, 216–224.

Lupica, C.R., Bell, J.A., Hoffman, A.F., Watson, P.L., Carl, R., Bell, J.A., Hoffman, A.F., and Watson, P.L. (2001). Contribution of the Hyperpolarization-Activated Current (Ih) to Membrane Potential and GABA Release in Hippocampal Interneurons. J. Neurophysiol. *86*, 261–268.

Macri, V., Mahida, S.N., Zhang, M.L., Moritz, F., Dolmatova, E. V, Tucker, N.R., Mclellan, M., Shea, M.A., Milan, D.J., Lunetta, K.L., et al. (2014). A Novel Trafficking-defective HCN4 Mutation is Associated with Early-Onset Atrial Fibrillation. Hear. Rhythm *11*, 1055–1062.

Magee, J.C. (2000). Dendritic Integration of Excitatory Synaptic Input. Nat. Rev. Neurosci. *1*, 181–190.

Magee, K.E.A., Madden, Z., and Young, E.C. (2015). HCN Channel C-Terminal Region Speeds Activation Rates Independently of Autoinhibition. J. Membr. Biol. *248*, 1043–1060.

Männikkö, R., Pandey, S., Larsson, H.P., and Elinder, F. (2005). Hysteresis in the Voltage Dependence of HCN Channels: Conversion between Two Modes Affects Pacemaker Properties. J. Gen. Physiol. *125*, 305–326.

Meuth, S.G., Kanyshkova, T., Meuth, P., Landgraf, P., Munsch, T., Ludwig, A., Hofmann, F., Pape, H., Budde, T., Sven, G., et al. (2019). Membrane Resting Potential of Thalamocortical Relay Neurons Is Shaped by the Interaction Among TASK3 and HCN2 Channels. J. Neurophysiol. *96*, 1517–1529.

Much, B., Wahl-schott, C., Zong, X., Schneider, A., Baumann, L., Moosmang, S., Ludwig, A., and Biel, M. (2003). Role of Subunit Heteromerization and N -Linked Glycosylation in the Formation of Functional Hyperpolarization-activated Cyclic Nucleotide-gated Channels. J. Biol. Chem. *278*, 43781–43786.

Nava, C., Dalle, C., Rastetter, A., Striano, P., de Kovel, C.G.F., Nabbout, R., Cancès, C., Ville, D., Brilstra, E.H., Gobbi, G., et al. (2014). De novo mutations in HCN1 cause early infantile epileptic encephalopathy. Nat. Genet. *46*, 640–645.

Netter, M.F., Zuzarte, M., Schlichthörl, G., Klöcker, N., Decher, N., Netter, M.F., Zuzarte, M., Schlichthörl, G., Klöcker, N., and Decher, N. (2012). The HCN4 channel mutation D553N associated with bradycardia has a C-linker mediated gating defect. Cell. Physiol. Biochem. *30*, 1227–1240.

Nolan, M.F., Lee, K.H., Gibbs, E., Dudman, J.T., Santoro, B., Yin, D., Thompson, R.F., Siegelbaum, S.A., Kandel, E.R., Morozov, A., et al. (2003). The Hyperpolarization-Activated HCN1 Channel Is Important for Motor Learning and Neuronal Integration by Cerebellar Purkinje Cells. Cell *115*, 551–564.

Nolan, M.F., Dudman, J.T., Buhl, D.L., Santoro, B., Gibbs, E., Vronskaya, S., Siegelbaum, S.A., Kandel, E.R., and Morozov, A. (2004). A Behavioral Role for Dendritic Integration : HCN1 Channels Constrain Spatial Memory and Plasticity at Inputs to Distal Dendrites of CA1 Pyramidal Neurons. Cell *119*, 719–732.

Nolan, M.F., Dudman, J.T., Dodson, P.D., and Santoro, B. (2007). HCN1 Channels Control Resting and Active Integrative Properties of Stellate Cells from Layer II of the Entorhinal Cortex. J. Neurosci. *27*, 12440–12451.

Pian, P., Bucchi, A., Robinson, R.B., and Siegelbaum, S. a (2006). Regulation of gating and rundown of HCN hyperpolarization-activated channels by exogenous and endogenous PIP2. J. Gen. Physiol. *128*, 593–604.

Pian, P., Bucchi, A., DeCostanzo, A., Robinson, R.B., and Siegelbaum, S. a. (2007). Modulation of cyclic nucleotide-regulated HCN channels by PIP2 and receptors coupled to phospholipase C. Pflugers Arch. Eur. J. Physiol. *455*, 125–145.

Prole, D.L., and Yellen, G. (2006). Reversal of HCN channel voltage dependence via bridging of the S4-S5 linker and Post-S6. J. Gen. Physiol. *128*, 273–282.

Puljung, M.C., and Zagotta, W.N. (2013). A secondary structural transition in the C-helix promotes gating of cyclic nucleotide-regulated ion channels. J. Biol. Chem. *288*, 12944–12956.

Santoro, B., and Tibbs, G.R. (1999). The HCN gene family: Molecular basis of the

hyperpolarization-activated pacemaker channels. Ann. N. Y. Acad. Sci. *868*, 741–764.

Santoro, B., Grant, S.G.N., Bartsch, D., and Kandel, E.R. (1997). Interactive cloning with the SH3 domain of N-src identifies a new brain specific ion channel protein, with homology to Eag and cyclic nucleotide-gated channels. Proc. Natl. Acad. Sci. *94*, 14815–14820.

Santoro, B., Liu, D.T., Yao, H., Bartsch, D., Kandel, E.R., Siegelbaum, S.A., and Tibbs, G.R. (1998). Identification of a Gene Encoding a Hyperpolarization-Activated Pacemaker Channel of Brain. Cell *93*, 717–729.

Santoro, B., Chen, S., Luthi, A., Pavlidis, P., Shumyatsky, G.P., Tibbs, G.R., and Siegelbaum, S.A. (2000). Molecular and functional heterogeneity of hyperpolarization-activated pacemaker channels in the mouse CNS. J. Neurosci. *20*, 5264–5275.

Santoro, B., Wainger, B.J., and Siegelbaum, S.A. (2004). Regulation of HCN Channel Surface Expression by a Novel C-Terminal Protein – Protein Interaction. J. Neurosci. *24*, 10750–10762.

Saponaro, A., Pauleta, S.R., Cantini, F., Matzapetakis, M., and Hammann, C. (2014). Structural basis for the mutual antagonism of cAMP and TRIP8b in regulating HCN channel function. Proc. Natl. Acad. Sci. *111*, 14577–14582.

Schulze-Bahr, E., Neu, A., Friederich, P., Kaupp, U.B., Breithardt, G., Pongs, O., and Isbrandt, D. (2003). Pacemaker channel dysfunction in a patient with sinus node disease. J. Clin. Invest. *111*, 1537–1545.

Schweizer, P.A., Duhme, N., Thomas, D., Becker, R., Zehelein, J., Draguhn, A., Bruehl, C., Katus, H.A., and Koenen, M. (2010). cAMP sensitivity of HCN pacemaker channels determines basal heart rate but is not critical for autonomic rate control. Circ. Arrhythmia Electrophysiol. *3*, 542–552.

Stieber, J., Herrmann, S., Feil, S., Loster, J., Feil, R., Biel, M., Hofmann, F., Ludwig, A., Löster, J., Feil, R., et al. (2003a). The hyperpolarization-activated channel HCN4 is required for the generation of pacemaker action potentials in the embryonic heart. Proc. Natl. Acad. Sci. *100*, 15235–15240.

Stieber, J., Thomer, A., Much, B., Schneider, A., Biel, M., and Hofmann, F. (2003b). Molecular Basis for the Different Activation Kinetics of the Pacemaker Channels HCN2 and HCN4. J. Biol. Chem. *278*, 33672–33680.

Stieber, J., Sto, G., Herrmann, S., Hassfurth, B., and Hofmann, F. (2005). Functional Expression of the Human HCN3 Channel. J. Biol. Chem. *280*, 34635–34643.

Taraska, J.W., Puljung, M.C., Olivier, N.B., Flynn, G.E., and Zagotta, W.N. (2009). Mapping the structure and conformational movements of proteins with transition metal ion FRET. Nat. Methods *6*, 532–537.

Tibbs, G.R., Liu, D.T., Leypold, B.G., and Siegelbaum, S. a. (1998). A state-independent interaction between ligand and a conserved arginine residue in cyclic nucleotide-gated channels reveals a functional polarity of the cyclic nucleotide binding site. J. Biol. Chem. *273*, 4497–4505.

Ueda, K., Nakamura, K., Hayashi, T., Inagaki, N., Takahashi, M., Arimura, T., Morita, H., Higashiuesato, Y., Hirano, Y., Yasunami, M., et al. (2004). Functional characterization of a trafficking-defective HCN4 mutation, D553N, associated with cardiac arrhythmia. J. Biol. Chem. *279*, 27194–27198.

Ueda, K., Hirano, Y., Higashiuesato, Y., Aizawa, Y., Hayashi, T., Inagaki, N., Tana, T., Ohya, Y., Takishita, S., Muratani, H., et al. (2009). Role of HCN4 channel in preventing ventricular arrhythmia. J. Hum. Genet. *54*, 115–121.

Vaidyanathan, R., and Makielski, J.C. (2014). Chapter 23 - Scaffolding Proteins and Ion Channel Diseases (Elsevier Inc.).

VanSchouwen, B., Akimoto, M., Sayadi, M., Fogolari, F., and Melacini, G. (2015). Role of Dynamics in the Autoinhibition and Activation of the Hyperpolarization-activated Cyclic Nucleotide-modulated (HCN) Ion Channels. J. Biol. Chem. *290*, 17642–17654.

Vemana, S., Pandey, S., and Larsson, H.P. (2004). S4 movement in a mammalian HCN channel. J. Gen. Physiol. *123*, 21–32.

Wahl-Schott, C., and Biel, M. (2009). HCN channels: Structure, cellular regulation and physiological function. Cell. Mol. Life Sci. *66*, 470–494.

Wainger, B.J., DeGennaro, M., Santoro, B., Siegelbaum, S. A, and Tibbs, G.R. (2001). Molecular mechanism of cAMP modulation of HCN pacemaker channels. Nature *411*, 805–810.

Wang, J., Chen, S., and Siegelbaum, S.A. (2001). Regulation of Hyperpolarization-Activated HCN Channel Gating and cAMP Modulation Due to Interactions of COOH Terminus and Core Transmembrane Regions. J. Gen. Physiol. *118*, 237–250.

Wang, J., Chen, S., Nolan, M.F., and Siegelbaum, S.A. (2002). Activity-dependent regulation of HCN pacemaker channels by cyclic AMP: Signaling through dynamic allosteric coupling. Neuron *36*, 451–461.

Wicks, N.L., Chan, K.S.C., Madden, Z., Santoro, B., and Young, E.C. (2009). Sensitivity of HCN channel deactivation to cAMP is amplified by an S4 mutation combined with activation mode shift. Pflugers Arch. *458*, 877–889.

Wicks, N.L., Wong, T., Sun, J., Madden, Z., and Young, E.C. (2011). Cytoplasmic cAMP-sensing domain of hyperpolarization-activated cation (HCN) channels uses two structurally distinct mechanisms to regulate voltage gating. Proc. Natl. Acad. Sci. U. S. A. *108*, 609–614.

Xu, X., Vysotskaya, Z. V., Liu, Q., and Zhou, L. (2010). Structural basis for the cAMP-dependent gating in the human HCN4 channel. J. Biol. Chem. *285*, 37082–37091.

Ye, B., and Nerbonne, J.M. (2009). Proteolytic Processing of HCN2 and Co-assembly with HCN4 in the Generation of Cardiac Pacemaker Channels. J. Biol. Chem. *284*, 25553–25559.

Zagotta, W.N., and Siegelbaum, S.A. (1996). Structure and Function of Cyclic Nucleotide-Gated Channels. Annu. Rev. Neurosci. *19*, 235–263.

Zagotta, W., Olivier, N., Black, K., and Young, E. (2003). Structural basis for modulation and agonist specificity of HCN pacemaker channels. Nature *425*, 200–205.

Zhou, J., Ding, W., Makiyama, T., Miyamoto, A., Matsumoto, Y., Kimura, H., Tarutani, Y., Zhao, J., Wu, J., Zang, W., et al. (2014). A Novel HCN4 Mutation, G1097 W, Is Associated With Atrioventricular Block. Circ. J. *78*, 938–942.

Zhou, L., Olivier, N.B., Yao, H., Young, E.C., Siegelbaum, S.A., Street, W., and York, N. (2004). A Conserved Tripeptide in CNG and HCN Channels Regulates Ligand Gating by Controlling C-Terminal Oligomerization. Neuron *44*, 823–834.

Zolles, G., Klöcker, N., Wenzel, D., Weisser-Thomas, J., Fleischmann, B.K., Roeper, J., and Fakler, B. (2006). Pacemaking by HCN Channels Requires Interaction with Phosphoinositides. Neuron *52*, 1027–1036.